ESL-TR-89-61

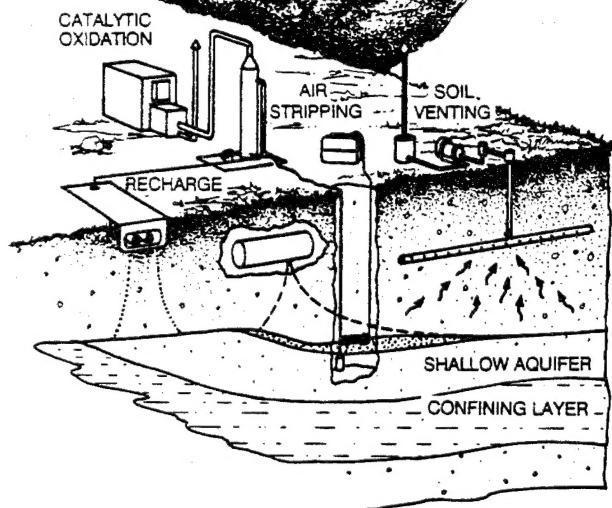# SPRAY COATING OF METALS, PHASE I: FEASIBILITY OF CONCEPT

S.A. Ploger, P.B. Hembree, L.D. Watson

HQ AIR FORCE CIVIL ENGINEERING SUPPORT AGENCY
AF CIVIL ENGINEERING LABORATORY
TYNDALL AFB FL 32403-5323

AUGUST 1995

FINAL REPORT
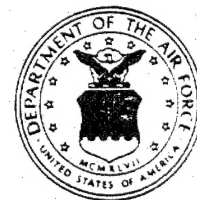
DECEMBER 1989 - JANUARY 1990

CATALYTIC
OXIDATION

AIR
STRIPPING

SOIL
VENTING

RECHARGE

SHALLOW AQUIFER

CONFINING LAYER

19960103 206

ENVIRONICS DIVISION
Air Force Civil Engineering Support Agency
Civil Engineering Laboratory
Tyndall Air Force Base, Florida 32403

NOTICE

PLEASE DO NOT REQUEST COPIES OF THIS REPORT FROM HQ AFCESA/RA (AIR FORCE CIVIL ENGINEERING SUPPORT AGENCY). ADDITIONAL COPIES MAY BE PURCHASED FROM:

NATIONAL TECHNICAL INFORMATION SERVICE
5285 PORT ROYAL ROAD
SPRINGFIELD, VIRGINIA 22161

FEDERAL GOVERNMENT AGENCIES AND THEIR CONTRACTORS REGISTERED WITH DEFENSE TECHNICAL INFORMATION CENTER SHOULD DIRECT REQUESTS FOR COPIES OF THIS REPORT TO:

DEFENSE TECHNICAL INFORMATION CENTER
CAMERON STATION
ALEXANDRIA, VIRGINIA 22314

REPORT DOCUMENTATION PAGE

Public reporting burden for this collection of information is estimated to average 1 hour per response, including the time for reviewing instructions, searching existing data sources, gathering and maintaining the data needed, and completing and reviewing the collection of information. Send comments regarding this burden estimate or any other aspect of this collection of information, including suggestions for reducing this burden to Washington Headquarters Services, Directorate for Information Operations and Reports, 1215 Jefferson Davis Highway, Suite 1204, Arlington, VA 22202-4302, and to the Office of Management and Budget, Paperwork Reduction Project (0704-0188), Washington, DC 20503.

1. AGENCY USE ONLY (Leave blank)	2. REPORT DATE August 1995	3. REPORT TYPE AND DATES COVERED Final

4. TITLE AND SUBTITLE Spray Coating of Metals, Phase I: Feasibility Of Concept, Interim Report	5. FUNDING NUMBERS DE-AC07-76ID01570

6. AUTHOR(S) Scott A. Ploger, Patricia B. Hembree, and Lloyd D. Watson	

7. PERFORMING ORGANIZATION NAME(S) AND ADDRESS(ES) Idaho National Engineering Laboratory EG&G Idaho, Inc. Idaho Falls, Idaho 83415-2050	8. PERFORMING ORGANIZATION REPORT NUMBER

9. SPONSORING/MONITORING AGENCY NAME(S) AND ADDRESS(ES) HQ AFCESA Tyndall AFB, FL 32403	10. SPONSORING/MONITORING AGENCY REPORT NUMBER ESL-TR-89-61

11. SUPPLEMENTARY NOTES

Prepared for the United States Air Force through the U. S. Department of Energy

12a. DISTRIBUTION/AVAILABILITY STATEMENT Unlimited Distribution	12b. DISTRIBUTION CODE

13. ABSTRACT (Maximum 200 words)

Idaho National Engineering Laboratory (INEL) is developing a new coating technique to eliminate hazardous wastes generated by electroplating processes at Air Logistics Centers. In this approach, molten metal is sprayed in fine droplets directly onto a base metal, with near-perfect conversion efficiency and without forming any hazardous liquid or airborne wastes. This phase I feasibility study confirmed that a low-melting-point metal can be deposited with excellent adhesion and negligible porosity, while strengthening the coating layer by rapid solidification. The low-temperature spray-coating system functioned smoothly, with minor modifications to complete the test matrix. The process was successful due to the basic suitability of the Controlled Aspiration Process (CAP) and to the careful, comprehensive approach adopted in development. Tin coatings were deposited onto low carbon steel at differing sets of conditions. Sealed chamber analyses found the CAP technique to be extremely safe and environmentally benign. The favorable Phase I findings suggest that spray-coating technology could be pursued along multiple paths, aimed toward several applications.

14. SUBJECT TERMS Spray Coating (U) Controlled Aspiration Process (U) Molten Metal Application (U)			15. NUMBER OF PAGES 16. PRICE CODE
17. SECURITY CLASSIFICATION OF REPORT UNCLASSIFIED	18. SECURITY CLASSIFICATION OF THIS PAGE UNCLASSIFIED	19. SECURITY CLASSIFICATION OF ABSTRACT UNCLASSIFIED	20. LIMITATION OF ABSTRACT UL

NSN 7540-01-280-5500

(The reverse of this page is blank.)

PREFACE

This report presents the results of an Idaho National Engineering Laboratory (INEL) coating technique study to eliminate hazardous wastes generated by electroplating processes at Air Logistics Centers. In this approach, molten metal is sprayed in fine droplets directly onto a base metal, with near-perfect conversion efficiency and without forming any hazardous liquid or airborne wastes. This phase I feasibility study confirmed that a low-melting-point metal can be deposited with excellent adhesion and negligible porosity, while strengthening the coating layer by rapid solidification. The favorable Phase I findings suggest that spray-coating technology could be pursued along multiple paths, aimed toward several applications.

This technical report has been reviewed by the Public Affairs Office (PA) and is releasable to the National Technical Information Service, where it will be available to the U. S. Government Agencies only because of the proprietary nature of the research.

This report has been reviewed and is approved for publication.

PHILLIP P. BROWN, 1LT, USAF, BSC
Environmental Engineer

MICHAEL G. KATONA
Chief Scientist

EDWARD N. COPPOLA, Maj, USAF
Chief, Environmental Compliance
Division

NEIL J. LAMB, Colonel, USAF, BSC
Chief, Environics Directorate

iii
(The reverse of this page is blank.)

EXECUTIVE SUMMARY

In response to increasingly stringent environmental regulations, the Idaho National Engineering Laboratory (INEL) is developing a new coating technique to the eliminate hazardous wastes generated by electroplating processes at Air Logistics Centers (ALCs). In this approach, molten metal is sprayed in fine droplets directly onto a base metal, with near-perfect conversion efficiency and without forming any hazardous liquid or airborne wastes. The Phase I feasibility study confirmed that a low-melting-point metal can be deposited with excellent adhesion and negligible porosity, while strengthening the coating layer by rapid solidification. This very encouraging behavior should extend to high-temperature alloys in Phase II.

A. OBJECTIVE

One way to minimize hazardous electroplating wastes is to develop an alternative metallization technique that prevents waste generation, rather than attempting to remediate the existing process cycle. The objective of the Spray Coating of Metals project is to investigate coating capabilities of spray-forming technology, whereby molten metals are nebulized into a jet of rapidly cooling droplets that consolidate upon impacting a base metal. Phase I goals consisted of designing, building, and successfully operating a bench-scale spray-coating system at low temperatures. This economical feasibility demonstration also required evaluating samples for several aspects of coating quality, plus assessing the prospects for spraying serviceable high-melting-point coatings in future phases.

B. BACKGROUND

Electroplating of corrosion- and wear-resistant coatings is currently a labor-intensive, time-consuming operation that generates residues laden with toxic "heavy" metals. Disposal costs are increasing rapidly from tightening environmental regulations and reduced landfill availability. Expenses to assure personnel safety are also rising. Moreover, preparing metal surfaces for electroplating often involves cleaning steps in harsh chemical solutions, which can be additional sources of hazardous waste.

Under the strong regulatory and budgetary driving forces, numerous coating processes have been surveyed as to their potential for replacing electroplating. The Controlled Aspiration Process (CAP) being developed at the INEL is one such candidate, where molten metal is drawn by suction from a heated reservoir into a converging/diverging nozzle. Liquid metal streams entering the nozzle throat are torn into fine droplets by a gas flow, much like gasoline in a venturi carburetor. Inert gas cools molten droplets rapidly in flight and accelerates them toward the base metal, where they consolidate and solidify into a dense deposit upon impact.

Spray forming offers several major advantages over electroplating. Most significantly, this direct metal-to-coating technology produces no liquid wastes, and measured conversion efficiencies exceed 99 percent. This process must be performed in an inert environment, so any remnant airborne particles can be completely filtered from the chamber exhaust.

Unlike electroplating, spray forming is not confined to pure elements, and the wide choice in available alloys may lead to better performance and increased service life. Superior coating properties may also be created by rapid solidification--as with state-of-the-art powder metallurgy--which freezes the molten composition, prevents defect formation from impurity segregation, and restricts metal grain growth. Furthermore, rapidly solidified alloys can often be machined to meet component dimensional tolerances, reducing grinding labor and associated personnel precautions.

C. SCOPE

Phase I consisted of five tasks to be performed on a $250,000 budget:

o   Design and fabricate a spray-coating system, including a chamber, furnace, nozzle, heated gas supply, base metal fixture, diagnostic instrumentation, and a computerized data acquisition system.

o   Operate the integrated system to verify computer interfaces, monitor chamber particulate concentrations, perform a scoping test on system behavior, and spray an initial coated specimen set.

o   Analyze the first set of tin-coated carbon steel samples for bend strength, adhesion strength, porosity, and thickness uniformity. Correlate performance results with operating parameters to refine ranges of key variables and design an optimization experiment.

o   Implement the designed optimization experiment to yield secondary samples over variable ranges identified for high coating quality.

o   Analyze process responses by testing the secondary specimen sets and correlating the results to spray-system operating conditions.

The first specimen set was to cover large parametric ranges, producing narrow thick coatings to wide thin coatings from cool to hot deposition temperatures. Test results were then to reduce ranges of interest, so secondary specimens could be sprayed at refined conditions likely to yield optimal tin-coated carbon steel. In practice, the base metal fixture and preheater were not versatile enough for all coating types. Substantial development was also required to prepare samples for adhesion testing and metallography, delaying feedback on coating performance. The test matrix was thus spread over the project duration, and most samples were extracted after spraying completion. All project objectives were still satisfied.

D. RATIONALE AND METHODOLOGY

Before this project, no coatings had been attempted by the Controlled Aspiration Process. However, INEL nebulizers offer major advantages for spraying uniform metal deposits, including uniquely fine droplet sizes and a rectangular configuration ideal for covering large areas with a constant coating thickness. In addition, these spray systems emphasize parametric versatility, assuring that an integrated configuration and a proper set of operating conditions could be found for spraying high-quality coatings.

A particularly important CAP feature is multiple-component thermal control, whereby precise amounts of heat can be injected at the furnace, nozzle/tundish assembly, gas manifold, and base metal fixture. This enables spraying metal deposits of varying thickness over a range of temperatures, permitting process optimization for specific applications. Superior coatings must be adherent and free of connected porosity, and flexibility in system operation is critical to achieving consolidation during deposition. This is especially true at the base metal interface, where any appreciable porosity would result in coating delamination.

The Phase I feasibility study was conducted on a small-scale system with tin chosen as the coating material, taking advantage of its 230°C melting point to limit equipment costs. A nozzle of circular geometry was also selected for reasons of economy, despite its tapered deposits. Later efforts will investigate serviceable, high-melting-point coatings with the novel rectangular nebulizer that sprays wide, uniformly thick deposits.

E. SPRAY SYSTEM CONFIGURATION

Successfully implementing spray forming on new applications requires obtaining comprehensive knowledge on individual components to understand the assembled system. The heart of this approach is combining measurement instrumentation with on-line data acquisition to expedite the component characterization exercises. Numerous baseline studies were conducted on the melt furnace, nebulizing gas heater, and nozzle/tundish assembly-- confirming intended functions before assembly of the functioning nebulizer system. Computerized data acquisition was also critical during on-line recording and subsequent data reduction for actual coating experiments.

All spray-system components performed essentially as designed. Proper nebulizer behavior reflected advance efforts with three prototype nozzles of different geometries, which optimized the design of the exit cone. The entire test matrix was successfully investigated, although changes had to be made to the base metal fixture and preheater for thin molten coatings.

Since the thrust of the Spray Coating of Metals project is minimizing waste generation, the cleanliness of the isolation chamber and filtered exhaust was a key consideration. Aerosol spectrometer measurements were obtained in baseline situations and while spraying tin under nominal and worst-case conditions. Particulate concentrations within the chamber remained more than 1000 times below potentially explosive levels for tin dust, assuring personnel safety in the event of an air leak. Comparing such concentrations to measured metal-spraying rates further established that droplet-to-deposit consolidation exceeded 99.8 percent efficiency, so virtually no solid waste would be produced by this technology.

Performance of the high-gas-volume, ultrafine particulate filter also surpassed requirements by a wide margin. It removed all detectable metal particles from the chamber exhaust stream. A very conservative analysis found the discharged gas to be extremely clean--at least 333 times less than the Permissible Exposure Limit set by the Occupational Safety and Health Administration. This calculation takes no credit for dilution of the chamber exhaust stream after exiting the laboratory stack.

F. EXPERIMENTAL COATING RESULTS

All of the coating types in the original test matrix were successfully sprayed. Early coatings were 1-inch wide at cool deposition temperatures, because of the relatively large 3-inch nozzle-to-base metal separation. With the considerable plume expansion and diffuse heat flux, preheating of the base metal to at least 100°C was necessary for thorough wetting by incident droplets. The base metal was shifted closer to the nozzle for the second set, producing narrower and hotter coatings, while thickness was controlled by adjusting gas pressure and the associated aspiration of molten tin. The higher thermal flux eliminated the need for a base metal preheater. However, the maximum speed of the base metal fixture was not fast enough for a thin molten film that would resist ridge formation under incident plume pressure. Consequently, the third set of coated specimens was sprayed with an improved fixture that moved vertical steel strips, instead of cylindrical sleeves of low carbon steel.

Both radial and horizontal patterns were grit-blasted onto the steel cylinders, which cleaned and roughened the surfaces to facilitate bonding. Several ceramic compounds and grit sizes were tried, but the different preparation techniques had no obvious influence on external appearances. The cool coatings displayed a dimpled, faceted appearance where droplet consolidation was not complete. This texture changed to a smooth, shiny surface with increasing heat flux. Completely molten coatings often were too deep, when wave-like ridges would form under incident gas turbulence.

Samples were extracted from coated steel specimens for assessing bend and adhesion strengths, plus for metallographic evaluations of coating porosity, interfacial matchup, and thickness uniformity. Appreciable development was required to prepare samples, and problems with adhesion testing and metallography were only resolved near the end of the studies.

G. OBSERVATIONS

After component performance and experimental conduct were summarized, sample test results were compiled to identify major parametric influences on overall coating quality. In general, coating thickness and base metal preparation were insignificant factors. Droplets consolidated well over the bulk of the coating layer, with nearly all porosity at the exterior. The absence of interfacial porosity caused excellent mechanical bonding. These findings suggest that spray-coated parts will not require harsh chemical cleaning in advance. They also compare favorably to commercial plasma spraying--where solid particles are injected into hot gas plumes.

Thermal deposition conditions played an important role, especially on adhesion strength. Wide cool coatings yielded the greatest strengths, but narrow hot deposits detached too easily--likely from differential thermal stress and resultant warping. Two adhesion samples surpassed 3000 pounds per square inch, which exceeds the 2100-psi tensile strength of wrought tin parent material. These high values illustrate strengths of mechanical bonds without high-temperature metallurgical bonding, as well as improved strength in the coating layer from rapid solidification. Spray forming thus offers superior coatings, plus major hazardous waste reductions.

H. CONCLUSIONS

The many conclusions from Phase I can be summarized as listed below:

o   The low-temperature spray-coating system functioned smoothly, with minor modifications to complete the test matrix. This success was due to the basic suitability of the Controlled Aspiration Process and to the careful, comprehesive approach adopted in development.

o   Tin coatings were successfully deposited onto low carbon steel at versatile sets of conditions. Base metal temperatures ranged from 50 to 225°C, depending upon plume expansion and preheating. Deposit widths varied from 0.4 to 1.1 inch and thicknesses from 0.004 to 0.025 inch, in response to flight distance, base metal speed, and the nozzle's pressure-dependent melt aspiration.

o   Sealed chamber analyses found the CAP technique to be extremely safe and environmentally benign. Worst-case margins of 1000 to 333 were determined for powder explosion hazards and atmospheric discharges, respectively. At least 99.8 percent of sprayed metal was consolidated into the deposits, showing excellent conversion efficiency and confirming negligible generation of wastes.

o   Bulk tin porosity was typically below 1 percent, independent of coating thicknesses and the grit used to clean and roughen steel surfaces. Excellent consolidation along the base metal interfaces enabled tight mechanical bonding. Superior adhesion strengths from cool deposition conditions demonstrated that high-temperature metallurgical bonds are not necessary and that benefits of rapid solidification can improve properties within the coating layer.

o   External surface roughness can be controlled according to spraying conditions. Rapidly cooled coatings display indentations at least 0.002-inch deep, while thin molten coatings can be mirror-smooth.

I. RECOMMENDATIONS

The favorable Phase I findings suggest that spray-coating technology could be pursued along multiple paths, aimed toward several applications. Tin results immediately indicate that most low-melting-point alloys can be sprayed at cool deposition temperatures--providing adherent metal coatings on plastics, cellulose fibers, and heat-sensitive metals. Possibilities for successfully replacing chromium electroplating at ALCs are encouraging for two main reasons: (1) the CAP approach is inherently flexible, so that coatings can be deposited at numerous spraying conditions; and (2) unlike electroplating, spray-coating technology can probably be used on modern alloys of superior wear and erosion resistance. However, spray behavior must be investigated soon on high-melting-point materials. Also, taking advantage of rapid solidification phenomena by the spray-forming approach could create high-performance coatings of Air Force interest beyond ALCs, where advanced properties may be more critical than minimizing waste. All of these applications would profit from the rectangular CAP nozzle, which appears ideal for covering large areas uniformly and economically.

TABLE OF CONTENTS

TABLE OF CONTENTS
(Concluded)

LIST OF FIGURES

LIST OF FIGURES
(Continued)

LIST OF FIGURES
(Continued)

LIST OF FIGURES
(Concluded)

SECTION I

OVERVIEW

Stringent local and national environmental regulations for the electroplating and metal-finishing industries are placing strict limits on hazardous waste discharges. Cleanup and disposal of these hazardous wastes cost millions of dollars each year. A practical solution to this problem is to develop alternative metallization processes that reduce or eliminate hazardous waste.

A. OBJECTIVE

The objective of the Spray Coating of Metals project is to design, construct, and test alternative metallization systems that minimize the generation of hazardous wastes. In Phase I, low-temperature tin coatings were placed onto low carbon steel templates. Samples were extracted from the coated specimens for determinations of adhesion strength, formability, porosity, and thickness uniformity to assess overall coating quality.

B. BACKGROUND

Electroplating of corrosion-resistant coatings is currently an expensive, waste-producing operation. Many of these elements (Cr, Ni, Cd, Pb, etc.) are considered hazardous materials and must be removed, treated to render them harmless, or disposed of as hazardous waste. Personnel safety precautions during electroplating and subsequent wastewater treatment or disposal are costly and labor-intensive.

In addition, electroplating is generally restricted to pure elemental coatings. That is, metallic alloys and intermetallic compounds can only rarely be electroplated due to very dissimilar "throwing powers" between the anode and cathode for different ionic species. This restriction may limit performances and service lives of coatings in certain applications.

1

With the Controlled Aspiration Process being developed at the Idaho National Engineering Laboratory (INEL), spray forming of metallic coatings has considerable potential for reducing or eliminating most associated sources of hazardous waste. In this nebulization process, molten metal is drawn by aspiration into the throat of a converging/diverging gas nozzle. The liquid stream is sheared by the gas flow into a spray of individual droplets that collect and solidify onto the surface to be coated. Such coatings can be sprayed directly from the melt with over 99 percent conversion efficiency, and any overspray can be collected and recycled.

Preliminary research indicates that, after scaleup, INEL nebulizers will spray wide, uniformly thick coatings with negligible porosity--owing to several fundamental design and operating advantages. The dimensional control thus afforded may minimize subsequent grinding to tolerances. This, in turn, should reduce hazardous airborne contaminants and related personnel exposure farther down the production line.

In contrast to conventional electroplating processes, the composition of a spray-formed coating is dictated solely by the melt makeup. Thus, for example, pure chromium electroplates can likely be replaced by coatings of stainless steel or other alloys of relatively low chromium content that exhibit superior resistance to wear, galling, and corrosion. This flexibility in materials selection may altogether eliminate some hazardous substances from the coating process. It may also reduce U.S. dependence on foreign sources of some strategic elements.

Spray forming offers extra benefits, because of the inherently rapid solidification behavior. Spray-formed metals can often be made stronger and harder than conventional parent materials, due to small grain sizes, freezing of metastable alloy phases, and negligible defect formation from impurity segregation. Furthermore, spray-forming technology has the potential of replacing conventional crystalline coatings with metallic glass layers. Amorphous coatings would be unequalled in corrosion and erosion resistance because no grain boundaries exist. Many compositions are available, offering flexibility in glass transition temperatures. Advanced coatings of either type could significantly reduce the frequency at which U.S. Air Force components must be stripped and recoated.

2

C. SCOPE

Phase I had a $250,000 budget to verify the feasibility of replacing
electroplating of corrosion-resistant and wear-resistant coatings with the
INEL spray-coating process. Phase I consisted of five interrelated tasks.

1. Task 1: Design and Fabricate Spray-Coating System

   o Design and construct a spray-system isolation chamber.

   o Provide a gas supply with temperature control and monitoring.

   o Establish metal melting and handling procedures with temperature
      control and monitoring.

   o Design, construct, and characterize a spray-coating nozzle.

   o Design and install fixturing for controlled movement of base metal
      test plates, including speed and temperature monitoring.

   o Provide computer/sensor interfaces and develop software for spray
      process diagnostics.

2. Task 2: Operate Integrated Spray System

   o Verify computer interfaces for parameter monitoring and control.

   o Monitor spray-system output for safety analyses.

   o Perform initial integrated tests to study primary effects of base
      metal position, droplet characteristics, and temperatures of base
      metal, molten metal, nebulizing gas, and nozzle/tundish assembly.

   o Operate the spray system over large ranges of operating parameters
      to generate a coated specimen set for visual inspections and other
      preliminary evaluations of coating quality.

3. Task 3: Evaluate Initial Coating Trials

o   Analyze first set of tin-coated carbon steel specimens for
    porosity, adhesion strength, bend strength, etc.

o   Correlate coating performance results with spray-system operating
    parameters to identify conditions most likely to produce high-
    quality coatings.

o   Design experiments for subsequent specimen sets to be sprayed over
    a refined range of operating parameters for further investigations
    of spray-coating process variables.

4. Task 4: Implement Coating Optimization Designed Experiment

o   Generate secondary specimen sets by systematically varying the key
    process variables determined in Task 3 over the ranges of interest
    identified for high-quality coatings. (This exercise extended the
    data base on coating properties to cover significantly different
    ranges of deposition temperature and coating thickness.)

5. Task 5: Analyze Coating Process Responses

o   Subject all specimens produced in Task 4 to coating integrity
    tests, including assessments of bond strength and corrosion
    resistance.

o   Correlate coating performance results to spraying conditions.

SECTION II

RATIONALE AND METHODOLOGY

INEL-designed nebulizers possess fundamental operational and geometric advantages for spraying uniform metal deposits. In addition, the unique features of the Controlled Aspiration Process allow tailoring of spray plume characteristics for demanding applications. This unique combination of nebulizer features and operational control offers excellent prospects for a new metallization process that will surpass U.S. Air Force coating standards and, at the same time, dramatically reduce hazardous wastes.

Coatings that resist corrosion and in-service wear must satisfy a number of exacting requirements. Deposited material must adhere tightly to the base metal. To prevent corrosion, a coating must not contain any connected porosity; the best coatings are fully consolidated. Also, to be cost-effective, coatings must be uniform in thickness, which minimizes subsequent grinding or machining to fit close dimensional tolerances.

The approach adopted for development of spray forming emphasizes parametric versatility. Primary process variables such as nebulizing gas pressure and melt feed rate are carefully monitored to control important plume characteristics such as droplet size distributions, gas/metal mass ratios, and spatially consistent mass impingement patterns (Reference 1). Governing such features is critical for complete droplet consolidation upon impacting the base metal. Uniform wetting of the base metal by the first droplets to arrive at the leading plume edge is also essential to avoid interfacial porosity, which can cause coating delamination.

The nebulizing system also permits temperature control at multiple-component stages: the furnace (superheating the molten metal), the nozzle/tundish assembly, the gas delivery manifold, and the base metal itself. This heat balance flexibility enables deposits of varying thickness to be sprayed over wide ranges of operating conditions. The inherent process flexibility also allows latitude in secondary aspects including overall energy expenditures, nebulizing gas recycling, and selection of component materials for lowest cost and ease of fabrication.

5

Nebulizer parameters can then be optimized for specific applications such as high-quality coatings. For example, the extent to which a base metal can be directly heated is often constrained by preserving mechanical properties; e.g., excessive base metal heating might induce embrittlement, loss of temper, etc. However, spray forming cools droplets in flight by radiation and convection, which restricts heat transfer to the coated surface and leaves the base metal bulk relatively cool. Yet, under proper operating conditions, the incident droplets will still wet the base metal surface, consolidate into a high-density deposit, and produce an adherent coating through mechanical interlinkage between interfacial surfaces-- avoiding the necessity for high-temperature metallurgical bonding.

In addition, the patented converging/diverging nebulizer design (Reference 2) has already been extended into a slot-type configuration with a rectangular cross section ideal for spraying flat metal parts. This version holds the most promise for eventual application of coatings for restoring worn components where uniform coatings must be deposited rapidly over large surface areas. It also requires no flight distance for plume expansion, therefore offering the highest overall cooling rates for maximum rapid solidification benefits. Nevertheless, due to the relatively massive gas and metal throughputs, this rectangular design is not as suitable for bench-scale feasibility studies as smaller versions with circular cross sections.

Besides economical nebulizers of circular geometry, low-melting-point materials were used in early spraying investigations to hold down costs of laboratory equipment. Depositing tin coatings on low carbon steel base metal was the principal objective of Phase I, although research performed is directly related to the needs of high-temperature systems.

As approved for Fiscal Year 1990, Phase II will involve a major increase in melt temperature of the sprayed material to include chromium or chromium alloys (e.g., stainless steels). This work will also be performed on an economical bench scale for proof of principle.

6

SECTION III

SPRAY-SYSTEM CONFIGURATION

A. INTRODUCTION

Tasks 1 and 2 of this project required building and testing a complete spray-coating system, before producing the first set of tin-coated steel specimens. The entire system is physically represented in Figure 1. As shown, system elements can be grouped into two major assemblies: the spray chamber and its integral components, and instrumentation for measuring and recording experimental data.

Very briefly, a regulated flow of inert gas is heated and fed into a converging/diverging nozzle. Meanwhile, as indicated in Figure 2, tin melted by a nearby furnace is poured into a heated tundish directly above the nozzle body. With the Controlled Aspiration Process, molten tin is aspirated into the nozzle throat over a narrow range of gas pressures, where it is nebulized into a droplet mist sprayed against a moving piece of low carbon steel. While the tin droplets cool rapidly in flight, they are not fully solidified upon impacting the base metal. Under suitable conditions, the droplets will consolidate into a dense adherent coating.

The nebulization process occurs in an enclosed chamber, both to afford personnel safety and to restrict oxidation of hot metal, including heating elements. Inert purging gas was used to reduce oxygen levels inside the chamber prior to melting tin and raising component temperatures, as well as to sweep unconsolidated particles (overspray) into a filter bank before discharging out the laboratory stack exhaust. Particulate concentrations are measured before and after filtration by laser aerosol spectrometers.

Considerable instrumentation is required to control this process, to acquire on-line data, and to subsequently analyze dynamic influences on coating quality. This hardware and software will be described in detail before specific information on spray-chamber components is presented, because the baseline studies discussed there on component behavior were performed with the aid of the data system.

7
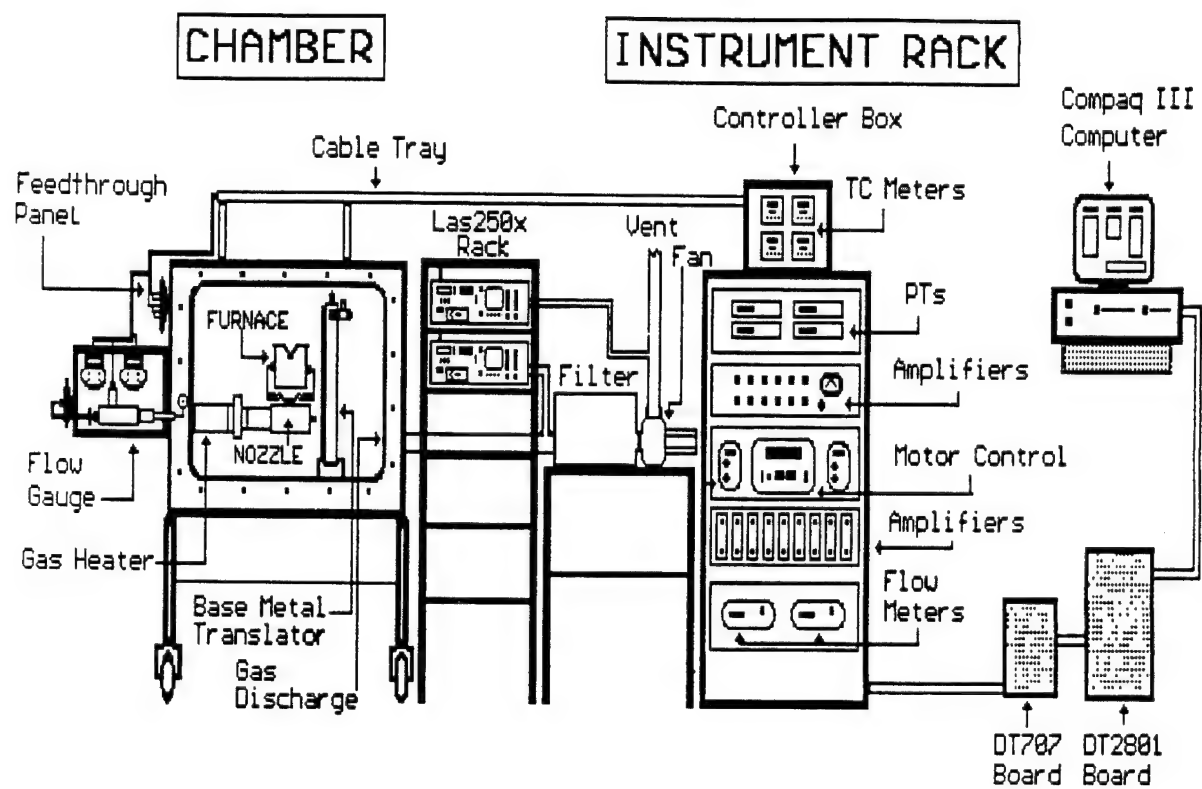
Figure 1.   Simplified Spray-System Arrangement.

8
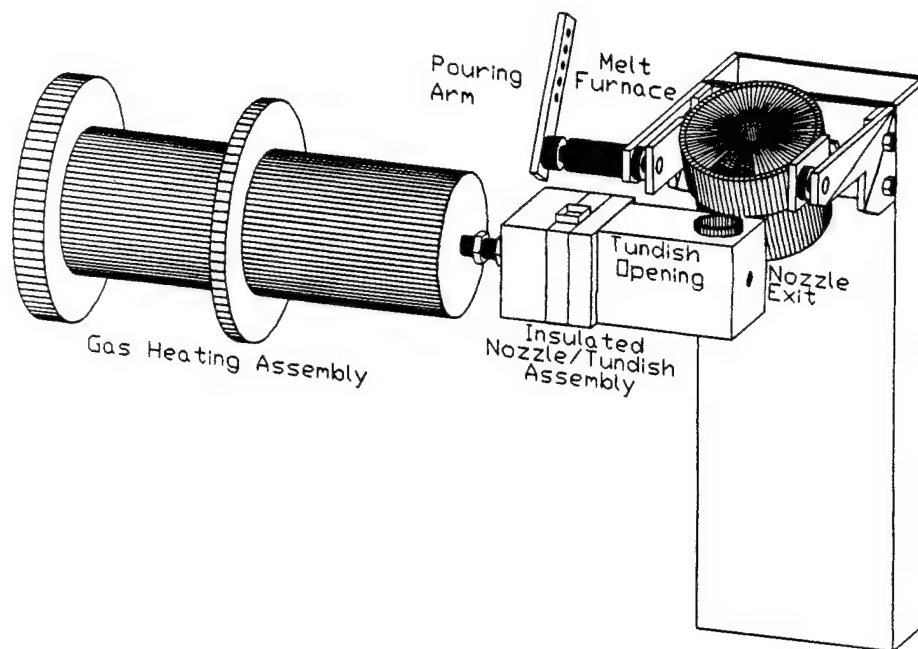
Figure 2.   Primary Components of the Molten Metal Nebulizer.
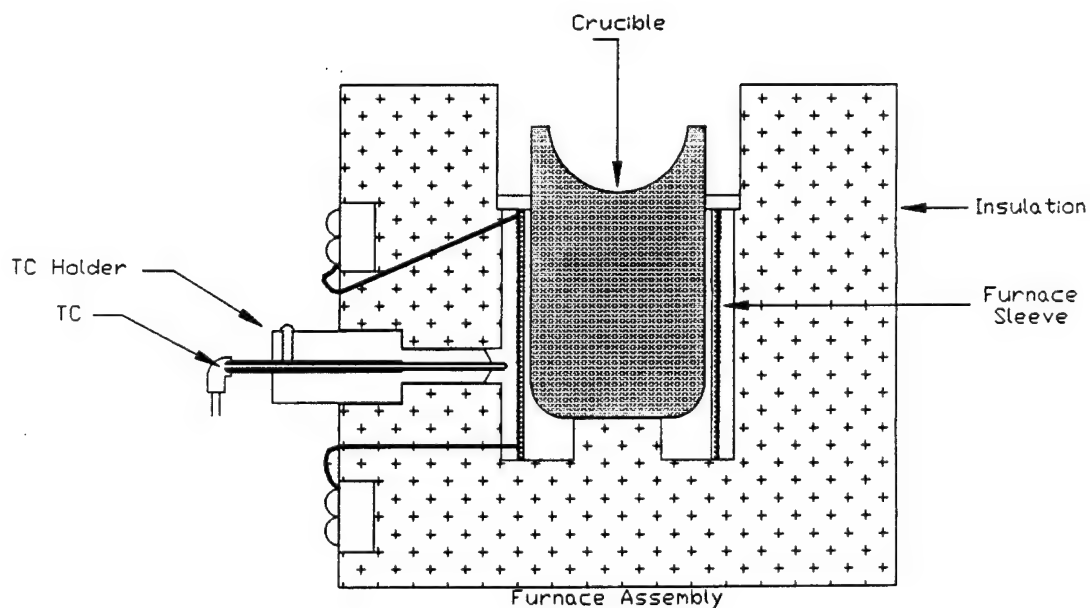
Figure 3.   Cross Section of Low-Temperature Furnace Assembly.

9

B. DATA ACQUISITION ELECTRONICS

The right half of Figure 1 displays numerous meters, controllers, and signal conditioners, along with a computer and related interface boards. This electronic array was assembled primarily to measure and record data from multiple transducers, either during spray-forming experiments or during baseline characterizations of spray-system components. A second portable computer (not shown) is used to record data on particulate sizes and concentrations from the two laser aerosol spectrometers.

Measurement sensors include pressure transducers (PTs) mounted inside and outside the spray chamber and upstream of the gas heater/nozzle; a gas flow meter upstream of the nozzle; thermocouples (TCs) on the melt furnace, nozzle/tundish body, gas heater outlet, and base metal; and a drive-mechanism encoder to monitor the speed of base metal movements. TC signals are also fed to temperature controllers that switch power supplies on and off, thereby maintaining preselected temperatures in the nozzle/tundish assembly and in the molten metal, prior to pouring.

All signals are routed through a patch panel and low-noise cables to signal conditioners for amplification and noise isolation. Along with panel meters and commercial transducers, the conditioners were checked upon receipt from the respective vendors to verify expected performance. All such instruments are periodically recalled by the INEL Standards and Calibration Laboratory for inspection and recertification. In addition, in-place calibration techniques were implemented via the computer, which confirms that the sensors and conditioners are functioning properly when connected. This approach is also essential for thermocouples, which are designed and fabricated in-house to satisfy exacting geometric constraints and which are tied to a cold reference junction for maximum accuracy.

The amplified outputs from the transducer signal conditioners must be digitized before computer processing. After routing through a DT707 terminal, each signal feeds a dedicated channel on a DT2801 interface. (Both boards are from Data Translation, Inc.) Up to 16 analogue-to-digital converters can be used for data acquisition, and two digital-to-analogue channels are available for programmable control functions.

10

A Compaq III Model 40 portable computer was used during Phase I for data acquisition. Features include a 12-megaHertz 80286 microprocessor (Intel Corp.), a 40-megabyte fixed disk drive, a 1.2-megabyte diskette drive, 640 kilobytes of random-access memory, both serial and parallel interfaces, and a real-time clock/calendar. It is fully IBM-compatible, and incorporates a MS-DOS Version III operating system (Microsoft Corp.).

As noted previously, the data acquisition system was used during both actual coating experiments and baseline characterizations of spray-system components, plus in-place measurement calibrations. A versatile software package called Labtech Notebook was procured to streamline execution of these diverse tasks. Each channel is provided with its own setup file, which permits different scale factors, offset constants, buffer sizes, and high- and low-value alarm limits.

Besides enabling input channels to be scaled into meaningful units, Labtech Notebook allows customized design of screen formats with individually labeled windows for dynamic data display. Data can be presented (averaged over preselected time intervals) either as on-line numerical values or as stored graphical plots. The prompt feedback thus provides immediate assurance that all instruments are functioning properly and that each experiment is being conducted as planned.

Labtech Notebook is not limited to a single-purpose display. Instead, a menu-driven screen was developed and stored for each acquisition mode desired. Specific programs were written for evaluating performances of the furnace, gas heater, spray nozzle, and the entire integrated system. As well as improving the convenience and productivity of data acquisition, this menu-driven approach ensured consistent data-recording formats over the project duration. Standardized testing proved helpful for subsequent reduction and analysis of data, which were performed after down-loading files to Lotus worksheets (Lotus Development Corp.).

Developing and debugging this data acquisition system constitutes a lasting accomplishment, because most hardware and software will be used on Phase II. Sensors of different ranges will be accommodated, and several currently manual functions will be controlled then directly by computer.

11

C. FURNACE/MELT DELIVERY SYSTEM

Molten tin was supplied to the nebulizer (nozzle/tundish assembly) by a furnace whose cross section is displayed in Figure 3. Melt is contained within a zirconia crucible, which is surrounded by a ceramic sleeve wound with nickel-chromium wire. This furnace can raise metal up to 1000°C by resistance heating, although tin temperatures of 400°C were generally adequate for Phase I purposes. Insulation is provided by a machined cylinder of fused silica. Not shown is an upper rim/pour spout cast from ceramic cement, which encloses the upper crucible portion.

Alumina-sheathed Type K chromel/alumel thermocouples measured melt temperature (by immersion) and heater coil temperature. As indicated in Figure 3, the coil TC is offset from the wire position by a small distance to avoid electrical shorts and eutectic reactions between the Type K TC junction and the NiCr wire. The primary purpose of the coil TC is to assure that the NiCr melting point is not approached, but it also serves as a backup indicator of melt temperature in the event of melt TC failure.

This furnace fits inside a steel container connected to a tilt mechanism, as illustrated in Figure 2. The tilt device is actuated by an external lever for remotely pouring metal into the nebulizer tundish. Any surplus metal can be discharged into a mold swung under the pour spout by a second remotely operated lever assembly.

Measured melt and wire temperatures are plotted in Figure 4, along with the furnace powers calculated from measured heater voltages and amperages. Indicated coil temperatures are systematically lower than melt temperatures, due to the NiCr wire-coil TC gap. Power was increased at 30-minute intervals, both with and without an insulating cover on the furnace. Comparing Figures 4a and 4b reveals that stable temperatures were achieved more rapidly with an insulating cover, as one would expect. However, the power level required to attain a certain melt temperature was only slightly larger without a cover, and the power required to stabilize a given temperature was not prohibitively large in any case. Accordingly, the decision was made to operate without a furnace cover--mainly for the sake of convenience, but also to permit visual inspections.

12
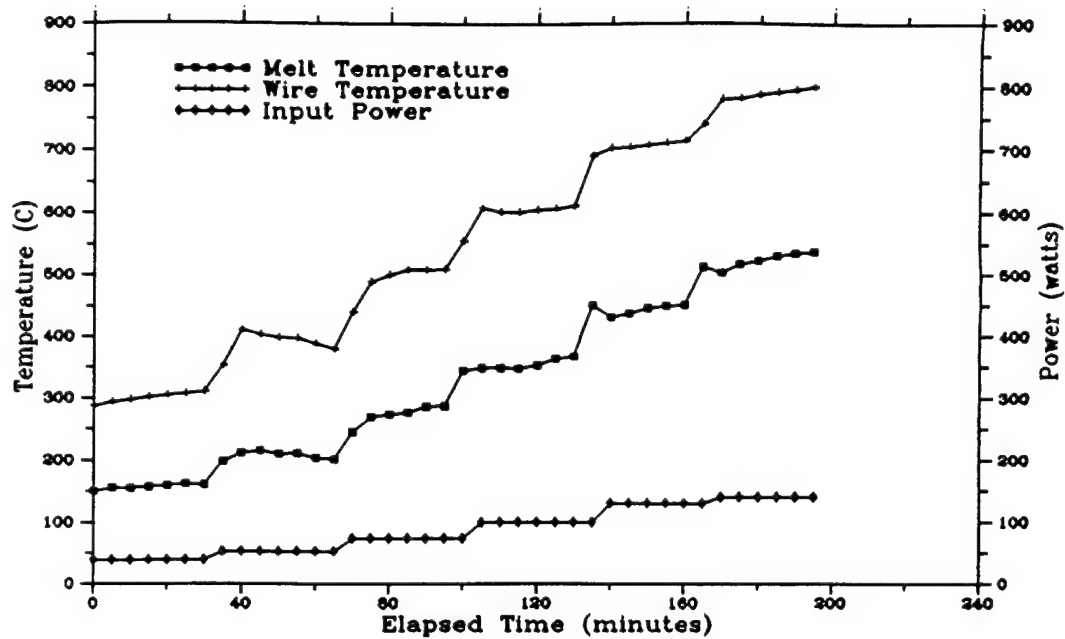
a) Without furnace cover
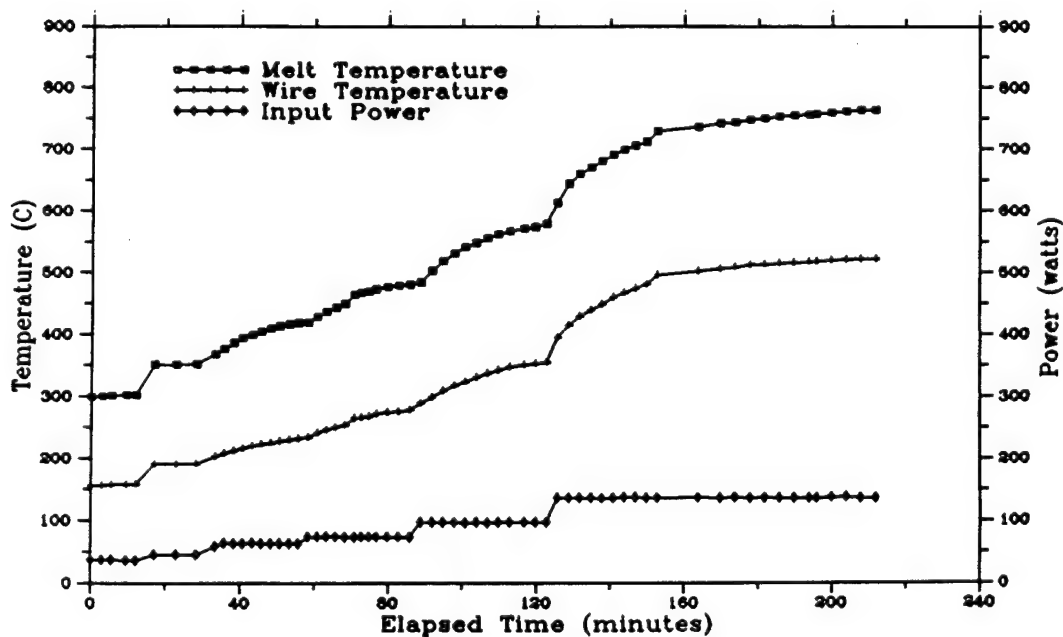
b) With furnace cover

Figure 4. Power Needed in Furnace Windings to Reach Various Melt Temperatures with and without a Furnace Cover.

13

Heat losses by radiation from a well-insulated furnace should be small, so most power would be dissipated to the surroundings by conduction and, in the absence of a cover, predominately by convection. If this assumption is correct, power losses will be proportional to temperature differences between the furnace and the environment. Figure 5 verifies that this is indeed the case, where the stabilizing power levels from Figure 4a clearly have a linear relationship with the corresponding differential temperatures (melt minus ambient). Furthermore, because this furnace can be operated over 600 Watts (240-Volt power supply) with temperature monitoring and automated control, the loss values in Figure 5 could be tolerated easily across the temperature range of interest.

Another furnace characterization experiment is presented in Figures 6 and 7. Here 110 grams of tin (a full crucible charge) was first melted, then raised to 800°C at an arbitrary input power of 324 Watts, and then allowed to cool after shutting off the furnace. Data points were collected at 10-second intervals to provide a continuous comparison of melt and indicated NiCr wire temperatures--as a calibration curve in the event of melt TC failure. However, much more information can be derived.

Multiplying 110 grams of molten tin by its specific heat capacity reveals that 25 Joules of energy is required to raise the crucible charge each degree of temperature. If all 324 Watts of input power reached the metal, a temperature increase rate of 13°C/second would result. Allowing for power lost to the surrounding environment would still yield 8°C/second. Yet, the melt TC plot in Figure 6 shows measured melt temperature rising between 1.5 and 1.0°C/second, which indicates that the crucible, ceramic sleeve, pour spout, and adjacent insulation also must be heated. Similarly, the exponential decrease in melt temperature would be expected to proceed with a larger time constant (ie. decrease faster) than shown in Figure 7, if only the molten tin had to cool.

A very useful concept for treating heat-sink effects of all furnace components is that of effective thermal mass, which can be derived by summing the products of each component mass and its heat capacity. Rather than performing such a calculation, however, accurate estimates can be produced directly from characterization data by two complementary methods.

14
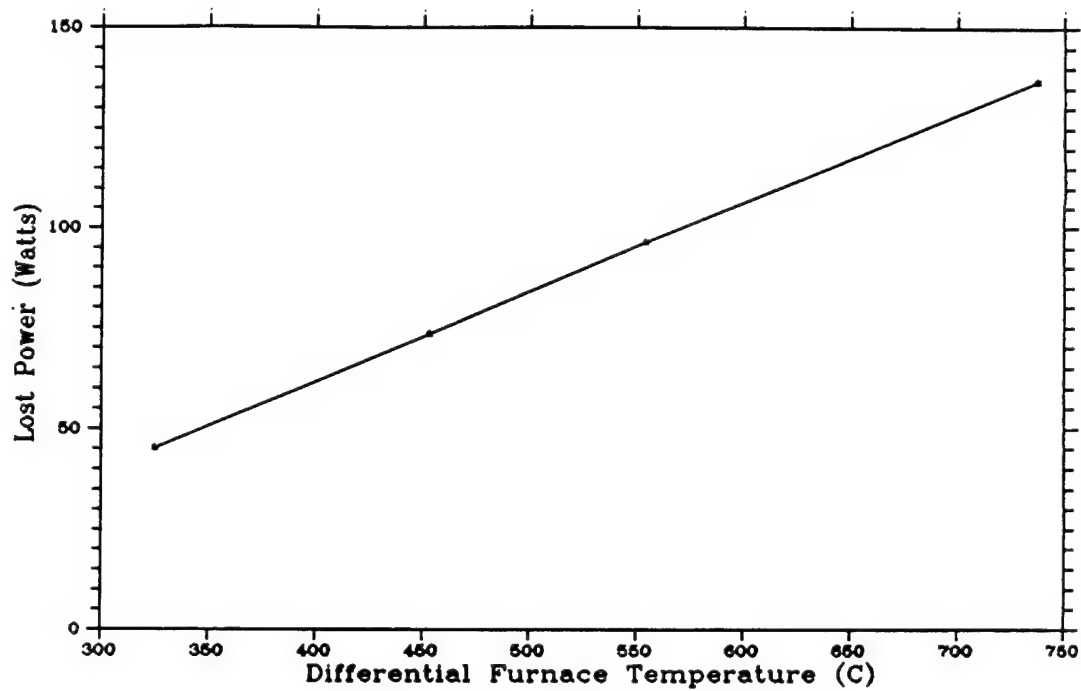
Figure 5.   Linear Relationship between Lost Furnace Power and the
Difference between Melt Temperature and Room
Temperature.
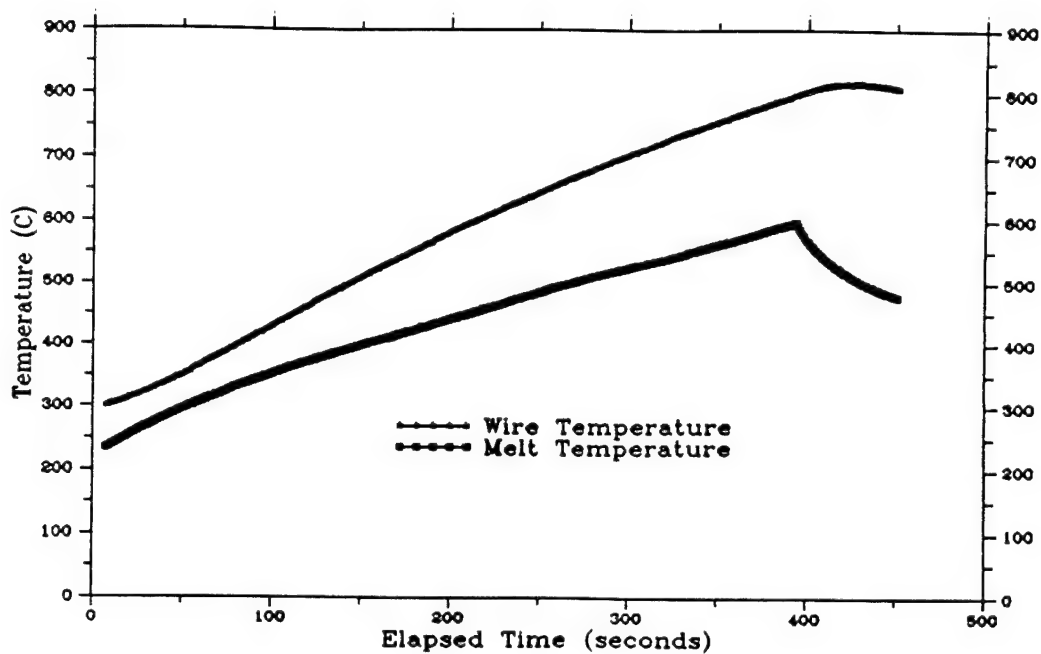
Figure 6. Furnace Heating Rates Measured at 324 Watts of
Input Power.
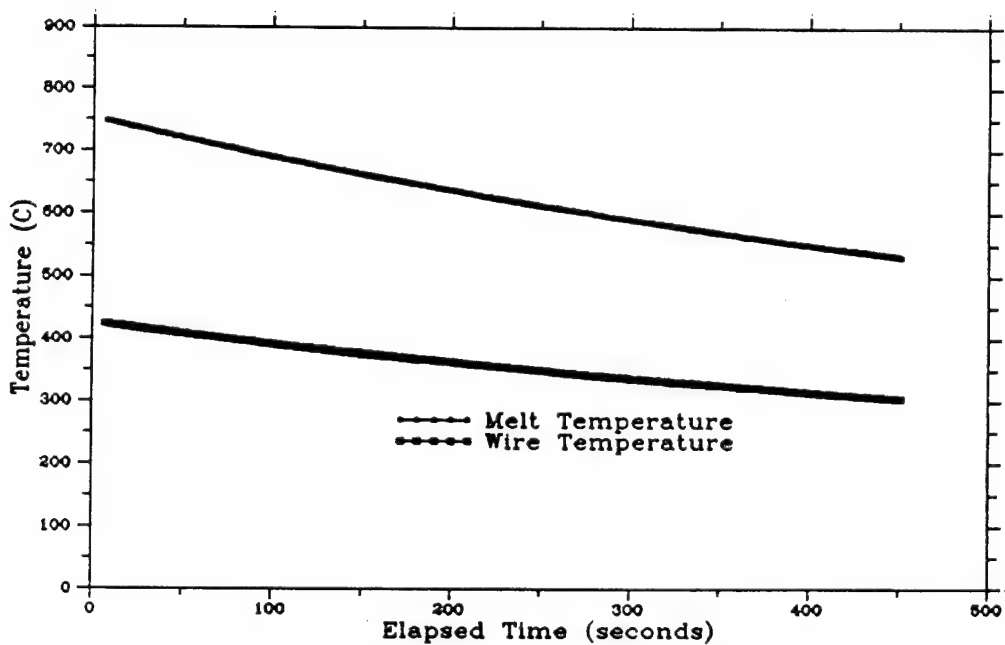
Figure 7. Measured Furnace Cooldown Rates.

16

The first approach is to obtain a power-loss value at a specific temperature from Figure 5 and then divide this value by the melt cooldown rate at the same temperature on Figure 7--assuming that the rate of heat loss to the environment during heatup is equivalent to the rate of heat removal during cooldown. The second method is to subtract the power-loss value from the input power (324 Watts) and then to divide this net heating power by the corresponding melt heatup rate in Figure 6. No matter what particular temperature is selected, both of these estimation techniques consistently yield an effective thermal mass of nearly 200 J/°C--eight times the thermal mass of the tin charge. Because this approximated value is independent of temperature, it can be used to predict the actual melt heatup rate for any choice of input power--with allowance for different heat loss rates in Figure 5.

Effective thermal mass is also a valid criterion for rating furnace designs. This value simultaneously considers insulation efficiency, heat transfer coupling between the coil and crucible charge, overall thermal response relative to input power, and total heat sink mass relative to the heated metal mass. Since a similar characterization sequence is conducted for each furnace involved in INEL spray-forming research, a substantial data base is steadily evolving on various design features, including relative merits of alternative component materials and dimensions. Consequently, newer, larger furnace designs can be developed as spray-forming projects are begun or extended, with a high degree of confidence that they will perform as required.

D. GAS SUPPLY HEATER

Past INEL spray-forming research has found it highly desirable to heat the nebulizing gas before reaching the nozzle. The main reason is to provide an extra degree of freedom for precise control of the nebulizing process, including critical characteristics such as droplet cooling rates. Upstream gas heating also reduces demands on the nozzle heating element, making it relatively easy to stabilize nozzle and throat gas temperatures. In addition, because gas is blown through the nozzle just before spraying, the hot gas jet preheats the base metal for better wetting behavior.

For this small-scale coating project, the gas heater was designed to raise inert gas temperatures up to 600°C, allowing for nebulization of tin (235°C melting point) with several hundred degrees of superheat, if needed. The gas heater was also designed to operate between inlet pressures of 12.4 (ambient) and 50 pounds-per-square-inch absolute (psia) and over flows from 0 to 10 standard cubic-feet-per-minute (scfm).

Figures 8 and 9 show three-dimensional and cross-sectional views of the gas heater, respectively. The heart of the assembly is a Leister Model 3000 resistance-heating unit, where power to the nickel-chromium coils can be manually adjusted up to 3000 Watts. It is surrounded by a custom-built stainless steel barrel that can be mounted onto inner or outer portions of the spray chamber. An annulus was incorporated for a cool internal flow of bypass gas, which restricts heating of the external barrel, so the gas heater can be used for bench-testing without risk of burn injuries. The bypass flow also cools internal thermal sensors that, upon becoming too warm, intermittently switch off power to the NiCr coils.

The essential performance characteristics of the gas heating assembly are illustrated in Figure 10, where temperatures of the outlet gas and the heater barrel are plotted over the full range of heater power settings for five representative flow rates. One Type K TC was centered in the outlet fitting (no wall contact) and another was attached nearby on the warmest part of the barrel housing. Outlet gas temperatures stabilized within two minutes of each power increase, and the heater barrel stayed cool in all cases. Lower outlet temperatures at the two lower flow rates reflect incomplete bypass cooling of the thermal switches and intermittent power.

Internal behavior of the assembly is shown in Figure 11, where free-standing thermocouples were placed inside the NiCr coil outlet and within the bypass annulus surrounding the heating elements. (See Figure 9.) Coil outlet temperatures follow very similar trends to those measured at the assembly outlet. However, the coil outlet temperatures are noticeably higher than at the assembly outlet, where mixing has occurred with the cool bypass stream, and the thermal response of the coil gas is faster than near the assembly outlet heat sinks. Consistently low temperatures found in the bypass region confirm the adequacy of this design feature.

18
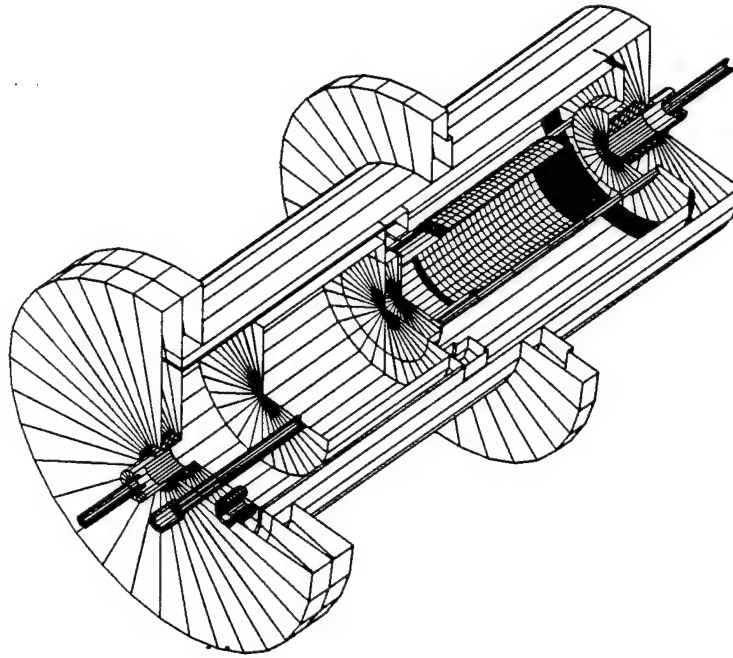
Figure 8. Three-Dimensional Plan View of Gas Heating Assembly.
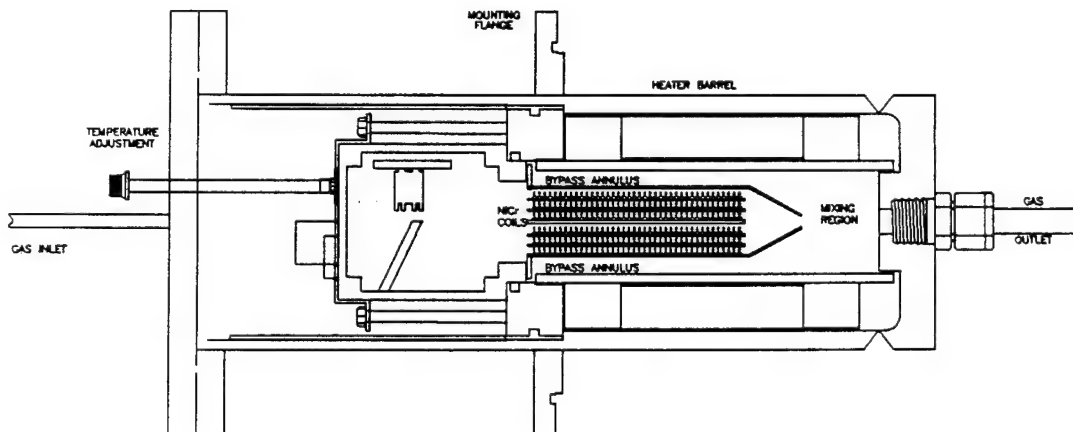
Figure 9. Cross Section of Gas Heating Assembly.
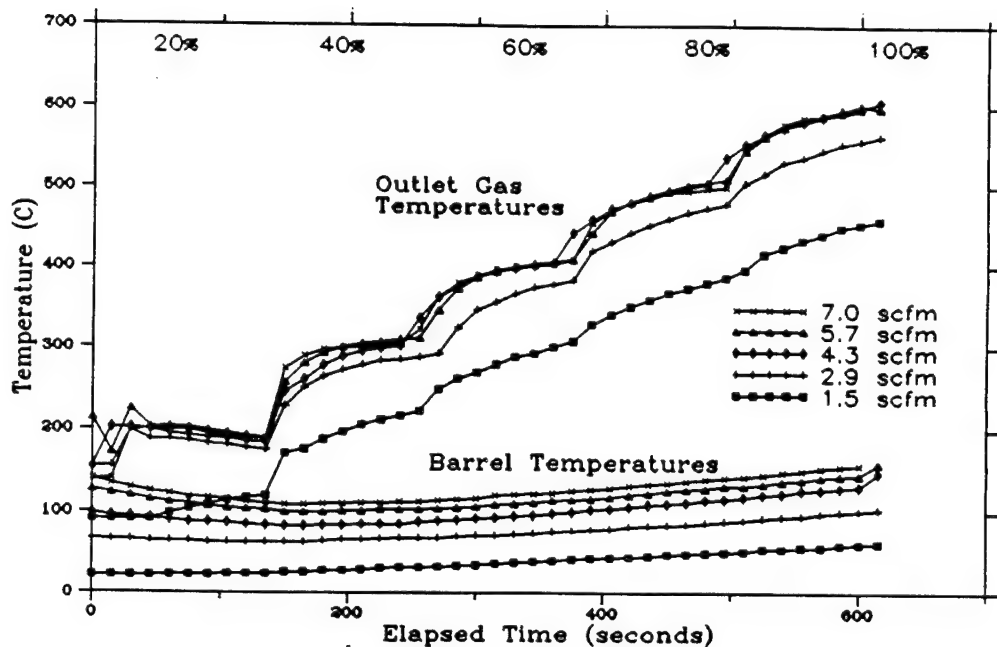
Figure 10. Gas Heater Outlet and Barrel Temperatures at Five Flow Rates and Five Heater Power Settings.
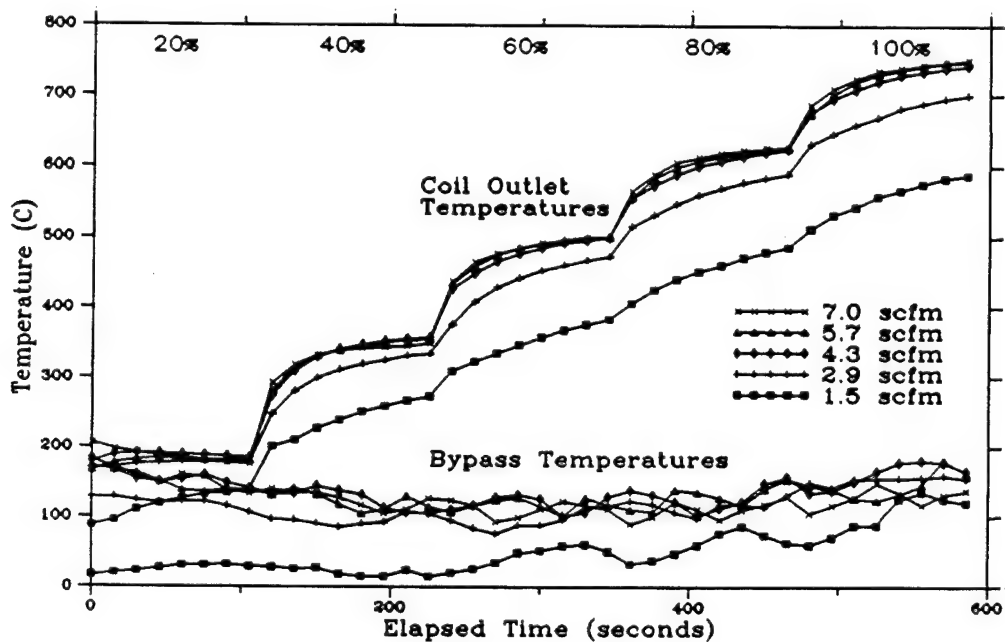
Figure 11. Gas Heater Internal Temperatures Measured at the NiCr Coil Outlet and within the Bypass Annulus.

Behavior of INEL spray nozzles is primarily governed by gas pressure, as discussed in the next section. Since the gas heater is located between the nozzle and where operating pressure is measured, an essential part of characterizing the gas heater is determining pressure drops across it as a function of process variables. Another benefit is computing heater power from downstream gas temperature and known flow and local pressure values. The results of this study are displayed in Figure 12. Differential pressure is strongly influenced by gas flow rate, and the pressure drop magnitudes become highly significant above 3 scfm. Appreciable pressure drops also occur with increasing heater power at specific flow rates.

Knowing the behavior of the gas heating assembly is doubly important because--as described below--the nozzle assembly was designed to accept gas flows above 3 scfm, where the gas heater operates more efficiently. That is, above 3 scfm the higher gas throughputs permit sufficient bypass cooling of the thermal switches for continuous heater coil operation. This design foresight again demonstrates the worth of thoroughly characterizing performance of individual system components.

E. NOZZLE/TUNDISH ASSEMBLY

To accomplish Phase I, a molten metal nebulizer had to be designed and built to confirm the feasibility of spray deposition for coating U.S. Air Force components. The approach taken at the INEL is to aspirate molten metal into the throat of a converging/diverging gas nozzle under tightly controlled conditions. Here the liquid stream of metal is transformed into a directed mist of rapidly cooling droplets. Moreover, the nebulizer assembly must readily accept molten metal poured from a furnace and hold it at a stable temperature until spraying commences.

Behavior of a converging/diverging nozzle is influenced by many design features. Among them are the entrance and throat diameters, the entrance cone angle, the throat length, and the angle and length of the exit cone. Past INEL research has narrowed the ranges for purposes of nebulizing liquid metals, particularly in the entrance region. However, exit cone dimensions frequently must be tailored for specific applications.

21
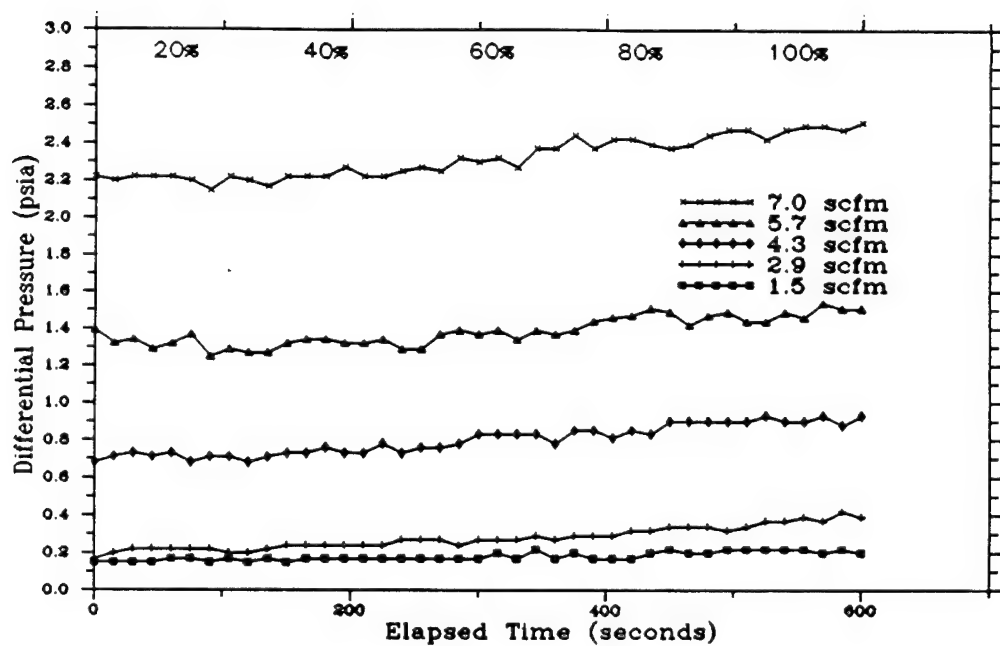
Figure 12. Pressure Drops between Gas Heater Inlet and Outlet
for Five Flow Rates and Heater Power Settings.

22

Simple converging/diverging nozzles were built with exit cone angles of 6, 10, and 18 degrees to begin this process. Small holes were drilled at predetermined increments along the exit wall of each nozzle, and the pressure was measured at each hole while sequentially increasing operating pressure. After data had been obtained for each nozzle at its original exit area-to-throat area ratio, this ratio was successively changed by trimming down the exit cone length on each nozzle while recording new wall pressure data sets. Four ratios were tried for the 10- and 18-degree nozzles, and three ratios were tried for the 6-degree nozzle. All measurements were performed at room temperature using argon gas.

These measurements were plotted in both as-recorded and normalized fashions, and the results are presented in Appendix A as Figures A-1 through A-12. Figure 13 provides an example of each plot type for the nozzle configuration that was ultimately selected for spraying coatings. In both Figure 13 and Appendix A, Areas 2 through 8 mean larger distances (one-sixth inch steps) from the throat (Area 1). Local wall pressures P were normalized to the nozzle operating pressure $P01$, while local cross-sectional exit cone areas A were normalized to the throat area At.

Close inspection of the Appendix A plots reveals little difference between the 10- and 18-degree nozzles in that both the as-recorded and normalized pressure profiles are consistently smooth along exit cone walls. Also, this behavior was not strongly influenced by changing the exit cone length, allowing design flexibility for other components. Plots from the 6-degree nozzle reveal irregular profiles, and trimming induces rather abrupt changes near the exit plane. Both trends suggest potential instabilities with respect to small changes in operating pressure.

Another important aspect of the 10- and 18-degree nozzles is that the throat wall pressure shows first a decrease below atmospheric pressure (ie. suction) and later an increase above it as operating pressure is increased. This design feature is essential for starting and stopping the metal-spraying process, besides using aspiration to precisely control the liquid feed rate into the throat when spraying. However, such inflections occur outside the 6-degree nozzle throat as well--along the exit cone wall--which again infers localized pressure discontinuities.

23
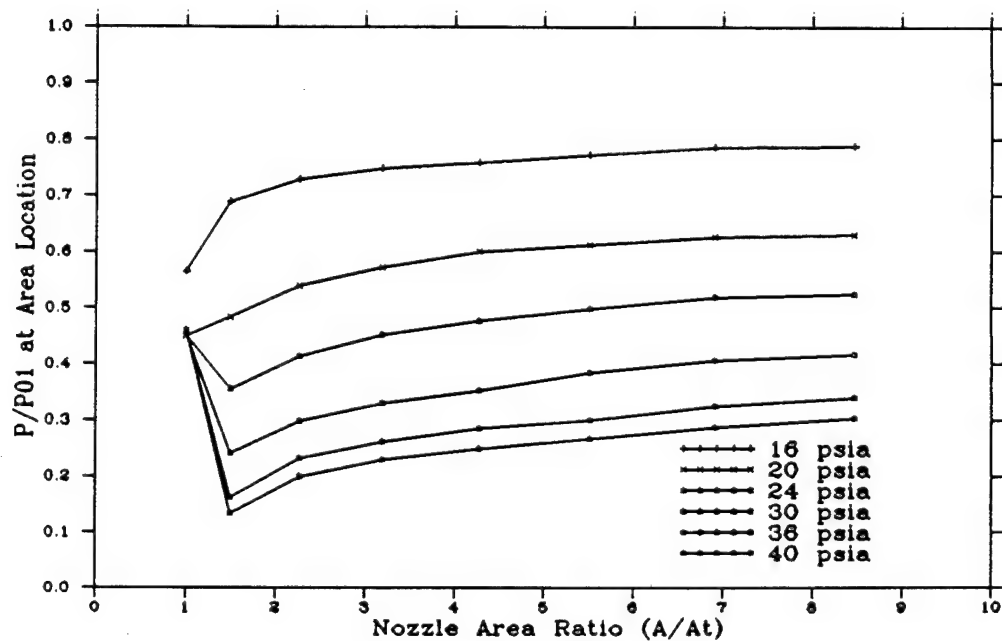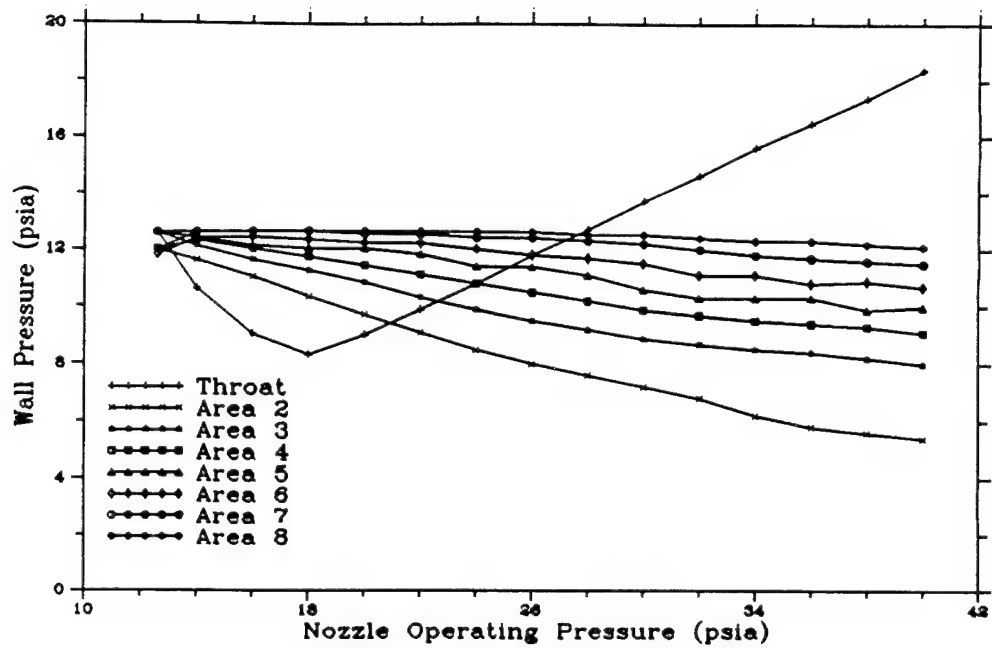
Figure 13. Pressure Measurements and Normalized Pressure Ratios along the Exit Cone Wall for 10-degree Nozzle with an Exit Area-to-Throat Area Ratio of 8.5.

The above considerations ruled out a 6-degree exit cone. A 10-degree design was finally selected over an 18-degree nozzle for two reasons. First, a narrower exit angle allows a longer exit cone for an equivalent exit area-to-throat area ratio, making possible a wider tundish opening for relative ease in pouring tin from the melt furnace. (See Figure 2.) Second, experience in spraying tin with an 18-degree nozzle had shown a tendency for droplets to gather and agglomerate in vortices near the exit plane. This observation indicated that an 18-degree exit cone was overly expanded for relatively low plume temperatures. That is, the flow stream was apparently separating from the walls before reaching the exit plane, creating small "eddies" near the walls that temporarily trapped tin droplets. The resulting agglomerated droplets could still be sprayed, but they cooled rather slowly--detracting from mechanical properties desired in the deposits from rapid solidification. Furthermore, their relatively large size produced a rougher surface finish than wanted on a coating.

It should be noted that some of the empiricism involved in nozzle design will be eliminated in future efforts, beginning with Phase II. As outlined in Appendix B--the approved Phase II work scope--predictive computer modeling will be employed extensively to refine basic nozzle configurations as new performance requirements emerge. In particular, a one-dimensional computer code following classical gas dynamics will be augmented to account for gas temperatures far above ambient, for heavy liquid loading of the gas stream (two-phase flow), and for two-dimensional effects (e.g. pressure differences between an exit cone centerline and the walls). Code predictions will be benchmarked against actual measurements, including the room-temperature data sets contained within Appendix A.

Figures 14 and 15 show the as-built nozzle/tundish assembly design in three-dimensional and cross-sectional views, respectively. The nozzle and tundish were made of boron nitride. Both were heated with NiCr wire, monitored with thermocouples, and insulated to minimize energy losses. The main purpose of the integral heaters is to prevent molten metal from freezing after pouring from the furnace and prior to spraying. However, the ability to directly control temperatures of these components--as well as the melt, nebulizing gas, and the base metal--is very important for both process flexibility and conducting precise parametric experiments.

25
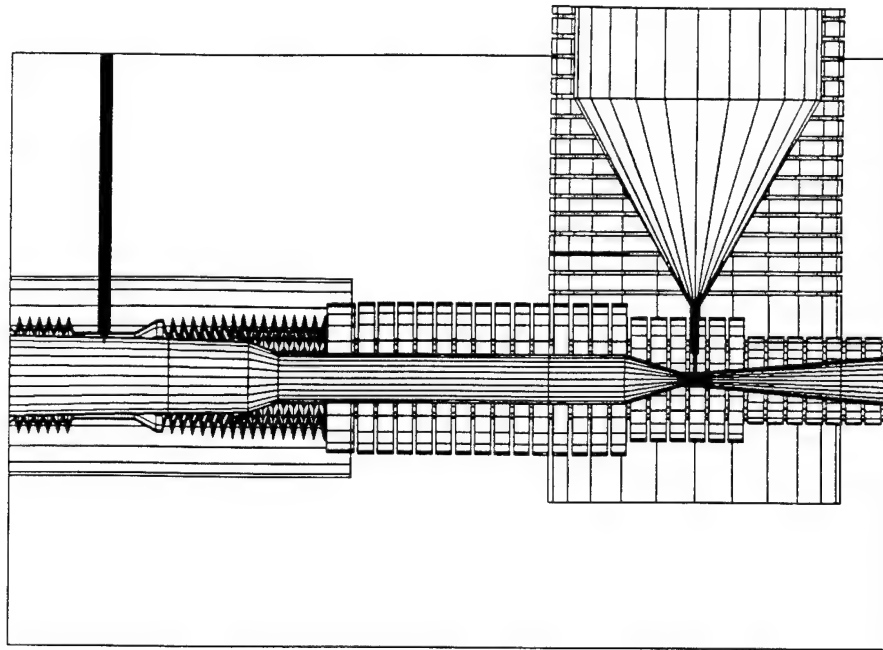
Figure 14.   Three-Dimensional Plan View of the
Nozzle/Tundish Assembly.
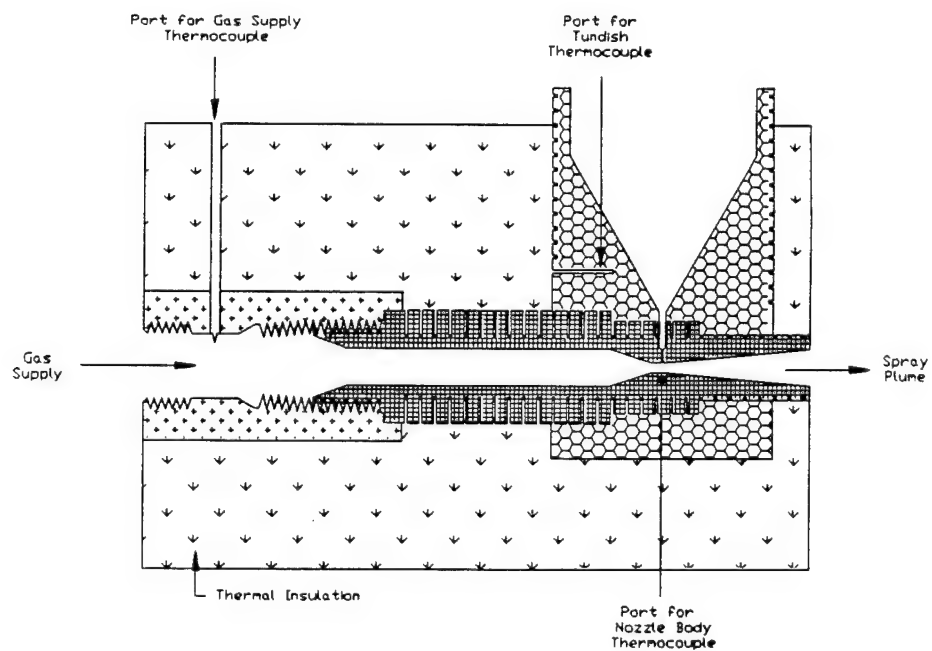
Figure 15.   Cross Section of the Nozzle/Tundish Assembly.

After the nozzle/tundish assembly was installed onto the gas heater in the spray chamber, the first step in characterizing the performance of this component was obtaining data at room temperature. The most urgent aspect of this exercise was confirming that the nozzle throat exhibited strong suction at the liquid orifice position for reasonably low operating pressures. Experience has established that peak suction values of at least 2 psi are required for successful metal spraying at low temperature.

The required behavior is shown in Figure 16, where the minimum pressure measured at the liquid orifice entrance (9.6 psia) converts to 2.8 psi of maximum suction after subtraction from 12.4 psia (ambient laboratory pressure). Moreover, the liquid orifice pressure rises above ambient at approximately 28 psia of operating pressure. Consequently, no molten metal is aspirated into the nozzle throat at operating pressures beyond this value, so spraying can be switched on and off at will by simply adjusting the pressure regulator upstream of the gas heating assembly. In addition, the suction parabola over the 12- to 28-psia operating range determines the melt feed rate when spraying. (Later efforts established a maximum spray rate of 0.5 gram/second of tin under maximum suction conditions. The spray rate decreased for pressures above an 18-psia nozzle entrance pressure as expected from this curve.)

Argon flow rate was recorded as part of the same experiment, and the results are given in Figure 17. As indicated there, flow through the nozzle throat never exceeded 3 scfm and was between 1 and 2 scfm for the operating pressure range that exhibited suction. Because these flow rates are so low, the pressure drops through the gas heater are negligible--less than 0.2 psi per Figure 12. That is, the true gas pressure entering the nozzle must be nearly equal to pressure measured upstream of the gas heater. Since real nozzle entrance pressure is displaced only slightly from measured operating pressure, the plot in Figure 16 can be interpreted as a fundamental spray nozzle characteristic.

Liquid orifice pressure can also be plotted as a function of argon flow rate, as presented in Figure 18. Maximum suction was achieved from 1.0 to 1.2 scfm, and suction ceased completely above 1.7 scfm. Here the nozzle behavior is totally independent of gas heater pressure drops.
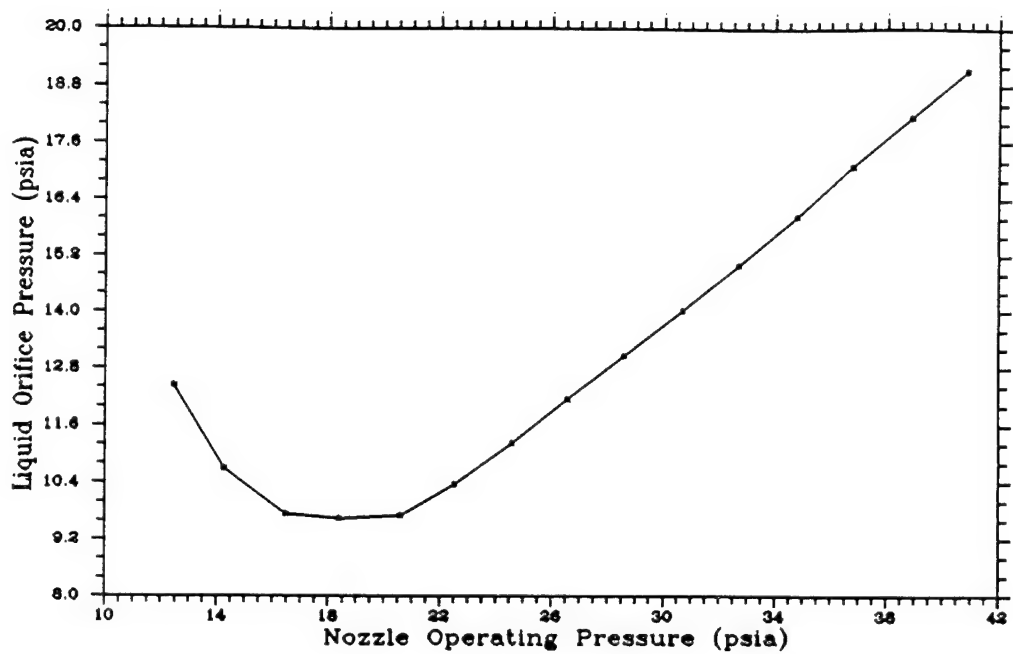
Figure 16.   Nozzle Suction Behavior Measured at Room Temperature.
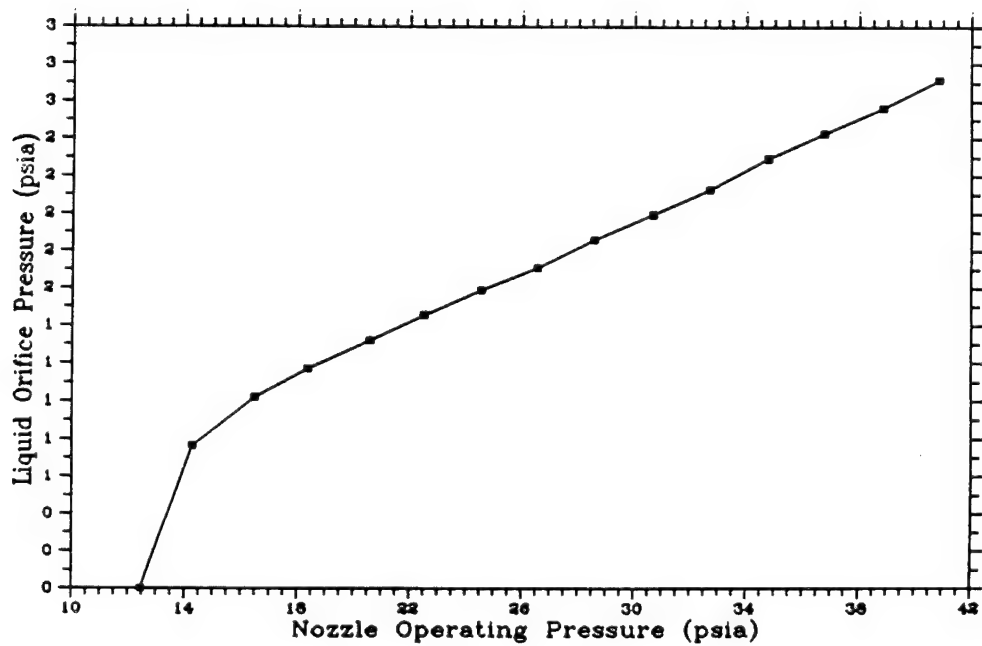
Figure 17.   Flow of Argon Gas through the Spray Nozzle Throat.
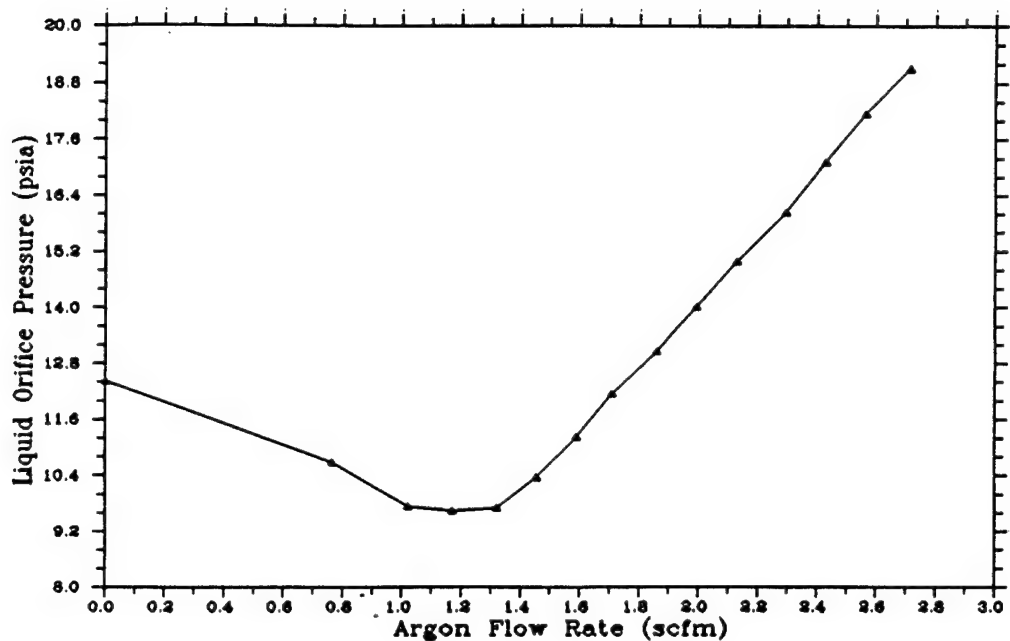
Figure 18.   Gas Flow Influence on Nozzle Suction Performance.
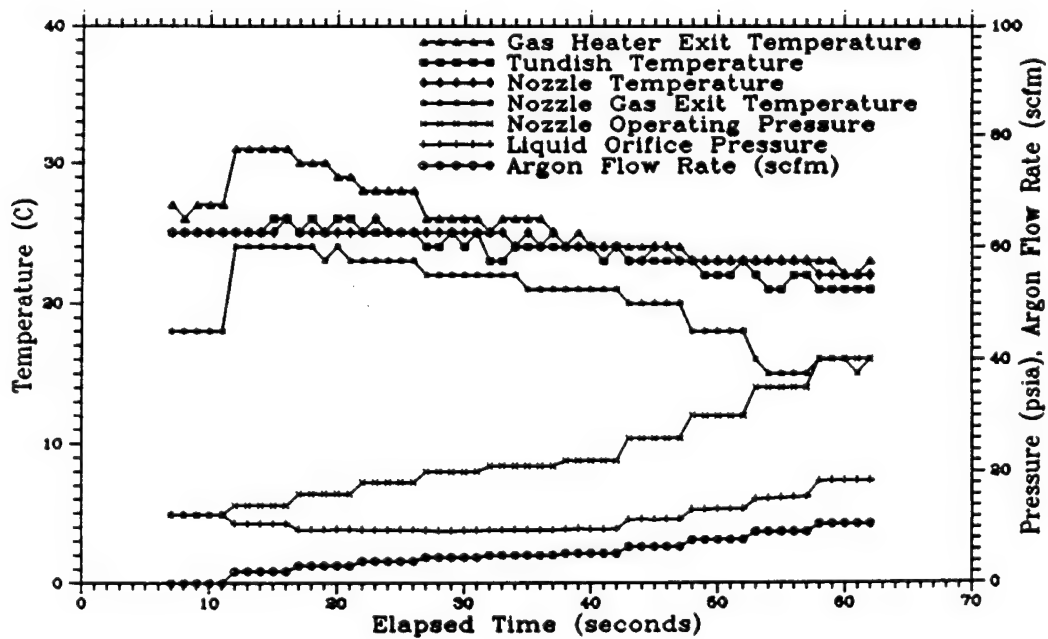
Figure 19.   Room-Temperature Nozzle Behavior with Bypass
             Installed.

As mentioned previously, argon flow rates above 3 scfm through the gas heater are necessary to cool internal thermal sensors that would otherwise intermittently switch off power to the heating coils. However, the room-temperature characterization data just discussed revealed that flows of merely 1 to 2 scfm would pass through the narrow nozzle throat while spraying. At such low flow rates, the gas heater would operate at only a fraction of its capacity--delivering lower gas temperatures for tin nebulization than might be necessary. (See Figure 10.)

This impasse was resolved by installing a low-turbulence tee between the gas heater exit and the nozzle entrance, such that a majority of the heated gas bypassed the nozzle. Specifically, a secondary gas orifice was built for the tee leg with five times the cross-sectional area of the nozzle throat in order to divert five-sixths of the flow. In the process, a Type K TC was inserted into the incoming flow stream to directly monitor gas heater exit temperature. The heated bypass gas was not wasted, but rather routed toward the base metal fixturing for preheating purposes. (More information on base metal preheating is provided later.) However, incorporating a heated gas bypass dictated acquiring new baseline information on the nebulizer as assembled in its final configuration.

Complete characterization results at room temperature are given in Figure 19. Most significantly, the bypass design was verified in that argon flow rates through the gas heater exceeded 3 scfm at nearly all nozzle operating pressures. Presence of the bypass did not interfere with critical suction behavior; in fact, maximum suction increased slightly from 2.8 to 3.0 psi. As expected from Figure 12, the increased flow rates induced larger pressure drops through the gas heater, such that measured operating pressure was no longer close to true nozzle entrance pressure. Consequently, maximum suction was found at an indicated operating pressure of 20 psia, rather than at 18 psia in Figure 16. (Pressure was actually 18 psia at the nozzle entrance in both cases.)

All temperature plots in Figure 19 show small cooling trends, due to expansion of argon gas initially at high compression in a cylinder bottle. But, cooling observed at the nozzle exit is more substantial--reflecting extra gas expansion while moving from the nozzle throat out the exit cone.

30

Having established that the room-temperature performance of the final nebulizer assembly was as desired, the next step in the characterization sequence was to obtain baseline data at operating temperatures. For this purpose the nozzle/tundish assembly was preheated to 400°C, while the gas heater was adjusted to 60 percent power. The recorded results are displayed in Figure 20. Both gas heater and nozzle exit temperatures rose rapidly at first, because the gas heater was turned on (at an extremely low gas flow) immediately before this experiment began. Internal gas heater components and the heat sinks surrounding the gas exit TC thus did not warm up to equilibrium temperatures, which would require several hundred seconds per Figure 10, allowing for extra heat sink effects of the line between the gas heater and the nozzle entrance. Since this entire experiment lasted less than 70 seconds, the peak gas exit temperature achieved (318°C) was nearly 100 degrees less than Figure 10 indicates for a 60 percent power setting.

The only unexpected finding in Figure 20 was the decrease in nozzle gas exit temperature that began above 30-psia operating pressure. It was apparently an artifact of TC placement at the exit plane rather than a fundamental effect, because gas heater exit temperature was still rising and nozzle/tundish temperatures were stable. That is, the most likely explanation was that the flow stream was separating from the exit cone walls at high operating pressures before reaching the exit plane. If so, cool gas outside the nozzle would be drawn in along the walls and would subsequently be entrained into the plume, dropping the average gas temperature at the plume centerline before arrival at the TC position.

To check on this hypothesis, the TC junction was moved inward along the cone centerline until close to the throat to obtain a gas temperature measurement free of any entrainment perturbations. And, the data shown in Figure 21 no longer reveal a decrease in nozzle gas exit temperature at high operating pressures. In fact, plotted values are steadily increasing through the end of the data set, in agreement with the continual rise observed in gas heater exit temperature. Both gas temperature plots in Figure 21 begin at higher values than in Figure 20, because Figure 21 data were gathered shortly after the Figure 20 experiment, without allowing heated components to cool down completely.

31
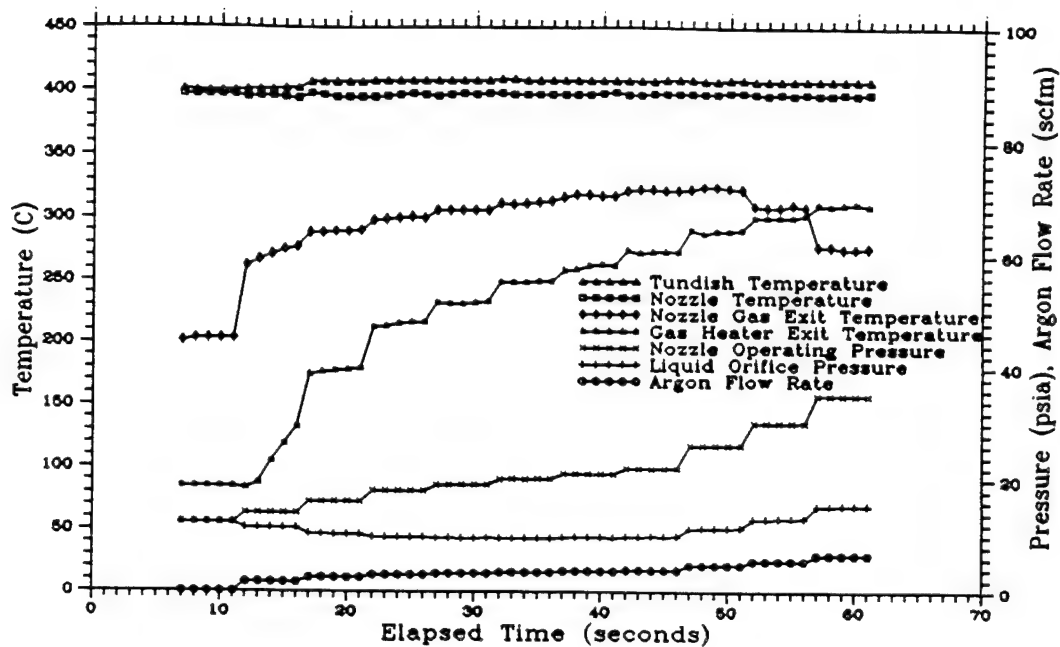
Figure 20. Operating-Temperature Characterization Data with Nozzle Gas Thermocouple near Exit Plane.
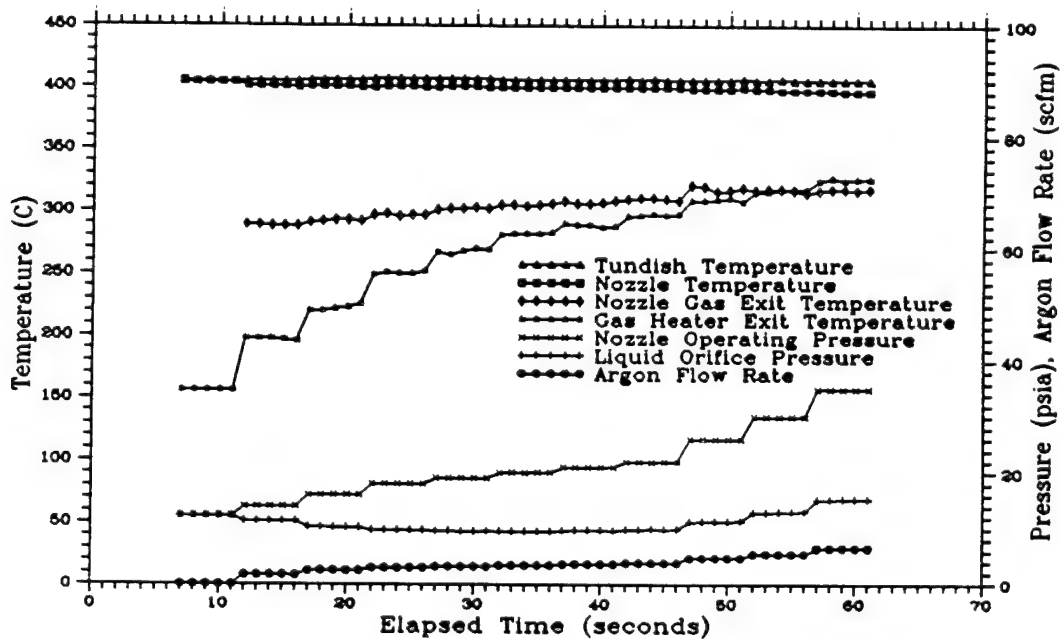
Figure 21. Operating-Temperature Characterization Results with Nozzle Gas Thermocouple near Throat.

The preceding elevated-temperature studies covered situations where the gas heater was set at 60 percent power and turned on shortly before data were recorded. Both the gas heater and the heat sinks downstream were still warming up rapidly when the nozzle/tundish characterizations began. As a consequence, precise predictions could not be made from these data on what gas temperatures would exist in the nozzle under steady-state conditions with longer warmup periods. Furthermore, a possibility existed that higher gas heater power settings might be necessary to adequately preheat base metal specimens for high-quality coatings. More baseline testing was thus necessary to understand fundamental nozzle behavior before introducing molten metal and adding another heat source.

To finish the nebulizer characterization effort, the nozzle/tundish heater was preheated to 400°C. Meanwhile, the gas heater was set at 60 percent power and allowed to warm up for eight minutes at a nozzle operating pressure of 16 psia and a low argon flow rate of 1.5 scfm. At this point, data were recorded on gas heater exit temperature, nozzle gas exit temperature, and argon flow rate, while operating pressures of 18, 20, and 22 psia were each maintained for over seven minutes. Then the exercise was repeated after equilibrating the gas heater at 100 percent power. An overlay plot of the two data sets is presented in Figure 22.

Several aspects of Figure 22 are worthy of commment. First of all, comparing the exit temperature data at 60 percent power with those in Figure 21 reveals that allowing the gas heater to warm up increases gas temperature leaving both the gas heater and nozzle by approximately 100°C. Running the gas heater at 60 percent power (after warmup) is a very stable mode, because the gas heater exit temperature is consistently close to 400°C; with the nozzle held at the same temperature, gas also leaves the nozzle at 400°C. Furthermore, as discussed later, molten tin was generally poured into the tundish after heating in the furnace to 400°C, so virtually no thermal gradients would exist under this set of circumstances. By comparison, operating the gas heater at 100 percent power would add heat to the molten tin droplets during the nebulization sequence, if so desired. Lastly, gas flow rates are lower at 100 percent heater power than at 60 percent for equivalent operating pressures, in response to the larger pressure drops indicated in Figure 12.
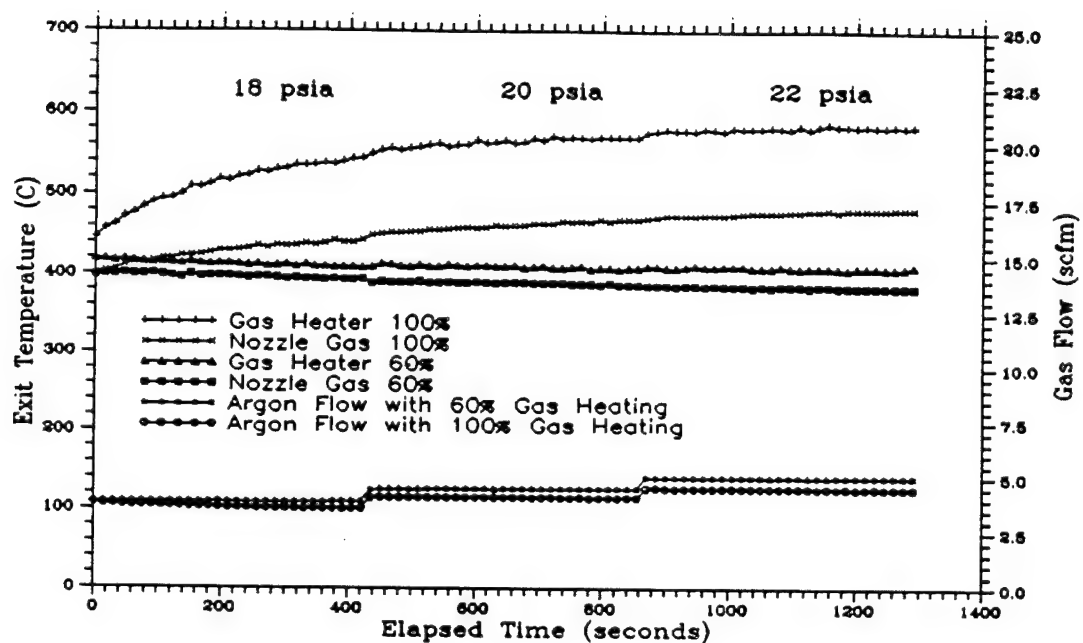
Figure 22. Characterization Data at Spraying Pressures for a
            400°C Nozzle with Gas Heater Equilibrated at 60 and
            100 Percent Powers.

34

F. BASE METAL FIXTURING

Base metal coupons must be properly positioned in front of the spray plume to control many coating characteristics. Nebulizer-to-base metal distance governs the extent of mixing between hot gas leaving the nozzle and cool chamber gas, the amount of droplet deceleration during the mixing process, and the plume width upon reaching the base metal according to the plume expansion angle. Consequently, this distance influences droplet temperatures upon impact, heat flux available to support consolidation, and convective gas cooling after deposition. Coating thickness is also determined in part by a coupon's speed of translation across the spray plume, in conjuction with nebulizer operating parameters.

Two general approaches on base metal fixturing were adopted during the course of Phase I to satisfy the position and speed control requirements. The first design is shown in Figure 23, where the low carbon steel sheet (0.010 inch thick) was coated in a cylindrical sleeve configuration. Each sleeve was first formed on a cylindrical mold, cut to size, and then spot-welded into the final shape. Before removing the mold, the outer sleeve surface was prepared for coating by grit-blasting, whereupon the sleeve was stored under a protective covering. Shortly before beginning a coating experiment, a sleeve would be slid over an aluminum drum with the same diameter (4.2 inches) but only half the length of the original mold. This drum was intended to maintain the sleeve shape and to allow the 8-inch long sleeve to be gripped by a three-jaw chuck that, in turn, was coupled to a variable-speed drive motor.

As displayed in Figure 23, coatings were sprayed on only the outer half of each sleeve--the 4-inch part not supported by the aluminum drum. Direct drum contact would have imposed a prohibitively large heat sink for purposes of preheating the base metal. Furthermore, while preheating or coating, the absence of the drum in this region permitted base metal temperature to be monitored from the back side--directly underneath the impact area of the nozzle plume (which aided in preheating) and close to the main base metal preheater. The main preheater used the nozzle bypass flow--five-sixths of the gas heater assembly output. At peak gas heater outlet temperatures, base metal sleeves could be raised to 150°C.

35
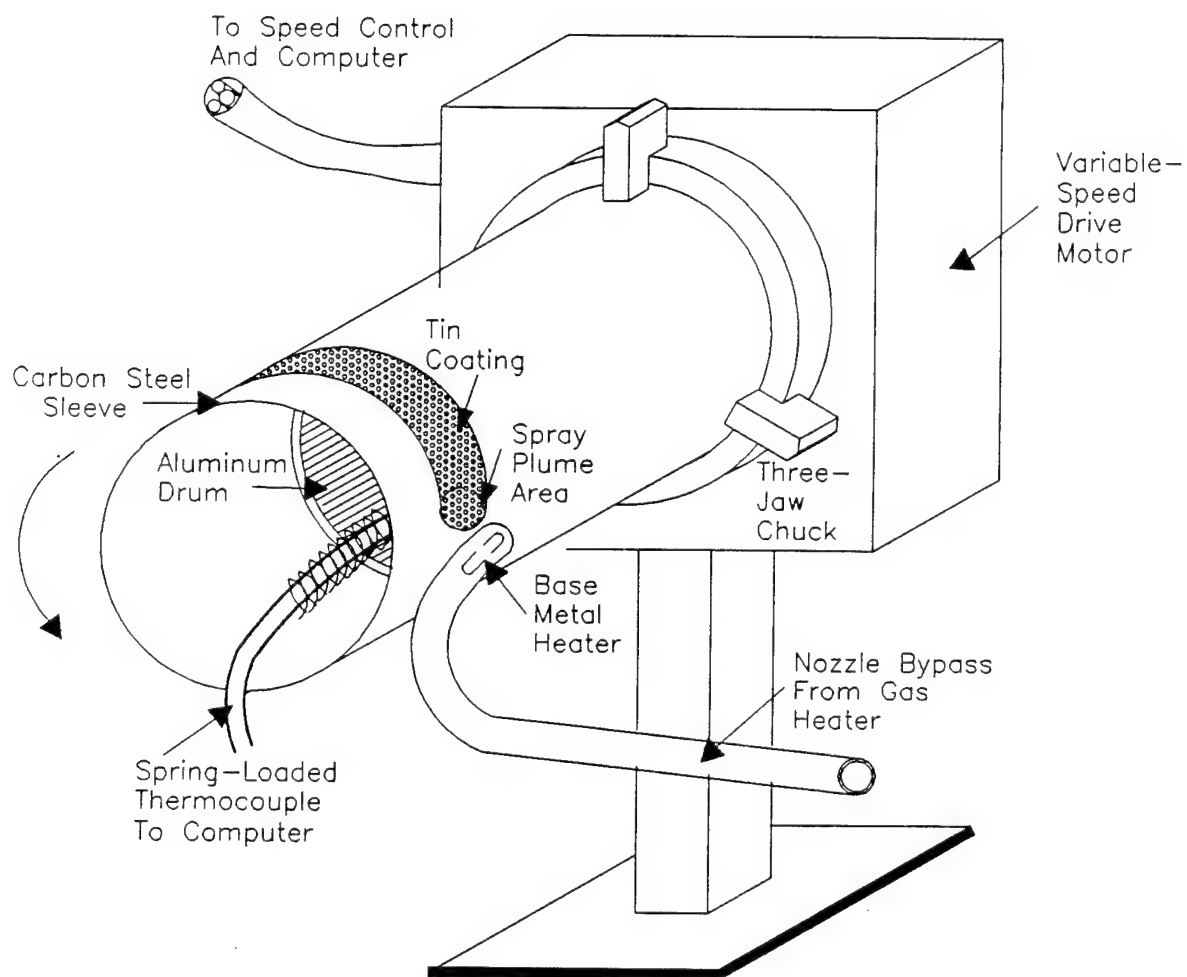
Figure 23.   Fixture for Rotating Base Metal Sleeves to Form
Tin Coatings on Low Carbon Steel.

36

Base metal temperature was measured by a spring-loaded Type K TC. This signal was sent directly to the data acquisition computer. Drive motor speed was controlled remotely by a potentiometer according to percentage of maximum voltage, which was also sent to the computer. A calibration curve had to be used in order to convert this percentage into revolutions per minute. Rotational speed then had to be converted into actual base metal speed according to the 13.3-inch sleeve circumference.

The first base metal fixture was adequate for spraying the first two sets of tin-coated specimens, as later described. However, a number of practical difficulties gradually emerged. The aluminum drum was not able to completely prevent sleeve eccentricity where coatings were deposited. Both the nozzle-to-base metal distance and the preheater-to-base metal distance continuously oscillated with peak amplitudes of up to several millimeters. The heavy base metal fixture had to be moved manually to set these distances before a spraying experiment, which proved to be rather awkward and imprecise. The main preheater was rigidly attached to the gas heating assembly, as was the nozzle/tundish assembly. Consequently, although the nozzle-to-base metal spacing could be increased at will, the base metal could not be moved close to the nozzle exit plane without first shortening the preheater tube length. Lastly, the cumbersome two-step conversion from the potentiometer setting to base metal translation speed made it difficult to display speeds dynamically on the computer screen.

For the above reasons, a radically different design was implemented for spraying the last set of coating specimens. The new fixture is illustrated in Figure 24. Here low carbon steel sheet (still 0.010 inch thick) was cut into strips--16 inches long by 2 inches wide--before grit-blasting. After surface preparation and shortly before coating, each strip was inserted between the guide rails and clamped at the top. As shown, the nozzle-to-base metal distance was adjusted remotely, and the base metal could be moved within an inch of the nozzle exit plane. When spray coating was in progress, the base metal was elevated by a cable connected to a light-weight variable-speed motor. A shaft encoder was attached to the remotely controlled motor, which enabled electronic rotation signals to be conveniently converted into translational speed on the data acquisition system.

37
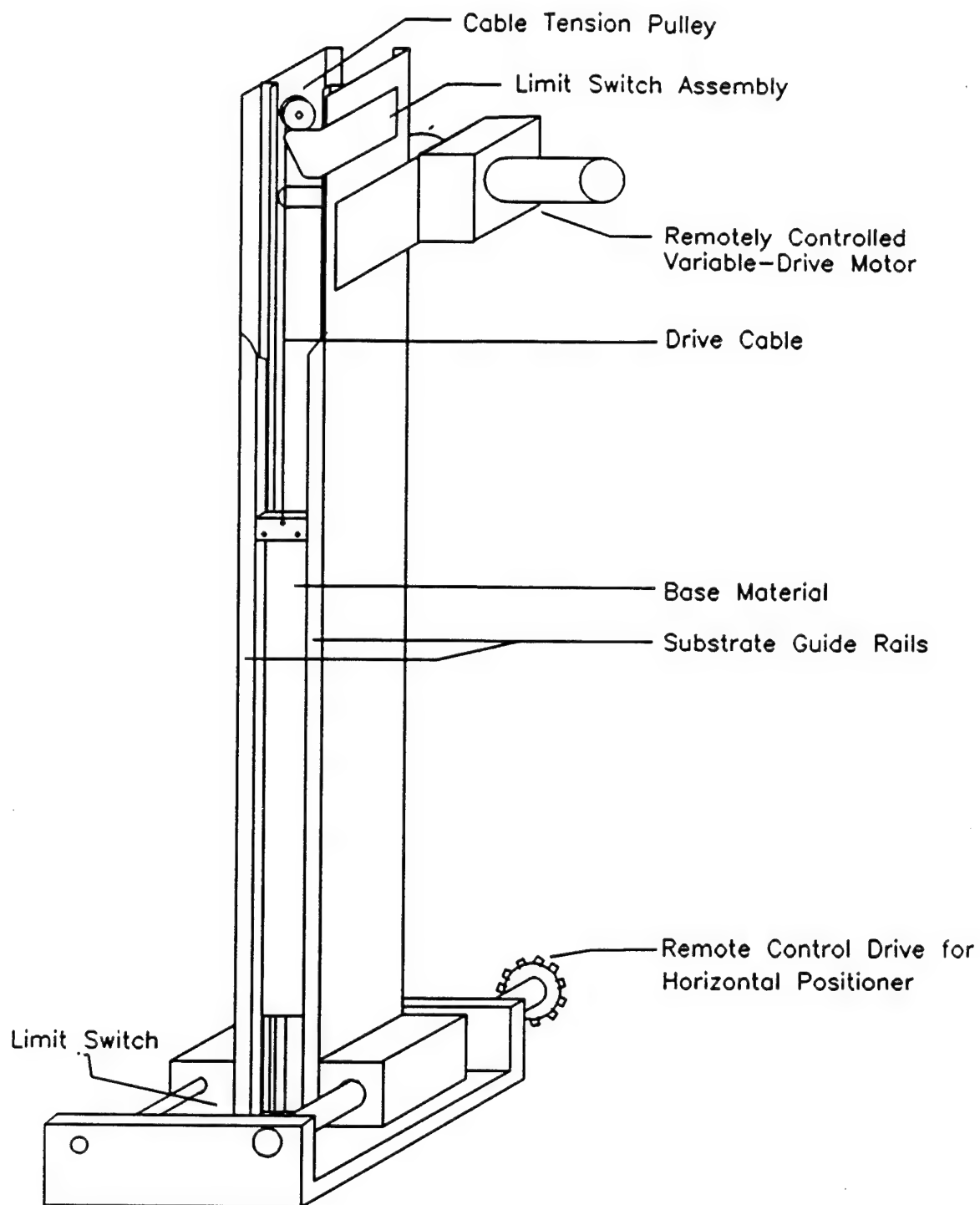
Figure 24.   Fixture for Elevating Steel Strips for Increased
Control of the Tin-Coating Process.

Two important features are not included in Figure 24. A spring-loaded Type K TC was attached to a guide rail to measure base metal temperature immediately underneath the plume impact area, on the surface facing the nozzle. The front base metal surface was monitored with the new fixture design, because hot gas from the main preheater was now blown against the back surface--again below the coating deposition region, opposite the TC position. Incoming tin droplets thus impacted a warm surface as the steel strip was raised by the cable assembly, while TC readings were not biased upward by direct exposure to the preheater flow.

The new fixture no longer used the heated flow of nozzle bypass gas, which was simply routed toward the chamber exhaust. Instead, a high-power gun-type blower was mounted on the guide rails, so the preheater flow consisted primarily of hot nitrogen--the chamber purge gas. Since the preheater now moved with the fixture, the nozzle-to-base metal distance was no longer constrained by interfering with the rigid nozzle bypass tube. Also, the preheater-to-base metal distance could be preselected and held constant, without restrictions imposed by the nozzle-to-base metal separation and without any perturbations from drum eccentricity.

The improved design offered several additional advantages. Preheating power could now be adjusted independently of the main argon heating assembly, whose operating conditions were largely dictated by nozzle spray parameters. The guide rails fixed the nozzle-to-base metal distance, so none of the earlier effects from drum eccentricity were encountered. However, centerline bowing of steel strips by plume pressure plume might have induced a comparable problem, if not for the counterbalancing force of the preheater flow stream. Directing the two flows against opposite sides of the base metal further eliminated any deflection of the nozzle plume, which occurred to some extent on the first fixture.

The ability to use flat base metal strips was by itself quite helpful. No forming and spot-welding were required, unlike the cylindrical sleeves. Post-coating cutting and mounting of strip samples were relatively simple, because the strips were already flat. By comparison, preparing coated sections of cylindrical drums for subsequent coating quality tests induced a risk of sample damage.

39

For reasons discussed later, the best overall coating quality results were obtained from certain cylindrical sleeve samples. Phase I feasibilty study objectives were thus achieved before the improved base metal fixture was implemented, although this fact was not demonstrated until subsequent performance tests on coating samples. However, the superiority of the sleeve samples reflected the spraying parameters used, rather than the rotating fixture design, and the benefits of the second fixture cannot be diminished. These design advantages will be fully realized in Phase II, when process control becomes more critical. The improvements in base metal fixturing thus represent work that could not have been avoided.

Another consideration that will receive increasing attention during Phase II is maintaining cleanliness of the grit-blasted base metal surfaces before coatings are deposited. To this end, preheating the base metal from the back side will become even more valuable, because chemical alterations on surfaces to be coated will be prevented from any reactive gas contaminants in the hot preheater flow stream.

G. SPRAY-SYSTEM ISOLATION CHAMBER

Spray forming had to be conducted in an inert, enclosed environment:

o   to protect laboratory personnel from dangerous situations (molten metal, exposed electrical wiring, inhaling particulates, etc.);

o   to develop filtration techniques for chamber exhaust streams that will prevent emissions of any hazardous materials out laboratory stacks during Phase I and post-Phase I efforts; and

o   to limit in-flight chemical reactions between metal droplets and gaseous contaminants that might alter deposit properties.

For similar considerations, controlled environments would also be likely in eventual commercial applications of spray-coating technology. In large-scale use, extra economic benefit could be derived from recycling both nebulizing gas and any unconsolidated metal powder (overspray).

40

The spray-system isolation chamber in which Phase I coatings were deposited is displayed in Figures 25 and 26--showing the sides containing the viewing window and the instrument access door, respectively. To reduce project costs, this chamber was constructed from a surplus glove box, where the original Plexiglas windows provide adequate protection for spraying low-melting-point metals. A large door allows convenient access to the melt furnace, nebulizer assembly, and base metal fixturing. Ports have been fitted with flanges holding instrument leads, electrical power feed-throughs, sampling penetrations, injection tubes for inert gases, and manipulation levers for pouring the furnace. A particulate filter and discharge pump are connected to the chamber exhaust port.

Plant-grade nitrogen gas (vented off a liquid nitrogen tank) was used to purge the chamber of oxygen. In order to verify the adequacy of this method, samples of the chamber atmosphere were extracted at 15-minute intervals for a two-hour period. Each sample was later analyzed for oxygen content by gas chromatography with a thermal conductivity sensor. An example of the gas analysis is provided in Figure 27 for a sample taken immediately before purging began. This exercise established that the chamber oxygen concentration was reduced within 15 minutes from 21 percent to less than 2 percent (the approximate background level for the syringe method used to extract samples). Later samples stayed below this level, which indicated a thorough nitrogen flush of the chamber with no trapped air spaces of significance. These results were sufficient for Phase I purposes, but more accurate methods will be employed during Phase II, when precise control of reactive gases likely will be of greater importance.

Once purging capabilities were verified, tin could be sprayed safely with the nebulizer for the first time in order to perform a particulate safety analysis on the spray chamber. This was important for confirming that the chamber exhaust stream was adequately filtered, such that no significant amount of tin particles would escape through the laboratory stack. In addition, concentrations entrained in the chamber atmosphere had to be measured to determine that no explosive hazards would exist in the event of a major air leak. In the process, valuable information was also obtained on melt-to-coating conversion efficiency--ie. how much of the metal sprayed was successfully consolidated into a dense deposit.

41
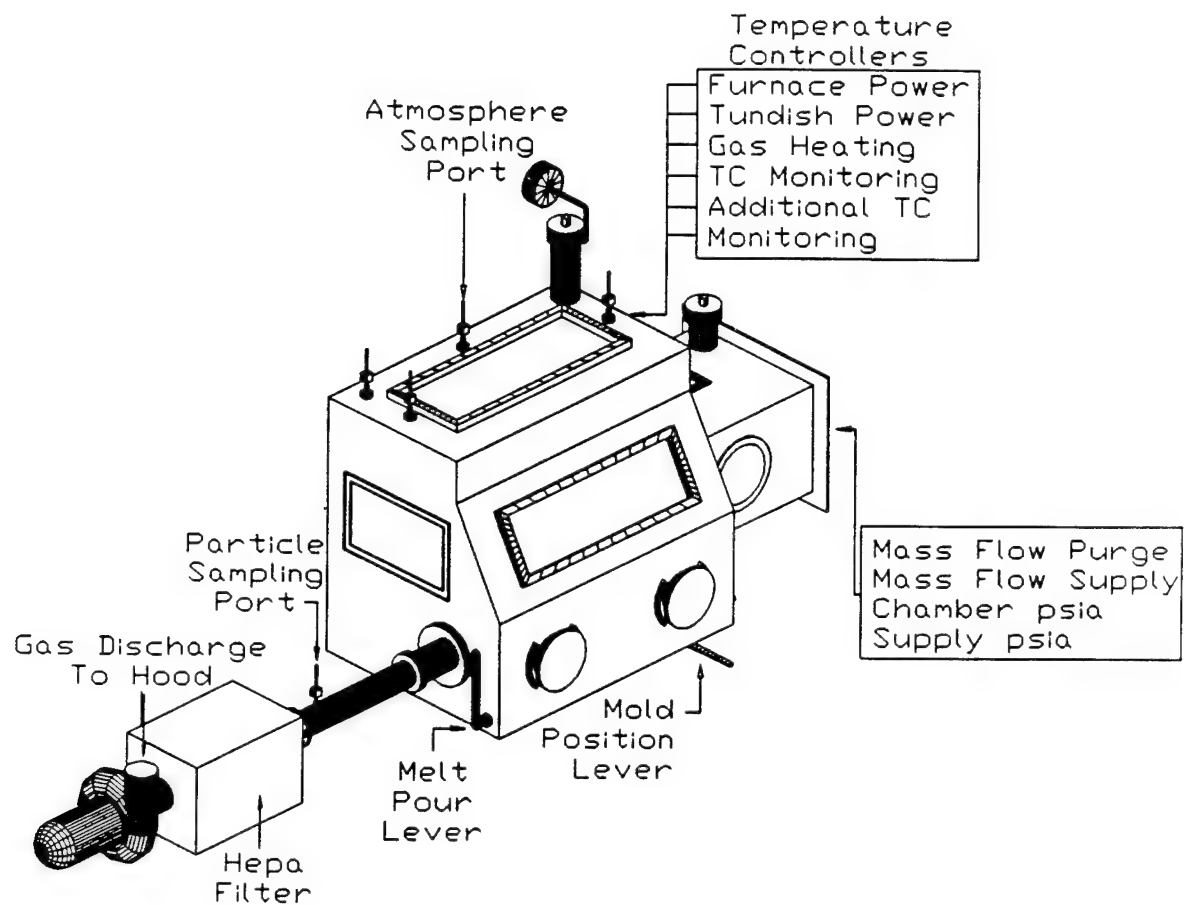
Figure 25.   Viewing Side of the Spray Chamber.

Temperature
Controllers

Furnace Power
Tundish Power
Gas Heating
TC Monitoring
Additional TC
Monitoring

Atmosphere
Sampling
Port

Particle
Sampling
Port

Gas
Discharge
To Hood

Access
Door

Mass Flow Purge
Mass Flow Supply
Chamber psia
Supply psia
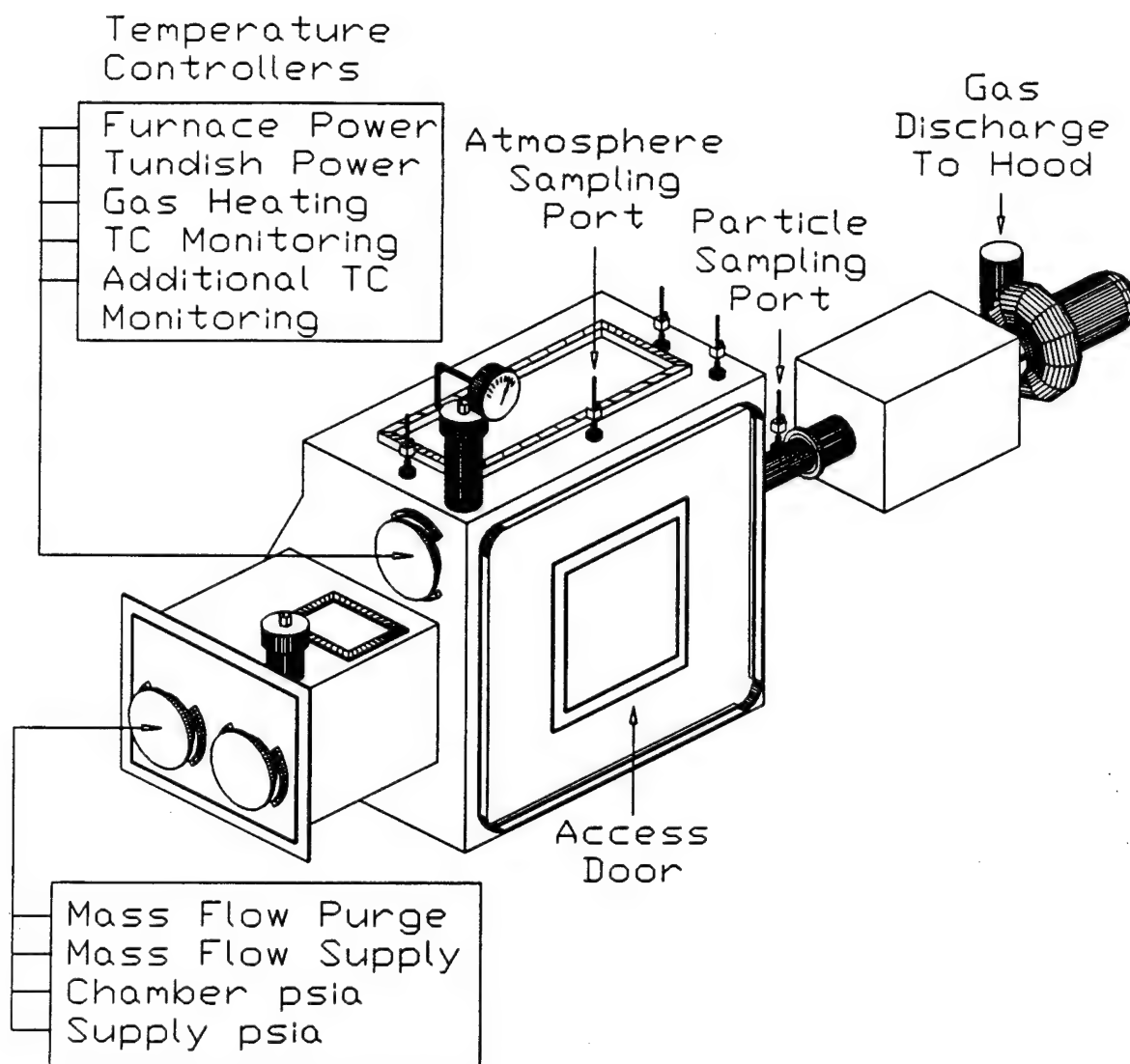
Figure 26.   Access Side of the Spray Chamber.

43

All measurements of particle size and concentration were performed by LAS 250X laser aerosol spectrometers (Particle Measurement Systems, Inc.). Two of these spectrometers are shown in Figure 1, with sampling lines connected to the chamber exhaust duct immediately before and after the high-volume ultrafine particle filter. Both spectrometers contain a small pump that extracts 0.01 of the exhaust volume for continuous analysis, where the pump throughputs and sample line diameters were carefully set to extract gas at the same velocity as it was flowing through the main duct. This "isokinetic" method assured that all samples were representative.

Each spectrometer segregated incoming particles into 16 size ranges according to scattered light intensity, where the size ranges must be calibrated periodically with appropriate aerosol standards. Particles in all 16 channels were counted for a preselected interval--typically 30 seconds to obtain accurate statistics--at which time the tallies were sent to a computer. Data were later reduced on Lotus worksheets.

Particle data were obtained under four conditions to properly assess chamber and filter performance: (1) at purge initiation shortly after sealing up the chamber, while the furnace was melting tin and the other components were being raised to operating temperatures; (2) while spraying tin at a low nozzle operating pressure to induce maximum melt aspiration and maximum droplet output; (3) while spraying tin at a high pressure to reduce aspiration and form a high-velocity plume of relatively cool droplets that do not consolidate as well (worst case); and (4) seven minutes after spraying was stopped, while continuing chamber purging. These exercises were conducted by spraying tin against flat substrates in conjunction with other nebulizer performance studies (plume widths, melt aspiration rates, etc.). The other basic experiments are discussed in the next section, where more detail on spray-system parameters is presented.

Spectrometer results from pre-filtering samples are given in one form in Figure 28. The cumulative mass distributions were derived by first converting diameters to spherical volumes, then multiplying by particle counts to yield total particle volume in each size range, converting each volume to mass (using the density of tin), dividing throughout by the grand mass total, and progressively summing normalized mass percentages.

ANAL 1 DET 2 METH 6 6 FILE 266

RUN 4

SENSITIVITIES 150 4
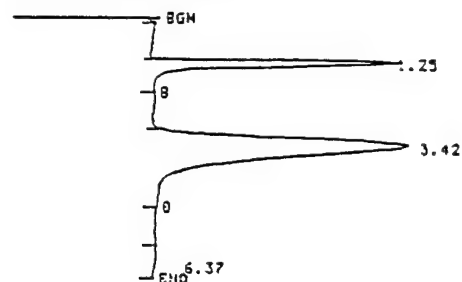
ANAL 1 DET 2 METH 6 6 FILE 266

RUN 4 7 : 44.9 2 / 24 / 89

SENSITIVITIES 150 4

TIME	AREA	BC	RRT	RF	C	NAME
1.25	0.4895		0.125	1.000	20.3339	!
3.42	1.9442		0.342	1.000	78.5064	!
6.37	0.0153		0.637	1.000	0.6547	!

Figure 27. Example of Chamber Oxygen Analyses.
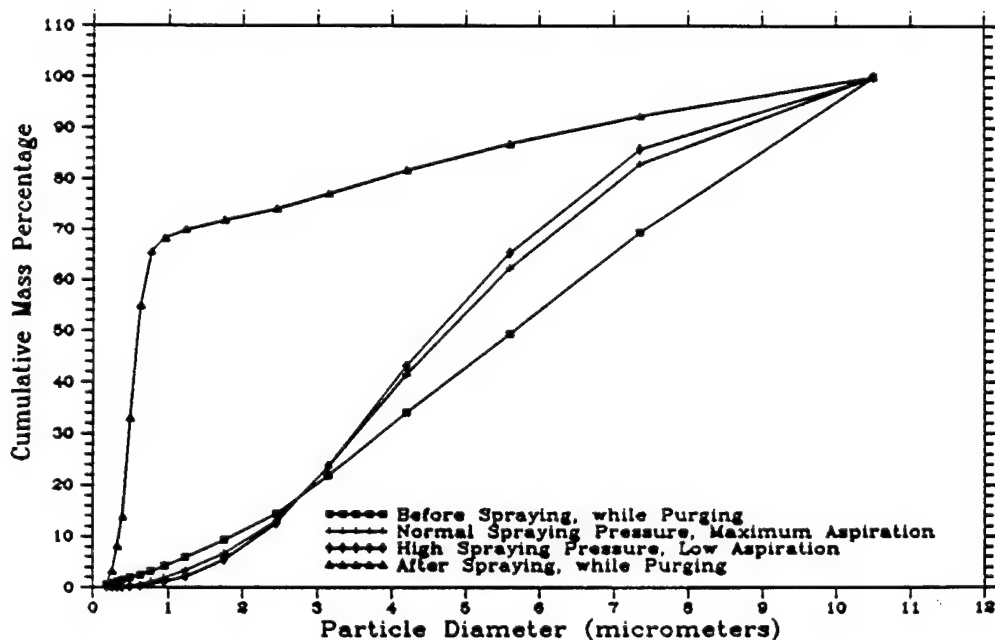
Figure 28. Cumulative Mass Distribution for Sixteen Particle Sizes in the Chamber Exhaust Stream at Various Sampling Conditions.

45

Comprehension of Figure 28 is aided by considering specific cases. The chamber's mass distribution gathered before spraying at the start of purging is almost a straight line. Here the aggregate particle mass is spread uniformly across the size ranges, which is characteristic of dust and pollen in moving air. On this plot the cumulative 50 percent value occurs at 5.6 micrometers--the mass median diameter--which evenly divides the total mass into particles less than or greater than this diameter.

By comparison, the mass distribution obtained well after spraying had ceased is much different. Nearly 70 percent of the mass is carried by submicron particles, primarily representing the clean nitrogen purging flow. Dust and other airborne contaminants inside the chamber when it was sealed have been swept into the filter, along with any fine tin solids.

Airborne contaminants had also been largely removed by purging when tin spraying began. Consequently, the mass distributions taken while spraying are primarily due to unconsolidated tin droplets that became entrained in the chamber exhaust. Occasionally, metal droplets will solidify completely in flight and recoil away from a surface. In most cases, however, such overspray occurs when incoming droplets impact small molten areas on a deposit surface, causing splashes. Most overspray mass here is between 3 and 8 micrometers, whereas Reference 1 established that INEL nebulizers spray nearly all tin droplets from 8 to 12 micrometers in size, with a mass median of 11 micrometers. Moreover, recoiling would be expected more often at higher spraying pressures, but no size differences are found in Figure 28 between the high- and low-spraying-pressure plots.

The same prefiltering data set is displayed in a more conventional histogram fashion in Figure 29, instead of as a cumulative distribution. Particle counts in each size range were converted to mass, as before. However, rather than normalizing by the grand mass total, here the mass in each channel was simply divided by the 30-second measurement interval. Each of the 16 values were then multiplied by 100 to extrapolate the particle masses found in the sampling line to those flowing in the chamber exhaust stream. At equilibrium conditions, the assumption can be made that particulate mass concentrations swept into the exhaust flow are identical to those that would be measured within the chamber itself.

46

Mass entrainment rates in Figure 29 taken before and after spraying reveal very little particulate activity in the chamber. That is, the chamber was quite clean in both cases, despite the indications of dust movement in Figure 28 at purge initiation. By contrast, chamber activity became significant when tin was sprayed at a low pressure for maximum aspiration, and the measured particle mass rose appreciably when spraying pressure was increased. Most mass was found in the 3- to 8-micrometer range under both conditions, as deduced from Figure 28. But, the larger entrainment rate at high pressure suggests that "splashing" of incident droplets occurred more often or more violently at high impact velocities.

Spraying results in Figure 29 can be summed over all 16 size ranges to yield total mass entrainment rates--88 and 310 micrograms/second for low- and high-pressure spraying, respectively. These values can be compared to measured tin-spraying rates at the two operating conditions, which are 0.50 and 0.17 gram/second, per studies described in the next section. For normal spraying situations, measured overspray is less than 0.02 percent, rising to only 0.18 percent for the worst-case, high-operating-pressure condition. Thus virtually all of the metal sprayed was consolidated into a deposit. These calculations do not incorporate any unusually large, unconsolidated particles that were too heavy to be carried by the exhaust flow. No such particles were observed on the chamber floor afterward, but they could have been collected and remelted, had any occurred.

A total tin entrainment rate can also be converted into a volumetric mass concentration by considering the 0.005-cubic meter/second (10.6-scfm) flow of gas through the chamber, which includes both the nitrogen purge and the argon nebulizing gas. This yields volumetric mass concentrations of 18 and 62 milligrams/cubic meter for low and high operating pressures, respectively. Such concentrations would pose absolutely no hazard of explosion if the chamber were to be suddenly filled with air. According to Reference 3, tin dust is considered moderately explosive, but only at concentrations from 100 to 500 grams/cubic meter. A thousand-fold safety margin would even exist for highly explosive metals powders (Al, Mg, Zr) that become dangerous at concentrations of 20 to 50 grams/cubic meter. These findings will likely extend to large-scale applications, since the ratio of metal spraying rate to chamber gas flow will not change by much.

47
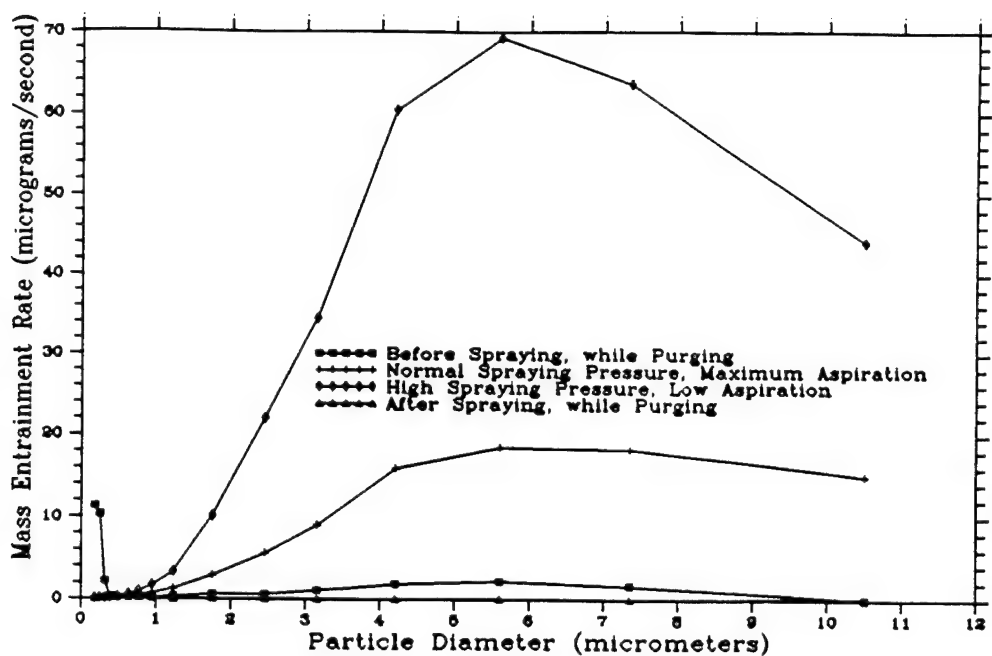
Figure 29. Rate of Particulate Mass Entrainment in Chamber
Exhaust Stream for Sixteen Particle Sizes at Various
Sampling Conditions.
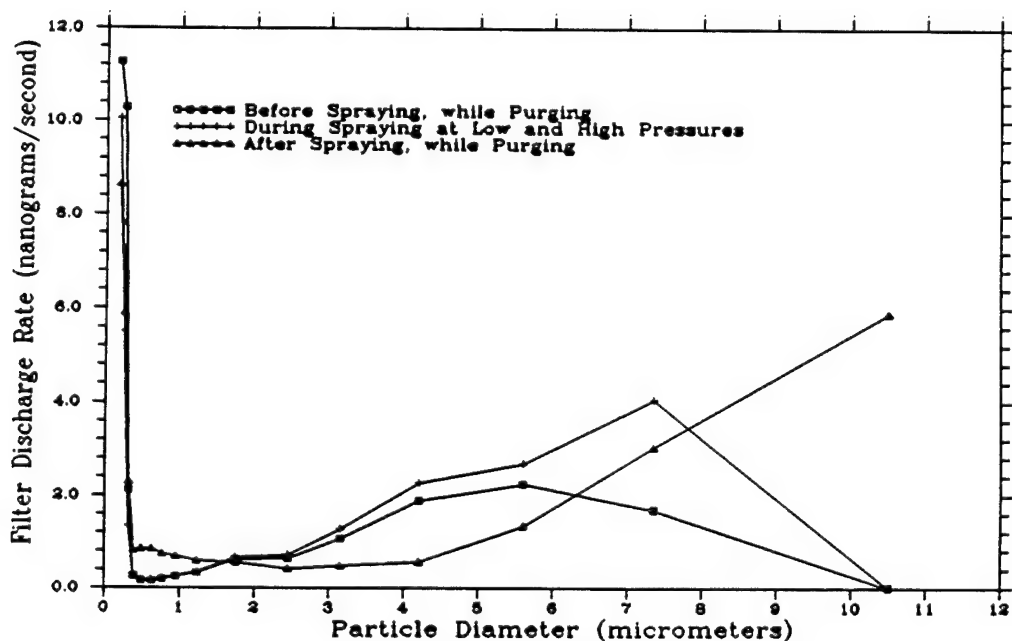
Figure 30. Mass Discharge Rate after Filtering as a Function of
Particle Size before, during, and after Spraying Tin.

48

Particle data sampled after the filter are displayed as a histogram in Figure 30. Note the scale change to nanograms/second, by comparison to micrograms/second in Figure 29. Only the very smallest of particles were able to pass through the filter in measurably significant quantities. It is doubtful that these ultrafine particulates are tin, because discharge rates are equivalent before, during, and after spraying. Similarly, a few tin particles between 3 and 8 micrometers may have escaped through the laboratory stack, but this is by no means certain, because the differences among the three sampling conditions are not statistically meaningful.

When masses from all sixteen channels are summed, the aggregate mass discharge rates calculated before, during, and after spraying are 33, 30, and 34 nanograms/second, respectively. Again, there is no indication that any tin was passed by the filter. Nevertheless, the very conservative assumption will be made that all 30 nanograms/second of particle mass detected after the filter while spraying represent nebulized tin.

This filter discharge rate can be converted into a volumetric mass concentration by dividing by 0.005 cubic meter/second--the total gas flow rate through the chamber, yielding 6 micrograms/cubic meter. Without taking credit for dilution after emerging from the stack, this value is 333 times less than the Occupational Safety and Health Administration's Permissible Exposure Limit for tin dust (2 milligrams/cubic meter, per Reference 3). That is, the filtered stack exhaust could be breathed safely and indefinitely, were it not for the lack of oxygen. Furthermore, such very clean gas could be recycled in large-scale use, if the purging and nebulizing flows both consisted of relatively valuable argon.

Since tin dust is not considered particularly toxic, the conservative 0.006-milligram/cubic meter discharge estimate should also be compared to OSHA PELs for other metals. Chromium, copper, and nickel are regulated at 1 milligram/cubic meter, while the continuous exposure limit for iron and aluminum is 10 milligrams/cubic meter. Lead is more tightly controlled at 0.050 milligram/cubic meter, but ample margin exists for it without taking credit for dilution after leaving the stack. Clearly, spray coating must be regarded as an environmentally benign process, when performed in a sealed enclosure and when the exhaust stream is properly filtered.

EXPERIMENTAL COATING RESULTS

A. INTRODUCTION

The task breakdown outlined in Section I enumerated an intended plan for the Phase I feasibility study, which can be summarized as follows. Once the spray-system components had been designed, tested, and assembled, an initial set of tin-coated steel specimens were to be produced over very wide ranges of operating parameters. As envisioned, this first set would cover wide thin coatings to narrow thick coatings and from cool to hot deposition temperatures. Samples representing this broad test matrix were then to be evaluated for several aspects of coating quality. Based upon preliminary evaluation results, a secondary set of specimens were to be coated under refined ranges of conditions most likely to yield high-quality coatings. Finally, coating property evaluations on samples from the second specimen set would identify near-optimal process parameters.

The intended task sequence relied upon several key assumptions. In particular, it presumed that all major components of the original spray-coating system would function as desired without modification. However, although most components performed very well without alterations, numerous improvements were made to the base metal fixture and preheater over the course of Phase I. Thus the experimental apparatus acquired sufficient versatility to handle all possible conditions only near the project's end.

Similarly, the initial task breakdown assumed that tests of coating quality could be achieved readily and that feedback would be promptly available to guide later experiments. In practice, parallel efforts had to be commissioned on metallographic studies and adhesion measurements. As described later, developing grinding and polishing techniques for metallographic samples that did not obscure interfaces or smear much grit into the soft tin layer posed a major challenge. Also, numerous epoxy formulations had to be tested to find a compound strong enough to permit adhesion tests. Accordingly, secondary specimens were coated without firm performance results on the first set to support timely project completion.

It must be recognized that these problems were overcome and that the Phase I feasibility study was not compromised. Indeed, tin coatings of surprisingly high quality were produced, almost from the beginning. The overall impact of the aforementioned difficulties was to rearrange the original test matrix, spreading it out over the whole project duration. The first sprayed coatings tended to be wide with relatively cool droplet deposition temperatures due to a large nozzle-to-base metal distance. For the next set, the base metal was moved closer to yield narrower coatings with a range of deposition temperatures. The third set was generally aimed at spraying thin molten coatings with high base metal temperatures. All three sets were subjected to thorough coating quality evaluations. Yet, because specimen samples could not be tested promptly, performance results could not be fed back iteratively into the experimental sequence.

For this reason, specific experimental results will be presented below in a topical format, instead of in an iterative fashion. Data recorded on-line during the various experiments will be discussed first in order to explain exactly how each effort was conducted. Bend test results will be described next, followed by adhesion measurement information. Finally, metallographic examinations of coating quality will be assessed.

B. EXPERIMENTAL SEQUENCE AND CONDUCT

1. Preliminary Tin-Spraying Trials

Before attempting actual coatings, basic nebulizer performance had to be studied while spraying tin. One effort was confirming that spraying could be governed by changes in operating pressure. After warming the nozzle to 400 °C and flowing hot argon through the nozzle at 32 psia, a 100-gram (four-ounce) crucible charge of 400°C tin was poured into the tundish. Gas bubbles emerged at the melt surface, indicating that the nozzle throat pressure exceeded the 12.4-psia chamber pressure. Reducing it to 30 psia nearly stopped the bubbling--balancing pressure across the liquid orifice, as predicted by Figure 21. Lowering pressure further created suction; molten tin was aspirated into the throat and sprayed onto a nearby target. The mist of droplets was too fine to see directly.

51

The next step was measuring the nebulizer's metal mass output as a function of operating pressure. Previously weighed coupons were attached to a wand that was inserted through a chamber port. Each coupon was held in front of the nozzle for 30 seconds while nozzle operating pressure was sequentially held at 20, 22, 24, and 26 psia, creating respective suctions of 3.0, 2.8, 2.4, and 1.0 psi. Corresponding metal spraying rates were 0.50, 0.47, 0.40, and 0.17 gram/second, in good agreement with the amount of aspiration expected from measured suction. Metal-spraying rates were not measured at pressures below 20 psia (maximum suction) because of the parabolic suction symmetry in Figures 16 and 21. In addition, as mentioned earlier, the low flow rates at lower pressures tended to cause inefficient gas heater use, and relatively high output temperatures were felt to be necessary for preheating base metal specimens.

Similar exercises with coupon targets established a coarse relationship between deposit width and nozzle-to-coupon distance. Deposit widths of 0.4, 0.7, and 1.1 inches were measured at 1, 2, and 3 inches from the exit plane. Allowing another inch from the nozzle throat to the exit, the spray plume was thus found to expand at approximately 10 degrees (the exit cone angle) when the width was measured close to the exit plane. Some additional divergence of the flow stream was observed with increasing separation, due to plume shearing against the stationary chamber gas and mixing-induced plume broadening. At 2 inches from the exit plane, the apparent plume expansion angle was nearly 12 degrees, increasing to almost 16 degrees with another inch of distance.

The most realistic preparatory tests were then conducted. A low carbon steel sheet (0.010 inch thick) was cut to size, wrapped around a mold, and spot-welded into a cylindrical sleeve for the rotating base metal fixture. (See Figure 23.) This sleeve was identical to those coated later, except that the outer surface was not grit-blasted. Meanwhile the preheater tube length was adjusted for a 3-inch sleeve-to-nozzle exit plane separation, aiming for 1-inch wide coatings. The nozzle was heated to 400°C, and the gas heater was warmed up at 60 percent power. At a 30-psia operating pressure, however, the preheating flow and hot nozzle plume were only able to raise the sleeve to 80°C. The gas heater was then changed to 100 percent power, heating the sleeve above 100°C.

52

Previous tin-spraying experience had shown that preheating a mold above 100°C was important for wetting mold surfaces and replicating engraved details. To deposit coatings with good adhesion, it was likely that base metal specimens would have to be preheated to at least this temperature. It was therefore decided to always operate the gas heater at 100 percent power for the spray-coating configuration in Figure 23.

At this point, the system was ready to spray tin onto the smooth steel sleeve; data recorded in this effort are displayed in Figure 31. At 20 seconds the operating pressure was increased to 32 psia--shortly before molten tin was poured into the tundish (indicated by a small decrease in melt temperature). At 80 seconds the base metal fixture was shifted for depositing tin near the end of the sleeve, which sharply lowered the base metal temperature to 105°C, because part of the preheater gas flow (emerging from a slot) now missed the sleeve. Tin spraying commenced at 210 seconds, when the operating pressure was lowered to 24 psia. Arrival of tin droplets at the base metal is shown by an abrupt 20°C rise in temperature. Subsequent oscillations in base metal temperature were due to sleeve eccentricity at its 1.38 revolutions-per-minute (rpm) rotational speed, which converts to a circumferential speed of 18.5 inches/minute.

Spraying lasted for nearly 100 seconds, which was long enough for more than two complete revolutions. However, the deposit separated cleanly from the smooth steel under the force of gravity, so tin was not sprayed onto itself. Throughout this period the operating pressure was adjusted by small amounts while effects on the deposit were visually observed. Ultimately, a 23.4-psia pressure was found to yield the best looking deposit for the relatively low 105°C base metal temperature.

Data shown in Figure 31 after 310 seconds are less important. The nebulizer ceased spraying after the operating pressure was increased to 32 psia, and the measured base metal temperature dropped accordingly. The sharp decrease in melt temperature at 380 seconds indicates when remaining molten tin in the furnace was poured into the tundish. Spraying was again initiated at 410 seconds with the drop in operating pressure to 23.4 psia. This pressure value was maintained while the tundish emptied, primarily to confirm the long-term stability of the nebulizer.

53
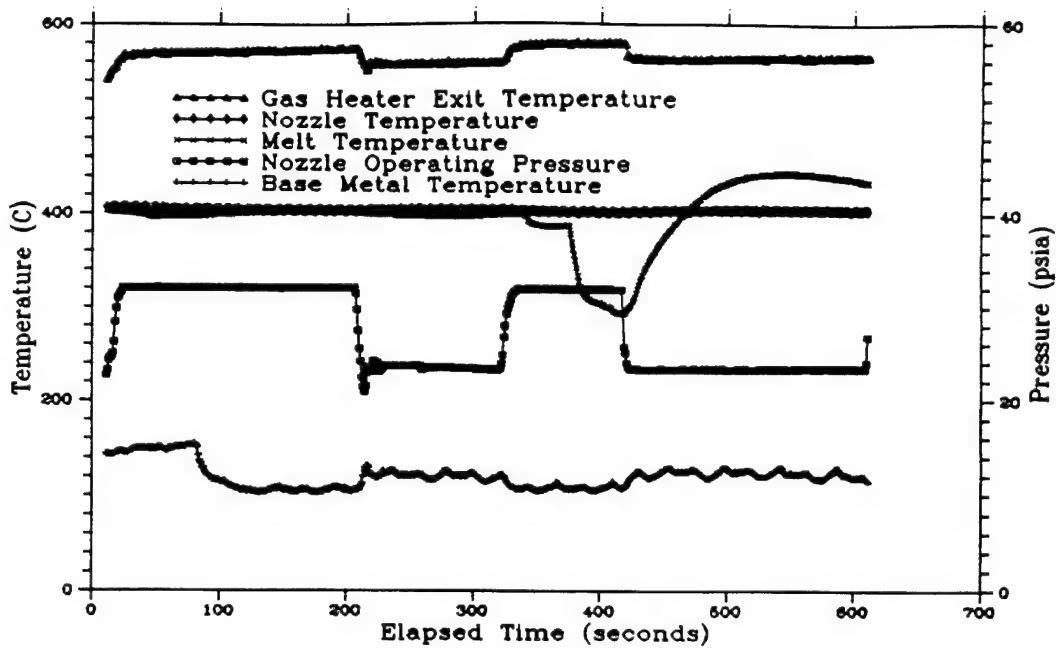
Figure 31. Tin-Spraying Test with Smooth Sleeve
Preheated to 105°C.
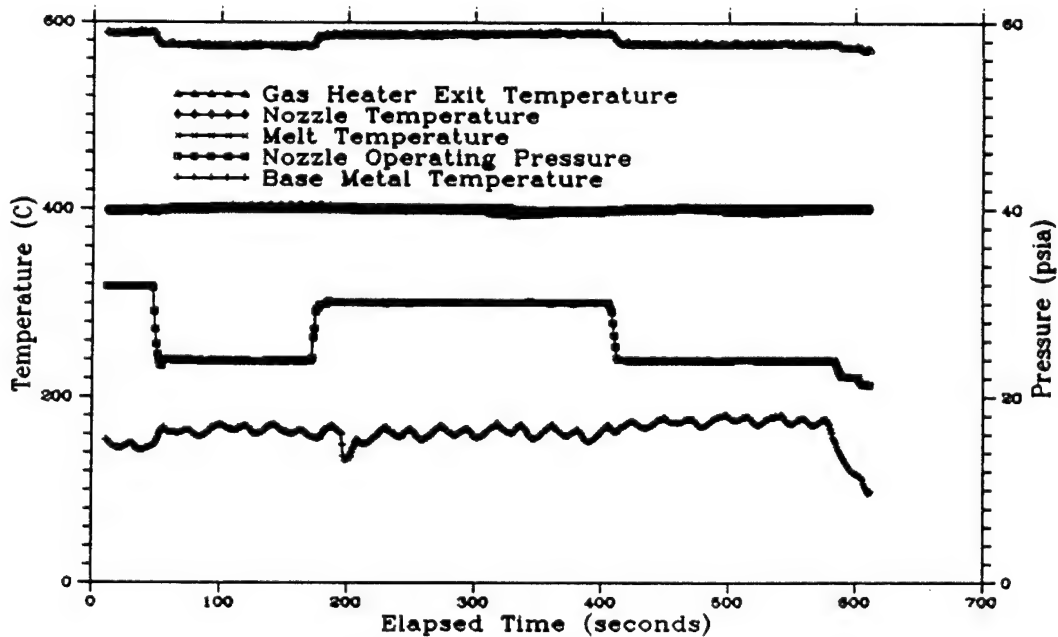
Figure 32. Tin-Spraying Test with Smooth Sleeve
Preheated to 145°C.

54

Somewhat later, the furnace was replentished with tin. While it melted and stabilized at 400°C, the base metal fixture was shifted to deposit tin approximately 2 inches inward from the sleeve end. Here all of the preheating flow contacted the base metal, resulting in an average base metal temperature of 145°C. The last precoating experiment was then conducted to ascertain the effects of this 40°C increase.

The data recorded are presented in Figure 32, where the recording interval began after tin had been poured into the tundish. Spraying commenced at 40 seconds with a drop in operating pressure to 24 psia, and tin deposition was again reflected by a 15°C rise in base metal temperature. Minor pressure adjustments established a visually optimal operating pressure of 23.9 psia for the warmer base metal.

Unlike the first deposition trial, however, the deposit did not detach under its own weight, so a multilayered deposit began to accrue after the 90-second mark. This condition was doubly anomalous, because the preheater remelted the tin surface on each pass. Consequently, only the first 50 seconds of spraying data were meaningful. Nevertheless, the continuous tin accumulation explains why base metal temperature did not decrease significantly in Figure 32 after spraying ceased at 180 seconds.

The last portion of Figure 32 represents a lateral shift of the base metal fixture to a region free of tin, as well as a slight movement of the sleeve toward the preheater. Virtually no clearance remained between the sleeve and the preheater tube, and the base metal temperature rose to an average value of 160°C. Upon initiation of spraying at 410 seconds, the base metal temperature increased to approximately 170°C. Once again, the deposit stuck to the smooth steel sleeve.

Preliminary tin-spraying findings can be summarized as follows. A 3-inch separation between the nozzle exit plane and base metal produced deposits over 1 inch wide--the target value. With the nozzle at this distance and the preheater placed next to the base metal, the gas heater (at full power) was able to heat most of the steel sleeve to 140°C, which encouraged tin to wet steel upon depositing. Operating pressures of 23 to 24 psia were best for spraying on a sleeve rotating at 1.4 rpm.

55

Certain terminology must be introduced before proceeding further. All computerized data files are listed according to the Julian date on which they were recorded. For example, May 30 was the 150th day of 1989. On two dates more than one experiment was performed, where the files were automatically incremented by 1, beginning with 0 (e.g. 160-0, 160-1, 160-2, etc.). However, the 160-1 file was created while testing a new component configuration, and no actual coated specimen was produced. Similarly, the 178-3 experiment was inadvertently performed without base metal preheating, so it was not studied further. Since each recording interval was ten minutes long, in some instances two separate coatings could be produced on the same data file. In these situations a letter designator was added, as with 160-2A, 160-2B, 160-3A, and 160-3B.

The above scheme uniquely identified each coating experiment, but extra designators were added to describe the base metal configuration. The first set of coated specimens came from two cylindrical steel sleeves radially (RDL) blasted with grit of varying sizes, where each portion of the sleeve length had the same roughness all around the circumference. (See Figure 23.) A horizontal (HOR) grit-blasting pattern was adopted for the second specimen set, where the sleeve was divided into 120-degree segments and each segment had the same roughness over its length. Three grades of surface roughness were thus coated in one circumferential pass under identical spraying conditions. Lastly, for the third specimen set, the improved base metal fixture raised vertical (VER) steel strips in front of the nebulizer to provide better overall process control.

2. The 150 RDL Experiment

Data recorded while spraying the first successful tin coating are given in Figure 33. (For simplicity, data taken before and after spraying are not presented, since characteristic features were already discussed while explaining Figures 31 and 32.) As with the preliminary exercises, the steel sleeve was positioned 3 inches from the nozzle exit plane and operating pressures ranged between 23 and 24 psia. Similarly, the sleeve was rotated at 1.38 rpm, which had been chosen earlier because it was midway in the drive motor speed range. Had it proven necessary, the circumferential speed could have been raised or lowered by large amounts.

56

As indicated in Figure 33, spraying lasted for 62 seconds--long enough for 1.5 passes--but tin was never sprayed onto itself. Instead, the base metal fixture was twice shifted toward the sleeve center after the first two 170-degree segments had been coated. The first segment was sprayed near the sleeve end, missing part of the preheater flow, while the other two segments received the full benefit of the preheater--which thus explains the net base metal temperature increase from 105 to 125°C.

The rate of increase in base metal temperature was exaggerated on the middle segment--between 36 and 48 seconds--by a tear-shaped globule formed on the deposit surface where the eccentric sleeve passed too close to the preheater slot. The globule ran continuously in the plume impact zone, leaving a shiny molten trail that was easily distinguished from the finely dimpled surface where partially solidified droplets consolidated. The globule refused to solidify at 40 seconds, when pressure was increased from 23.1 to 23.6 psia to lower the deposition rate and heat flux. This effect persisted until 52 seconds, when the fixture was shifted laterally, and it did not recur on the third coating segment. Despite its anomalous nature, the globule nevertheless simulated a standard hot-dip tin-coating process, and the shiny deposit was later sampled for detailed study.

The steel sleeve was grit-blasted in four parallel bands, each 1-inch wide around the circumference. The sleeve was 8 inches long, so only the outer half was prepared for coating--the half not supported by the aluminum drum in Figure 23. The outer band was slightly roughened by peening with glass beads of a wide size distribution. This was the surface coated by the first 170-degree segment. The second coating segment was sprayed onto a band blasted with a relatively fine Number 60 to 120 mixture of silica powder. The inner two bands were blasted with coarse Number 46 and Number 30 alundum grits, respectively. The third segment straddled the two bands to prevent overlapping the second segment.

Because the running globule altered the middle coating segment, the tin deposit on the band blasted with the fine alumina grit could not be compared to the first and third segments. Peening with glass beads could still be evaluated against blasting with coarse alumina, although the local temperatures were different on the first and third segments.

57
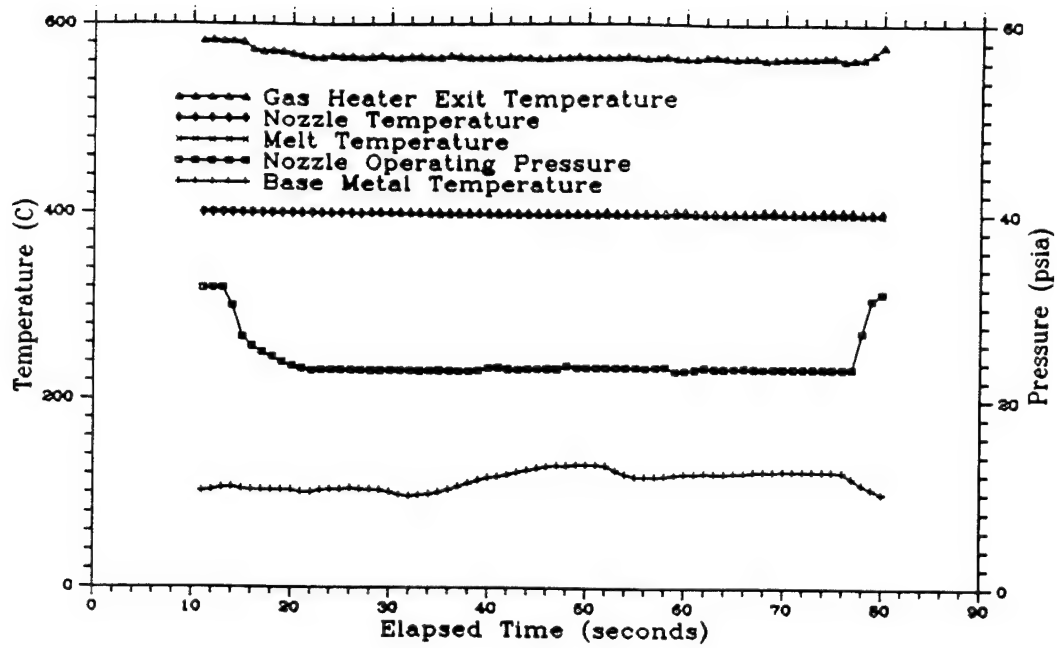
Figure 33. On-Line Coating Data from the 150 RDL Experiment.
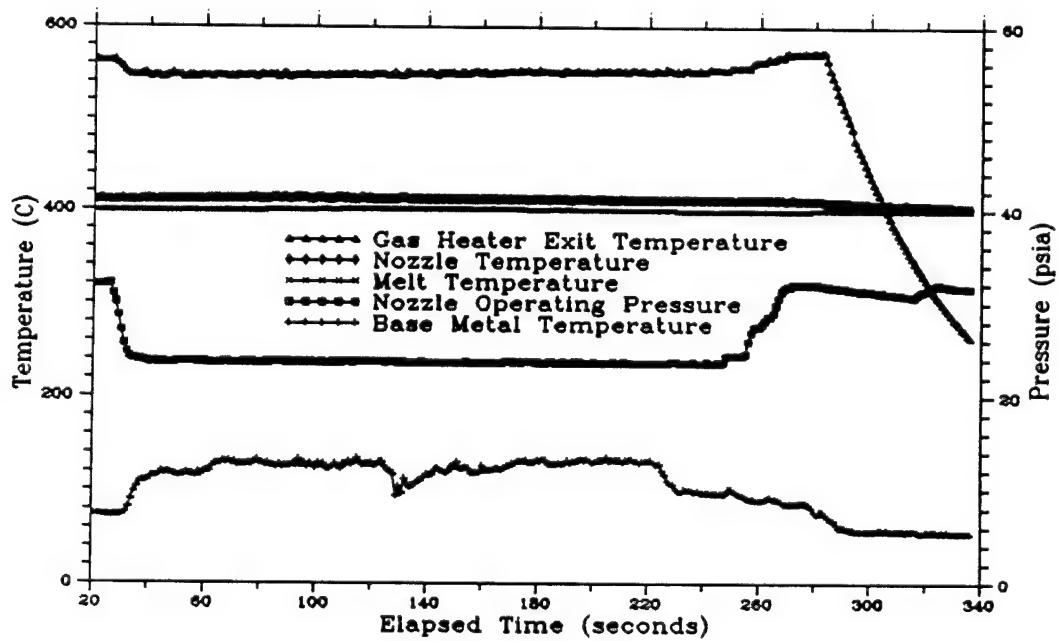
Figure 34. Data Recorded during the 153 RDL Coating Experiment.

58

3.   The 153 RDL Experiment

Initial examinations of the 150 RDL coatings revealed thicknesses of approximately 0.010 inch over most of the width, tapered down at the edges. As discussed in Reference 4, this value is somewhat thick for normal tin electroplates, but thinner than often necessary when hard chromium plating is performed to refurbish worn parts. Because the Spray Coating of Metals project is primarily aimed toward replacing the chromium electroplating process--thereby minimizing hazardous waste generation--the decision was made to produce substantially thicker coatings in the next experiment. This was accomplished by slowing the rotational speed of the base metal sleeve to 0.55 rpm (7.34 inches/minute) in order to achieve a thickness of approximately 0.025 inch. The steel sleeve was grit-blasted with an identical pattern to the first one.

Data from the 153 RDL coating experiment are displayed in Figure 34. Tin was sprayed from 30 to 260 seconds, as indicated by the reduction in operating pressure from 32.0 to 23.7 psia. This spraying pressure was deliberately set 0.6 psia above the 150 RDL value to lower the deposited heat flux, thereby compensating for poorer heat transfer through the thicker coating to the base metal heat sink. This alteration worked as desired in that no running globules formed. Furthermore, the outer coating surfaces typically had the same finely dimpled appearance as the first and third segments from 150 RDL.

Suitability of the operating pressure selected is demonstrated by the base metal temperature plot in Figure 34, as well. Despite the longer transit time through the plume impaction zone and accumulation of thicker deposits, the sleeve temperature stabilized at 130°C, within a few degrees of the first and third 150 RDL coating segments. The sharp drop in temperature at 130 seconds represents a lateral shift of the base metal fixture after coating over 320 degrees of rotation. This coating pass covered equal portions of the band peened with glass beads and the band blasted with fine silica grit. The sleeve temperature plateau from 140 to 220 seconds represents the second 320-degree segment, where the coating straddled the bands blasted with coarse Number 46 and Number 30 alundum grits. The sleeve was pulled away from the spray plume at 220 seconds.

4. The 160 HOR Experiments

Several difficulties were found with the radially grit-blasted steel sleeves used in the first two experiments. As mentioned earlier, the inch-wide bands were slightly narrower than the coated deposits, so some overlapping would occur at the edges if coatings were centered on a given band. The likelihood of overlapping was also increased by imprecise manual movements (through a chamber port) of the base metal fixture. Thus, coatings were sprayed along band boundaries to compare grit-size effects without risking overlaps. However, there was no guarantee of equally dividing a coating between bands. Another problem was unequal preheating of the sleeve while moving inward from the exposed end, such that grit effects on adhesion were confounded with thermal influences on wetting.

The solution chosen was blast 120-degree sleeve segments with each of three grit sizes over the full sleeve length. With this approach, all three types of roughness would be sprayed in a single circumferential pass, so several different sets of spray conditions could be explored on a single steel sleeve. In addition, with ample space along the length, precise lateral positioning was now not critical. Another advantage was that previously blasted surfaces had to be masked to prevent grit overlap during surface preparation of the old design, where the masks created a risk of surface contamination. By comparison, the modified pattern did not need masking, since only one-third (or so) of the circumference faced the blaster at a time and since any grit overlap along boundaries could merely affect a few degrees of a segment—a negligible concern.

Yet, with room to accommodate only three grit sizes on the new design, a choice was required on which sizes to use for the second set of coating specimens. Both the Number 30 and 46 grits appeared promising, based mostly on previous tin-spraying work with textured mold surfaces. Peening with glass beads seemed to barely roughen the steel sleeve surfaces, although the cleaning was clearly beneficial. Meanwhile, the mixture of Number 60 to 120 silica grits raised a possibility of changing size distributions with time, making preparation difficult to reproduce. Thus the coarse grit sizes were retained, but the glass beads and silica mixture were replaced with a uniformly fine Number 240 silica powder.

60

a. The 160-0 HOR Experiment. Because a distinctly different type of base metal preparation was being employed for the first time, the type of spraying conditions used while coating the first set of specimens was repeated as a control. This meant a 3-inch nozzle exit-to-base metal separation to produce 1-inch wide deposits. However, a 1.17-rpm rotating speed was chosen for a 0.012-inch nominal coating thickness. As shown in Figure 35, a 23.9-psia operating pressure was selected for a slightly lower molten metal aspiration rate in order to reduce the heat flux delivered to the base metal. The overall intention was to simulate the 150 RDL experiment without incurring any risk of running droplets. This concern remained with the new grit-blasting pattern, because the sleeve was still eccentric. At the open sleeve end where no support was received from the aluminum drum, diametral measurements differed by up to 0.2 inch.

Tin was sprayed for 50 seconds in the 160-0 HOR experiment-- long enough to finish a circumferential pass. The first 3 seconds are not shown in Figure 35, because the data acquisition system was not turned on quite early enough. (A 10-second lead time is needed for the system to come on line.) Although spraying ceased in time to prevent recoating the first layer, the base metal fixture was not pulled away from the preheater soon enough to prevent remelting of the first 50-degree deposit segment. Coincidentally, this portion of the sleeve had the greatest diametral deviance, and this segment made direct contact with the preheater slot. The tin layer here was physically scraped and smeared into a thin shiny coating that, nevertheless, accurately resembled a high-quality hot-dipped tin coating of commercial origin. It was tested later for comparison of coating properties to the remaining 300 degrees of spray-formed coating.

This experiment was recorded under intense stroboscopic illumination on high-speed videotape (1000 frames/second) with a Kodak EktaPro 1000 Motion Analyzer (Eastman Kodak Spin Physics Division). This state-of-the-art imaging system produced revealing slow-motion replays. In particular, individual droplets were observed impacting the base metal at 12X magnification. As the deposit accumulated, tiny "lakes" of molten metal would form on the surface and solidify within 0.01 second. With the base metal at 125°C and with the other spray conditions in Figure 35, approximately one-fourth of the surface was molten at a given instant.
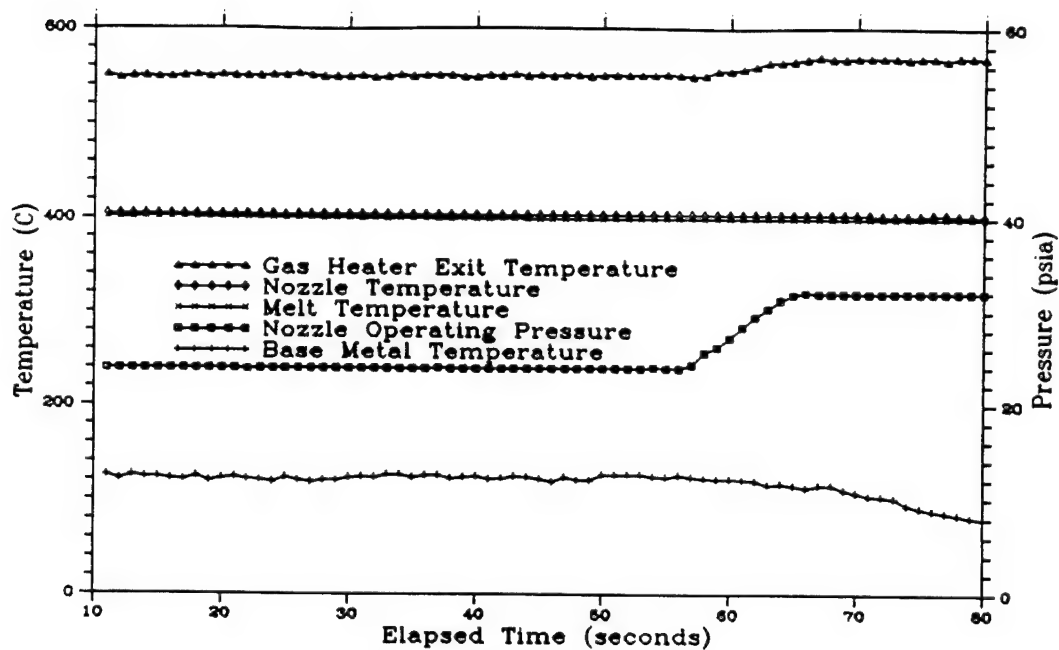
Figure 35.   Spraying Conditions for the 160-0 HOR
             Coating Experiment.
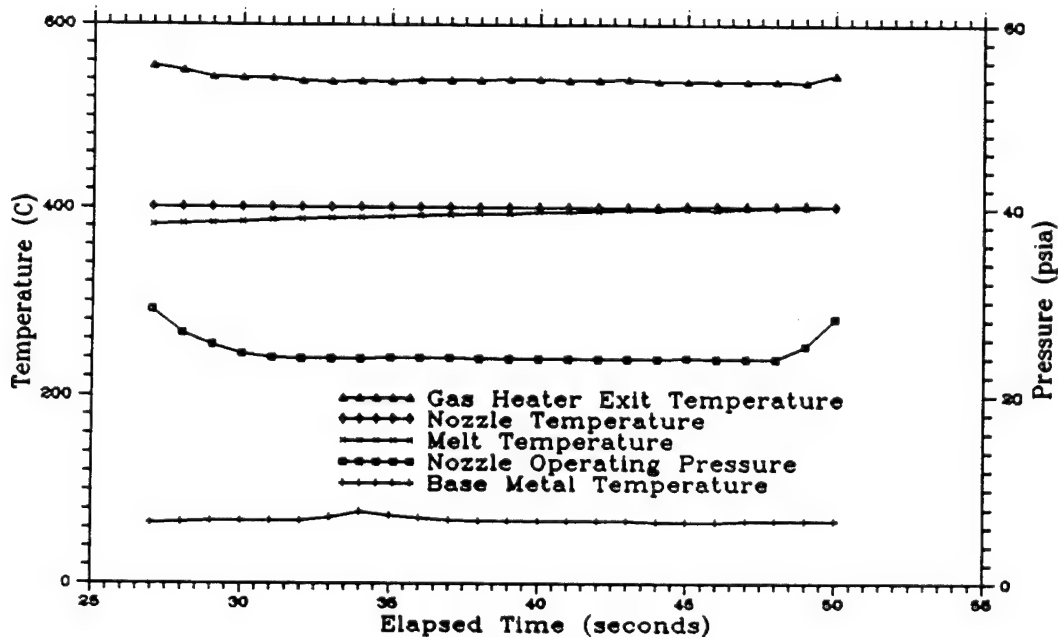
Figure 36.   Spray-Coating Data from the 160-2A HOR
             Experiment.

62

A reasonable range of conditions had now been investigated for wide coatings, so the base metal was moved closer to the nozzle. With less room for expansion, the tin plume was concentrated onto a smaller area of the base metal surface. This would create a high local heat flux, unless compensating methods were employed. One approach for lowering the heat deposition rate was to increase the base metal speed. Another option was to remove the preheater, since a doubt existed that preheating was absolutely required for successful coatings. That is, the leading edge of a concentrated plume might warm the base metal adequately by itself.

First, the nozzle bypass tube was rerouted toward the chamber exhaust port. Then a smooth steel sleeve was installed on the rotator to determine general spraying conditions. Preliminary tests on the 160-1 file established that droplet consolidation occurred without preheating at a 3.0-rpm rotational speed (40 inches/minute circumferential) within a 2-inch distance from the nozzle exit plane. However, deposits tended to detach under their own weight from the smooth steel surface.

b. The 160-2A HOR Experiment. For this effort the steel sleeve was placed 2 inches from the nozzle exit, which yielded a 0.70-inch wide coating. Due to the much faster speed of rotation, the coating thickness was reduced to 0.004 inch--another goal of this exercise. As indicated in Figure 36, an operating pressure of 23.9 psia was used for spraying, as with 160-0 HOR. The coating displayed the same finely dimpled exterior surface as seen earlier, although the base metal temperature was down to 66°C. The slight increase in temperature at 34 seconds was at the position where the eccentric sleeve was closest to the nozzle, but this small deviation left no detectable effect. The 160-2A HOR tin coating was sprayed at the coolest conditions in the first two sets of specimens.

c. The 160-2B HOR Experiment. The sleeve was moved to 1.2 inch from the nozzle exit plane, which reduced the coating width to 0.45 inch. As shown in Figure 37, the greater plume concentration raised the local base metal temperature above 90°C, and deposit thickness grew to 0.009 inch. Pressure was reduced at 453 seconds from 23.9 to 22.9 psia to increase tin aspiration and heat deposition. The faceted coating surface then became more reflective, suggesting incipient melting of the deposit.

63
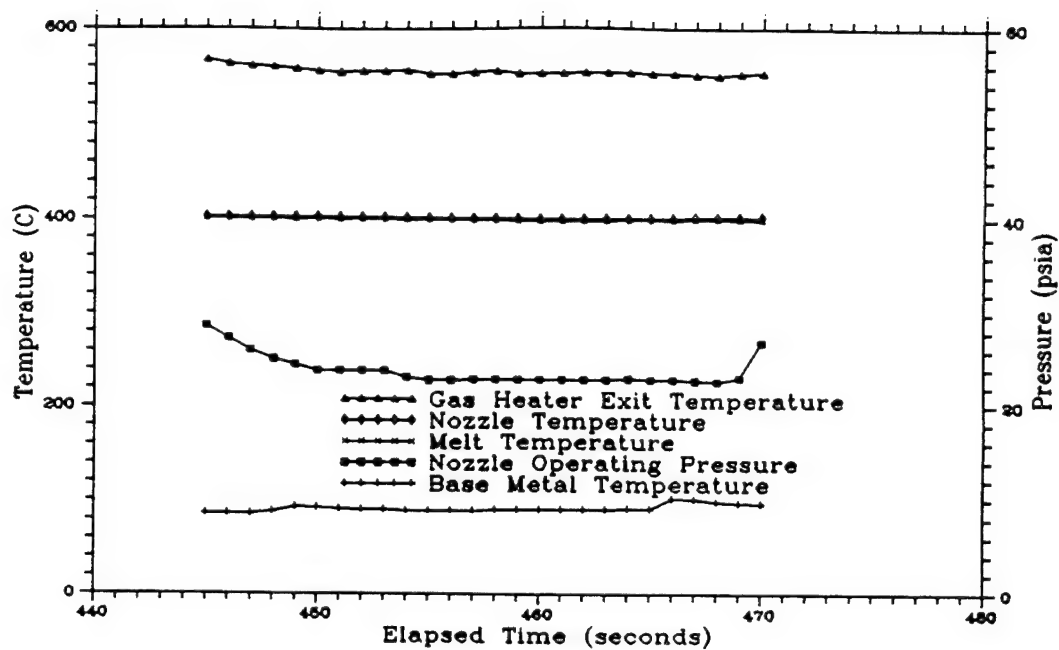
Figure 37. Data Recorded during the 160-2B HOR
             Coating Experiment.
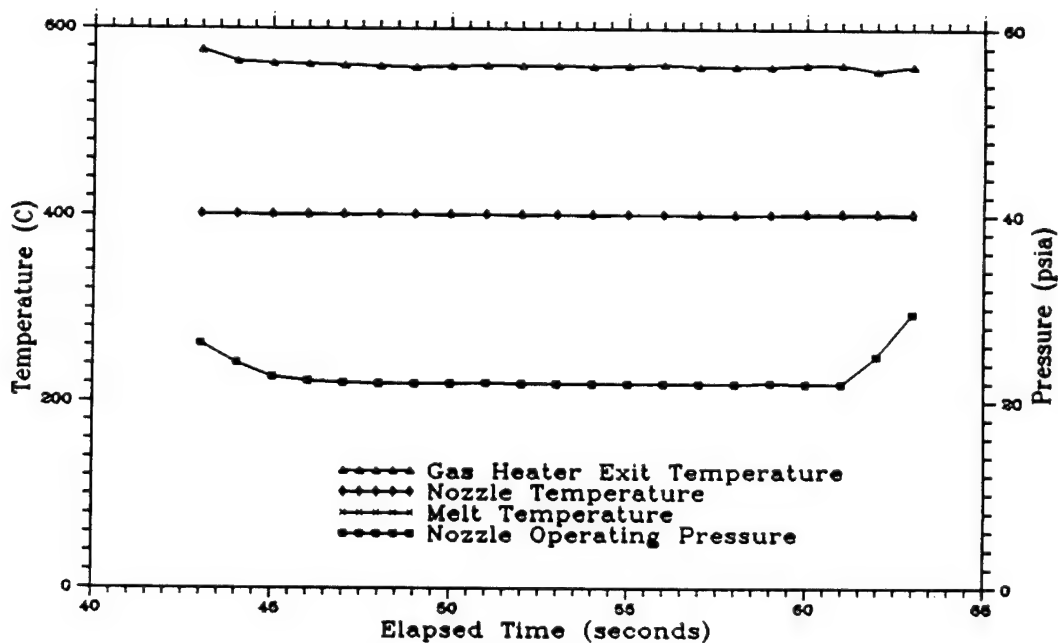
Figure 38. Spray-Coating Conditions for the 160-3A HOR
             Experiment.

64

d. The 160-3A HOR Experiment. Because increasing the metal mass flux and the heat flux in 160-2B HOR did not appear to adversely affect coating quality, the base metal was moved slightly closer in 160-3A HOR-- to a 1.0-inch separation. Unfortunately, the spring-loaded TC no longer made contact with the back sleeve surface, so base metal temperature is not plotted in Figure 38. Figure 38 also reveals that operating pressure was reduced still further to 22.0 psia for this experiment. The combined effect of the closer distance and higher melt aspiration was to produce a coating 0.41-inch wide and approximately 0.012-inch thick.

Despite the rapid 3-rpm speed, the high heat deposition rate created a visibly molten structure over most of the deposit width. This was intentional, because the main objective was finding out whether any metallurgical bonding might be induced by the increased heat content of the deposit. However, the nozzle plume exerted a profound influence on the broad molten film--pushing metal to both sides and piling it up into ridges--analogous to wave formation by a high wind. Consequently, the 0.012-inch coating thickness (measured by digital micrometer) primarily reflected maximum values at the peaks of the double-Gaussian profile.

e. The 160-3B HOR Experiment. The wave-like ridges in 160-3A HOR would pose prohibitive thickness variations for refurbishing worn parts. To reduce this phenomenon, the sleeve was moved away from the nozzle to a 1.5-inch separation. This produced a 0.50-inch deposit width. Yet, to maintain nearly the same heat load and encourage metallurgical bonding, the operating pressure was dropped to 21.0 psia, per Figure 39. The rate of metal spraying at this pressure (0.49 gram/second) was the highest tested in Phase I. The overall result was a 0.010-inch thickness on the wider deposit. A wide molten layer with wave-like ridges still formed, but the ridges were less pronounced than in 160-3A HOR.

Later visual inspection of coatings from the 160-3A HOR and 160-3B HOR experiments revealed that the influence of incident gas on the broad molten pools was more severe than at first recognized. Besides creating the very uneven surfaces just described, the steel sleeve surface was exposed at small isolated locations. Such "pinhole" defects would be totally unacceptable for applications requiring corrosion resistance.

65
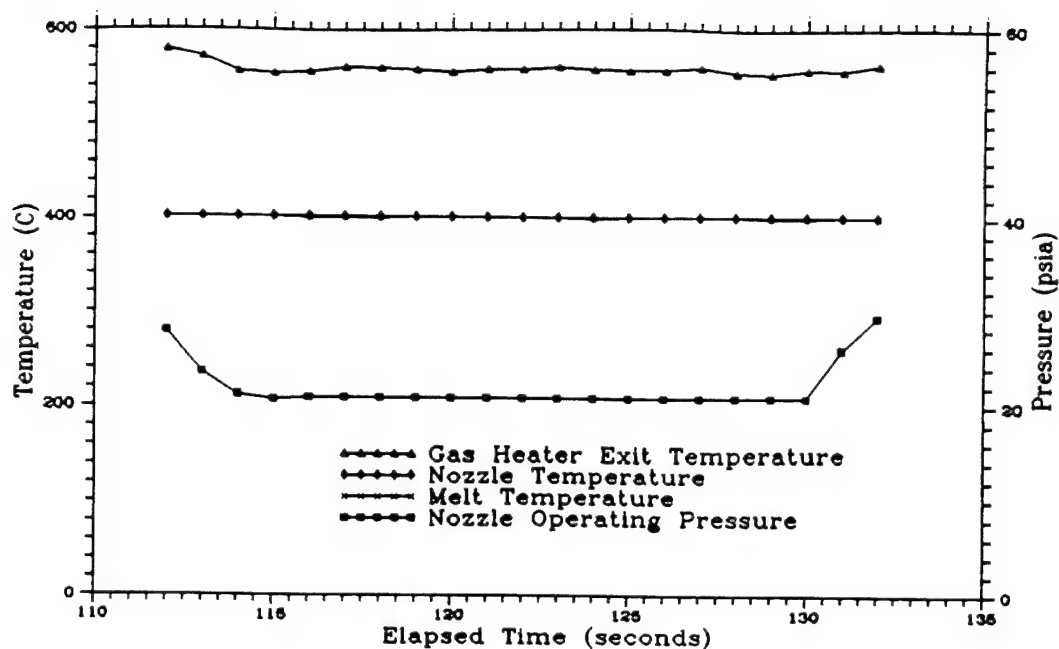
Figure 39.   Spraying Data from the 160-3B HOR
               Coating Experiment.
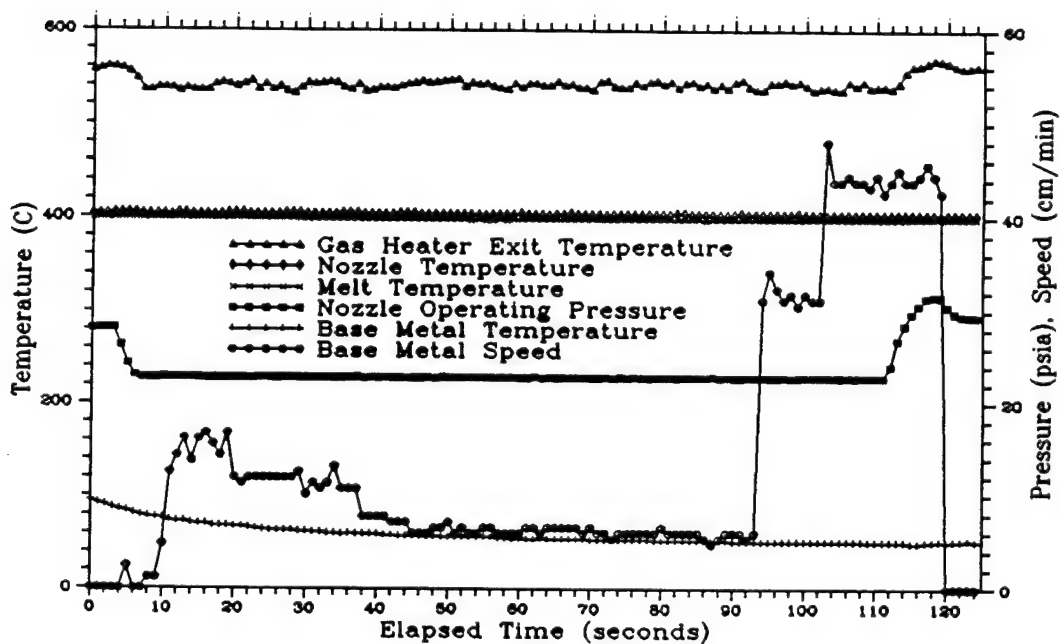
Figure 40.   On-Line Coating Data from the 178-1 VER Experiment.

66

5. The 178 VER Experiments.

When the 160 HOR experiments were conducted, no information was yet available from coating performance tests. Results presented later in this section demonstrate that broader coatings deposited at relatively cool temperatures were superior. But, in the absence of firm performance data, it was still felt that some metallurgical bonding would be essential for coatings with good adhesion properties. Consequently, the goal at the time remained producing coatings that exhibited a mostly molten surface.

Molten coating attempts in the 160 series were not satisfactory, due to wavy ridges forming under incident gas flow. For this fixed nozzle design, ridging dictated that molten coatings must be sprayed farther from the nozzle, where the plume would exert less influence. Thinner molten layers from extra plume expansion might be anchored by the wetted surface against ridging. But, thin molten coatings demanded preheating the base metal to augment the lower heat flux from a less concentrated spray plume.

The vertical fixture (Figure 24) became available at this time. Its sophisticated design was developed to surmount the rotating fixture limitations, as described in the experimental configuration section. But, for spraying thin molten coatings, the most valuable feature was its own preheater, which allowed total flexibility in nozzle-base metal distance.' Also, the computer display of base metal speed permitted adjusting this process variable dynamically, plus identifying speed ranges on samples.

At this stage of Phase I, most of the remaining budget had to be reserved for coated sample analyses and documentation of results, so a complete range of conditions could not be explored with the new fixture. An arbitrary choice was made to limit vertical coating to surfaces blasted with Number 30 alundum. Operating pressure was restricted to 22.9 psia, which yielded a partially molten coating without preheating in 160-2B HOR.

a. The 178-1 VER Experiment. As a control, the preheater element was not turned on. A pre-spraying nozzle pressure of 30 psia raised the base metal to 90°C, per Figure 40. The preheater blew cool gas onto the steel sleeve back to prevent deflection, which caused gradual cooling.

67

The nozzle-to-base metal distance in the 178-1 VER experiment
was 1.5 inch, which produced a 0.50-inch coating width--as in 160-3B HOR.
Coating thickness changed from 0.029 to 0.004 inch, depending on the base
metal speed. As plotted in Figure 40, the speed of the steel strip varied
from 6 to 44 centimeters/minute (2.4 to 17.2 inches/minute), which was
much slower than the 40 inches/minute used in the 160-3B HOR experiment.

Despite the slower base metal speed in 178-1 VER, no thick
molten layer formed on the deposit surface and no ridging occurred. This
was largely due to operating the nozzle at 22.9 psia--nearly 2 psi higher
than in the 160-3B HOR experiment. Here the reduced melt aspiration and
lower rate of heat deposition helped to inhibit formation of a molten tin
layer. Cool gas flow on the back strip surface (preventing steel strip
deflection from nozzle plume pressure on the front side) also kept molten
ridges from forming. This resulted in a dimpled texture much like the
early coatings deposited under relatively cool conditions.

b. The 178-2 VER Experiment. Because the 178-1 VER coating
displayed no incipient melting, the preheater element was set to its
maximum power setting. As shown in Figure 41, the temperature of the
nozzle/tundish assembly was increased to 500°C, as well, to superheat
the tin more and to increase the gas temperature exiting the nozzle. Both
measures were to guarantee ample heat at the base metal for fostering a
thin molten layer somewhere within the base metal speed range. Increasing
the nebulizer temperature was chosen over lowering operating pressure and
moving the base metal closer, because these alternatives would create
thicker deposits more susceptible to ridging. Again, the goal at the time
was spraying a thin molten coating that might bond metallurgically.

Figure 41 reveals that the initial base metal speed was slow--
6 to 14 centimeters/minute. Base metal temperature was below 140°C,
but a large, deep pool of molten tin formed, which was immediately pushed
sideways and piled into ridges. At the 7-second mark, the base metal was
accelerated to 36 centimeters/minute, creating an 0.011-inch thick coating
with an incipient melting structure much like the 160-2B HOR coating.
Yet, the small speed decrease at 14 seconds (combined with a warming base
metal surface) caused ridging to reoccur--persisting until 28 seconds.

68
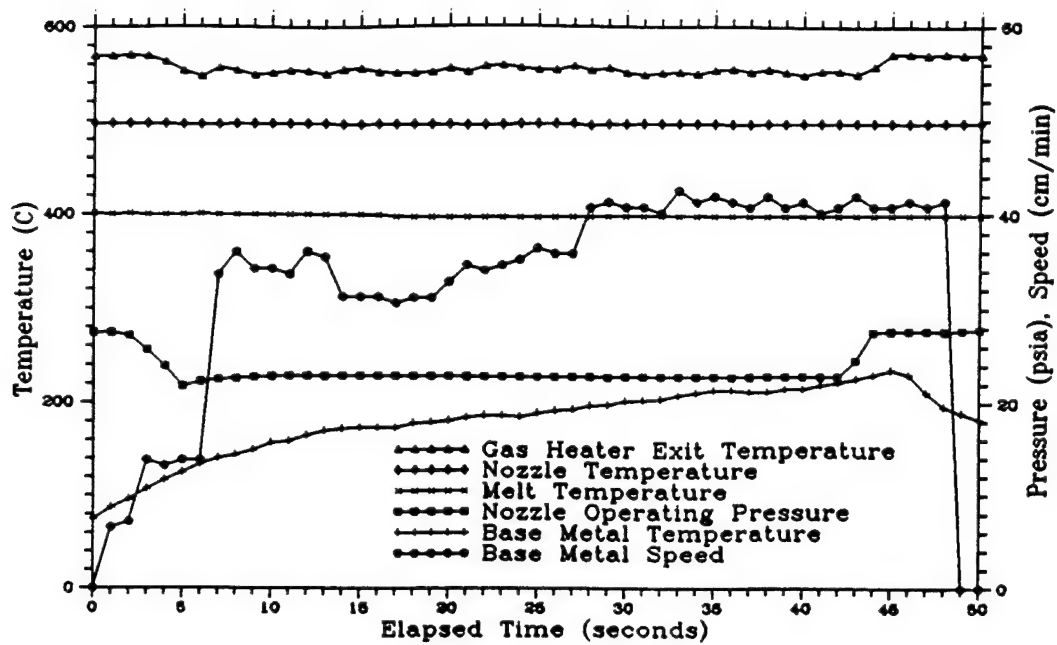
Figure 41. Spraying Conditions during the 178-2 VER Experiment.
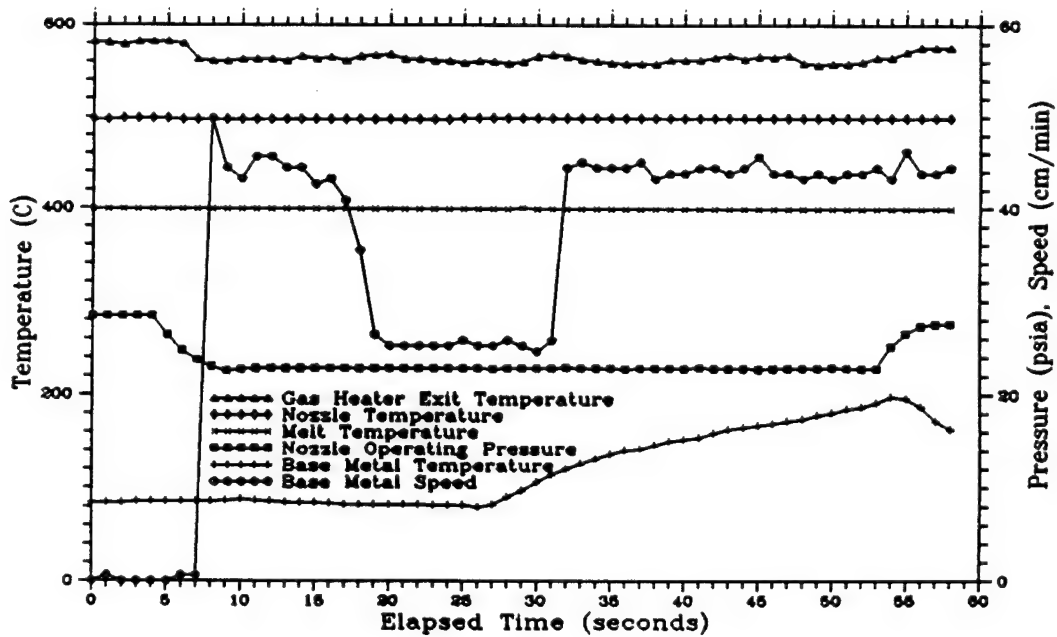
Figure 42. Coating Data Recorded during the 178-4 VER
Experiment.

69

Steel strip speed was then increased to 41 centimeters/minute, and the coating exhibited most of the target characteristics. The surface was shiny (conspicuously molten) over the full-thickness portion, and this region grew slightly in width as the base metal temperature increased from 200 to 225°C. No ridges were present in the molten zone, and the nominal thickness (excluding edge taper) was measured to be 0.009 inch.

c. The 178-4 VER Experiment. Successful spraying of a thin molten coating meant that the main objective of the 178 Series had been achieved. However, increasing the nebulizer temperature from 400 to 500°C had not been separately investigated. That is, effects of this increase were convoluted with influences of the preheater on the new base metal fixture.

Accordingly, the intention for the last experiment was to operate the nozzle at 500°C and at an operating pressure of 22.9 psia, as in the 178-2 VER effort. Meanwhile, the preheating element was to be turned off for the first half of the strip--as in 178-1 VER--with a cool gas flow directed against the back strip surface to counterbalance nozzle plume pressure. Then, at the halfway point, the heating element was to be turned on at full power to recreate the thin molten layer from 178-2 VER. When this was attempted on the 178-3 data file, the preheater gun was inadvertently left off entirely, including the cool gas flow. The plume deflected the steel strip and caused it to wobble severly, such that the nozzle separation distance changed constantly. This run was aborted, and the nonrepresentative sample was saved for archive purposes.

The next trial was free of any errors. A ridged molten layer formed initially, with the base metal shown at rest in Figure 42. This layer disappeared when the strip was accelerated to 44 centimeters/minute at 8 seconds, when the coating acquired a dimpled look from consolidation of partially solidified droplets. Here the coating thickness was measured at 0.010 inch, increasing to 0.016 inch at 20 seconds when the speed was slowed to 25 centimeters/minute. The overall appearance was identical to the 178-1 VER deposit. Molten ridging occurred almost instantly when the preheating element was engaged, and it persisted well after the base metal was speeded up. A uniformly thin molten layer like that in 178-2 VER did not emerge until near the end of the strip--at the 47-second mark.

70

C. BEND TEST RESULTS

Samples for coating performance tests were sectioned from each base
metal specimen. Each sample was sliced into three parts--two narrow parts
(0.25 inch wide) for bend tests and metallography, and a 1-inch wide part
for adhesion measurement. 150 RDL and 153 RDL samples were extracted by
shearing, when it became clear that this was causing weaker samples to
delaminate along the edges--especially because the cylindrical sleeves had
to be flattened in the process. A method was then adopted whereby slices
were made with a hand-held Dremel Moto-Tool equipped with a thin abrasive
cutting wheel, while the specimens were securely gripped in a vice.

The number of samples sectioned varied among specimens, depending on
how many different spraying conditions were covered in the course of an
experiment, along with how many ways the base metal surfaces had been
prepared. In general, one sample was extracted from each distinct region
for direct performance comparisons of varying spray-system parameters and
grit-blasting techniques. Unexpected anomalous areas were also examined.

Bend-testing provided the fastest feedback, due to minimal preparation
time and straightforward conduct. Each sample was slowly sqeezed in a
vice until the coating either fractured or separated from the steel base.
It was then photogaphed in place at approximately 10X magnification.
Lines were later drawn on photograph copies tangent to steel surfaces, and
the angle between them was measured by protractor. Positioning the
tangent lines was subjective--inducing an uncertainty of 5 degrees or so
in both directions--but the results are nevertheless a useful relative
indicator of both coating adhesion and ductility.

Samples from the 150 RDL experiment are shown in Figure 43. Four of
five behaved similarly, failing by coating fracture within 11 degrees of a
138-degree deflection, despite major differences in base metal preparation
(glass bead peening on Sample 1 to coarse alundum on Samples 4 and 5).
Unusually uneven Sample 3, sectioned across the "running globule" from the
second coating segment, performed consistently. Sample 2 failed quickly,
probably from shearing damage. Thickness appears asymmetric on Samples 1
and 2 (outer segment), since part of the plume missed the sleeve.

71

150 RDL-1
138 Degrees, Coating Fracture
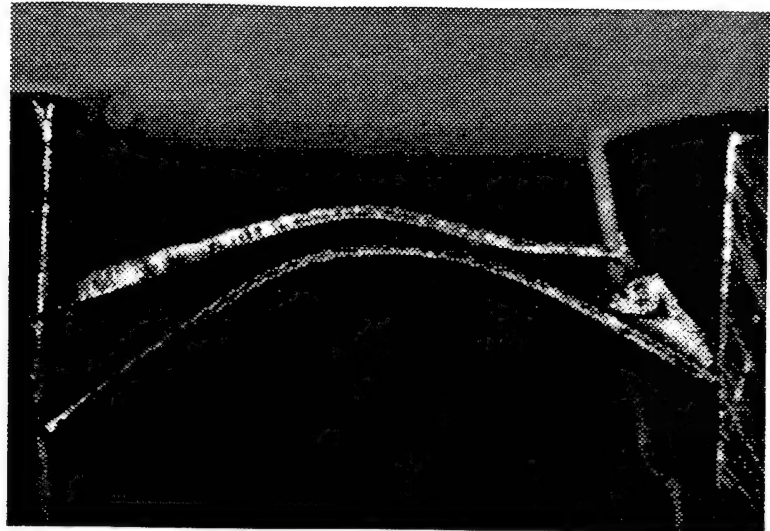
150 RDL-2
33 Degrees, Delamination

150 RDL-3
142 Degrees,
Coating Fracture
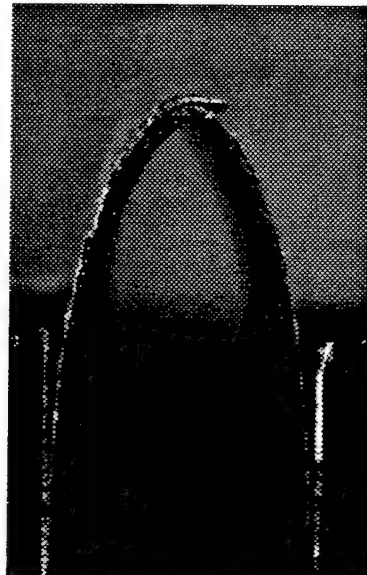
150 RDL-4
148 Degrees,
Coating Fracture
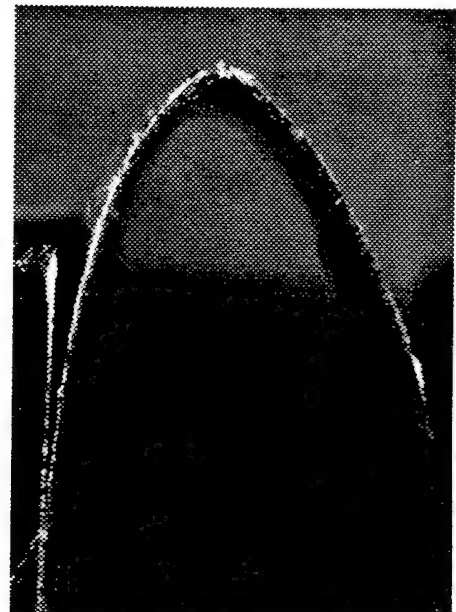
150 RDL-5
127 Degrees,
Coating Fracture

Figure 43.   Bend Test Specimens from First Carbon Steel Sleeve with Radial
Grit-Blasting Pattern.

The 153 RDL samples are displayed in Figure 44. Here the relatively
thick (0.025 inch) tin coating was able to accommodate very large bending
stress before fracturing, suggesting excellent ductility at low deposition
temperatures. No clear difference was seen from grit-blasting variations,
since Samples 1 and 2 straddled the boundary between the glass-beaded band
and the band blasted with fine silica, while Samples 3 and 4 straddled the
bands blasted with coarse Number 46 and 30 grits. The early coating
fracture on Sample 1 indicates a localized weakness of unknown origin.

Figure 45 demonstrates that thick coatings are not essential for
superior bend strength. Here the 0.012-inch thick 160-0 HOR coating did
almost as well as 153 RDL samples. Sample 1 was from the anomalous area
remelted and smeared into a thin layer by scraping against the preheater
slot, thus simulating a hot-dipped tin coating. The remaining samples
much more accurately represent spray-formed coatings and yielded virtually
identical results. Samples 2, 3, and 4 were sprayed onto surfaces blasted
with Number 46, Number 30, and Number 240 grit sizes, respectively.

Poorer overall performance is found in Figure 46 for the 160-2A HOR
and 160-2B HOR samples, which had nominal coating thicknesses of 0.004 and
0.009 inch. Only two samples are shown from each experiment--representing
Number 30 and 46 grit-blasted regions--because samples from the Number 240
areas both delaminated during cutting. The 160-2A HOR coating may not
have totally consolidated at the low 66°C deposition temperature,
while 160-2B HOR samples were coated at 90°C--near the normal range.

Number 240 grit-blasted regions are also absent in Figure 47, due to
premature delamination during sectioning. The samples from the 160-3A HOR
and 160-3B HOR experiments (one each from coarse Number 30 and Number 46
steel surfaces) failed by interfacial separation before the coatings could
fracture--again indicating weak adhesion for these mostly molten layers.

Samples cut from the first two flat strips are presented in Figure 48.
Sample 1 from the 178-1 VER experiment (no base metal preheating) was
deposited at a slow strip speed, and the 0.029-inch thick, asymmetric
coating separated very early. Sample 2 (0.004-inch thick) performed well,
showing no embrittlement from the low 50°C deposition temperature.

73
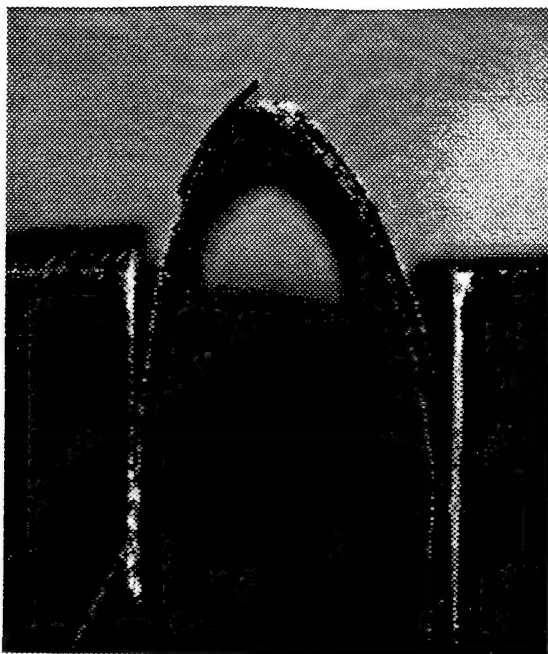
153 RDL-1
120 Degres, Coating Fracture
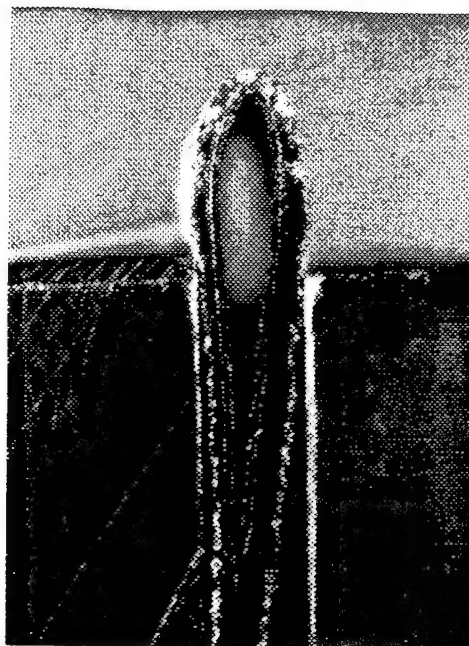
153 RDL-2
170 Degrees, Coating Fracture
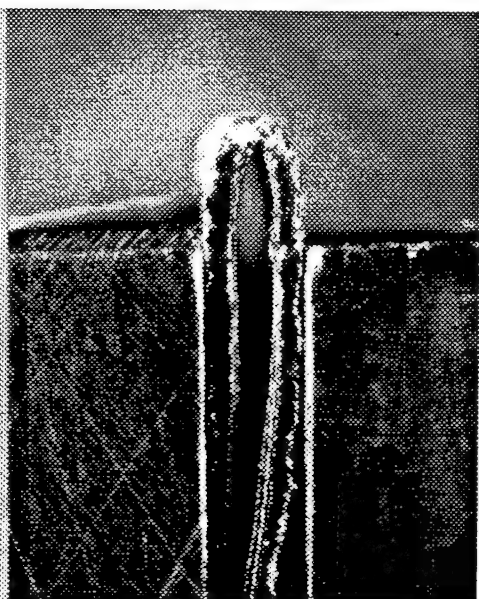
153 RDL-3
171 Degrees, Coating Fracture

153 RDL-4
173 Degrees, Coating Fracture

Figure 44.   Bend Test Specimens from Second Carbon Steel Sleeve with Radial
Grit-Blasting Pattern.

160-0 HOR-1
175 Degrees, Coating Fracture
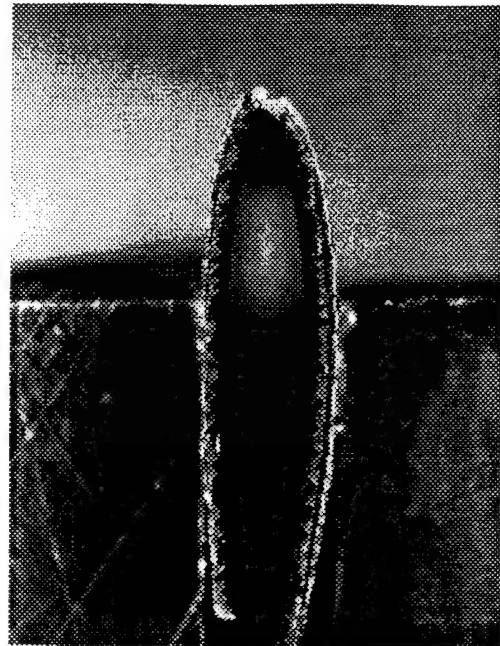
160-0 HOR-2
169 Degrees, Coating Fracture
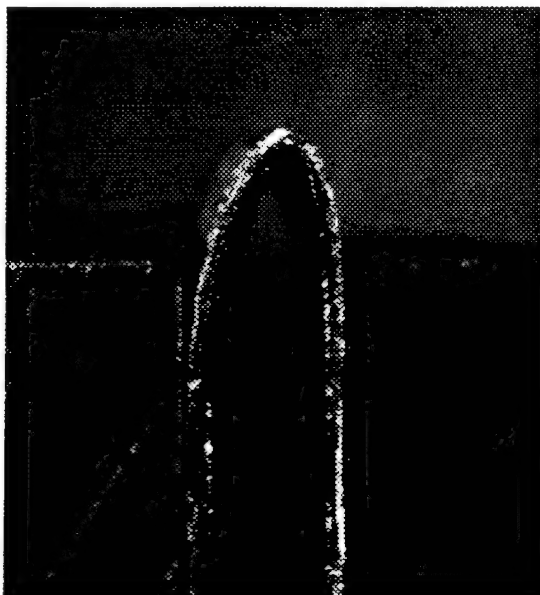
160-0 HOR-3
166 Degrees, Coating Fracture
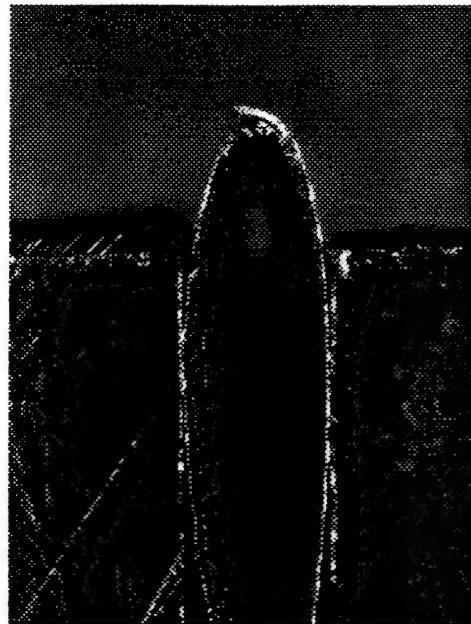
160-0 HOR-4
166 Degrees, Coating Fracture

Figure 45.   Bend Test Specimens from First Coating on Carbon Steel Sleeve with
Horizontal Grit-Blasting Pattern.

75
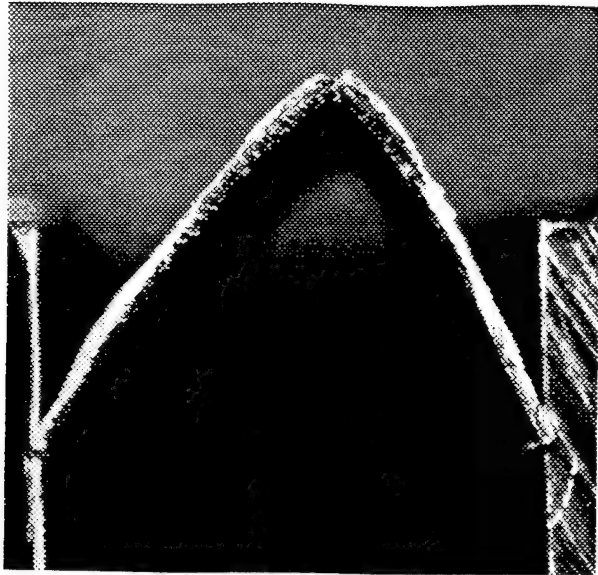
160-2A HOR-1
119 Degrees, Coating Fracture

160-2A HOR-2
122 Degrees, Coating Fracture
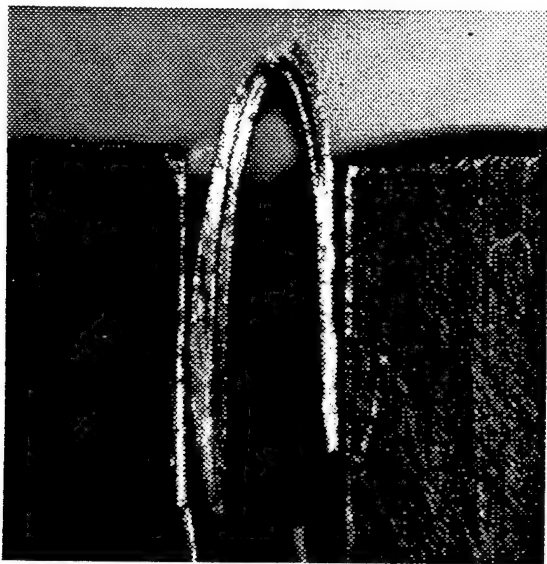
160-2B HOR-1
167 Degrees, Coating Fracture
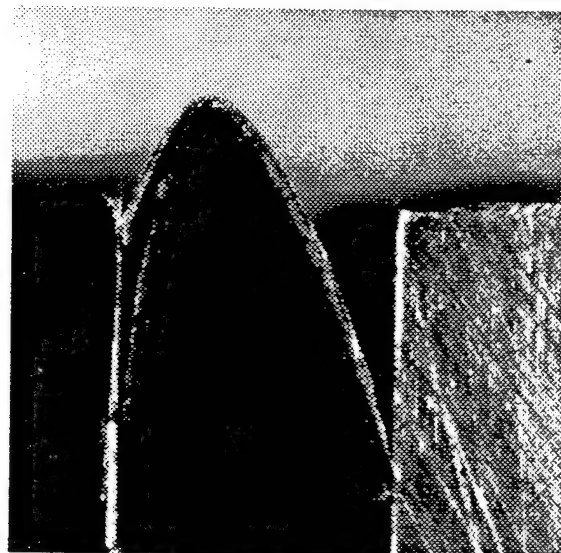
160-2B HOR-2
132 Degrees, Delamination

Figure 46.   Bend Test Specimens from Second Coating Experiment with
            Horizontal Grit-Blasting Pattern.
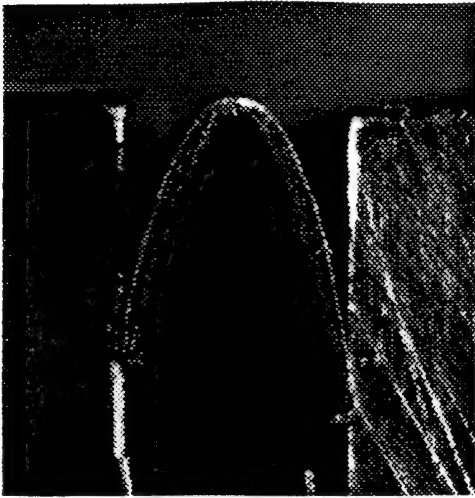
160-3A HOR-1
144 Degrees, Delamination
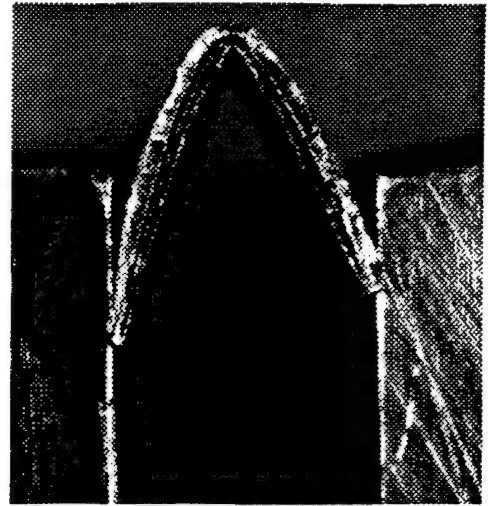
160-3A HOR-2
139 Degrees, Delamination
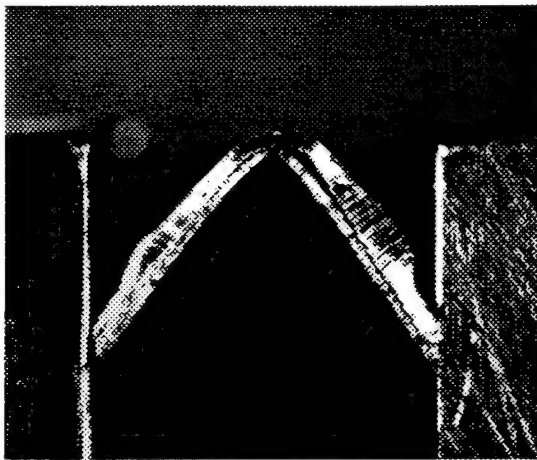
160-3B HOR-1
111 Degrees, Delamination

160-3B HOR-2
101 Degrees, Delamination

Figure 47.   Bend Test Specimens from Third Experiment with Horizontal
Grit-Blasting Pattern.

77

178-1 VER-1
15 Degrees, Delamination

178-1 VER-2
157 Degrees,
Coating Fracture
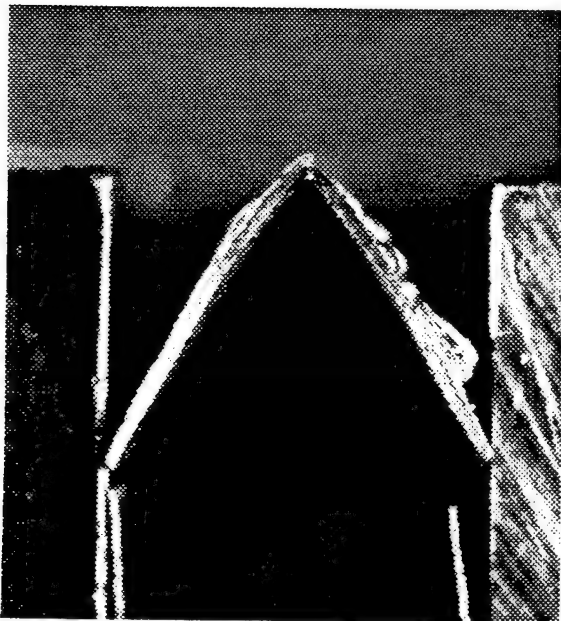
178-2 VER-1
116 Degrees, Coating Fracture
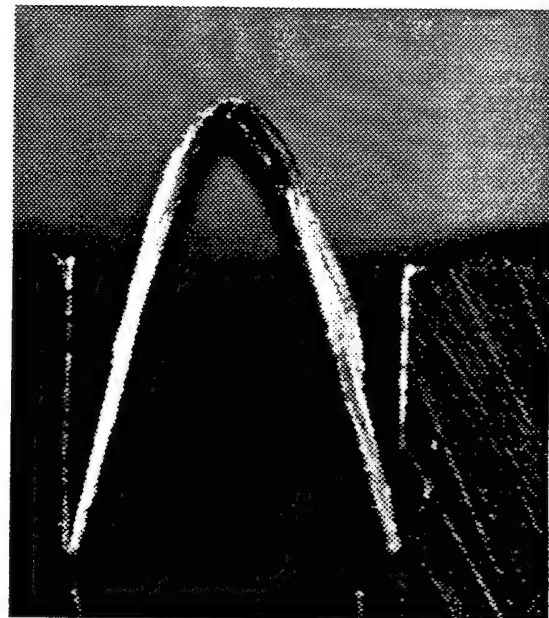
178-2 VER-2
146 Degrees, Coating Fracture

Figure 48.   Bend Test Specimens from the First Two Coatings Sprayed onto
Vertical Steel Strips.

78

The two samples from the 178-2 VER experiment in Figure 48 represent the high deposition temperatures achieved by preheating the back side of the strip. Sample 1 was extracted from the ridged region, where the incident nozzle plume exerted a strong influence on the deep molten layer there. Sample 1 fractured early during deformation, presumably because the major thickness variations from ridge formation prevented bend stress from being distributed equally. Bare spots may have existed on Sample 1, weakening fracture resistance even more. Unlike thicker ridged samples from 160-3A HOR and 160-3B HOR, Sample 1 did not fail by delamination.

Sample 2 from the 178-2 VER experiment was sectioned across the thin molten layer region that formed after the base metal speed was increased substantially, thereby eliminating ridge formation. Here the coating was nearly even at 0.009-inch thick, so bend stress was dispersed better than on Sample 1. Sample 178-2 VER-2 can be compared to Sample 160-2B HOR-2, which had the same thickness but lower deposition temperature (90°C versus 210°C). The thin, predominantly molten layer here performed slightly better (by 14 degrees) than the incipient molten coating there.

Three samples from the 178-4 VER experiment are shown in Figure 49. Samples 1 and 2 were taken from the cool deposition portion, where the preheater was not employed. Sample #2 had a 0.016-inch asymmetric crown and was 0.008-inch thick at the fracture point; it behaved like 160-2A HOR samples. Sample #1 was coated at a faster base metal speed, producing a 0.010-inch peak thickness, yet it fractured at least 20 degrees earlier than other samples of comparable thickness. It also did not approach the ductility of Sample 178-1 VER-2, which was 0.004-inch thick but also coated without preheating. Increasing the nozzle temperature to 500°C in 178-4 VER only raised the strip temperature to 85°C from 50°C in 178-1 VER, which does not clearly explain the different bend strengths.

Sample 3 in Figure 49 was sectioned from the 0.009-inch thick molten layer created by turning on the preheater midway through the 178-4 VER experiment and accelerating the steel strip speed to eliminate ridging. As such, Sample 178-4 VER-3 is virtually identical to Sample 178-2 VER-2 in terms of spraying parameters and base metal conditions. The similar bending deformations (only 9 degrees difference) thus should be expected.

79
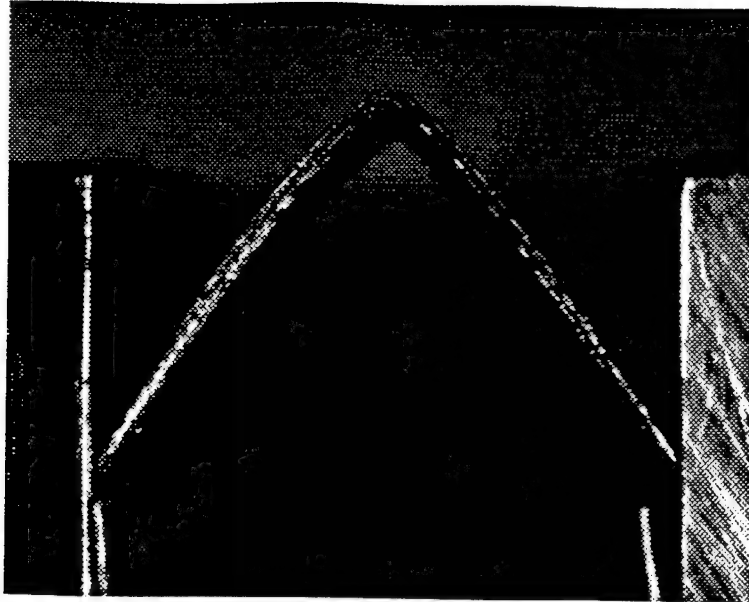
178-4 VER-1
108 Degrees, Coating Fracture
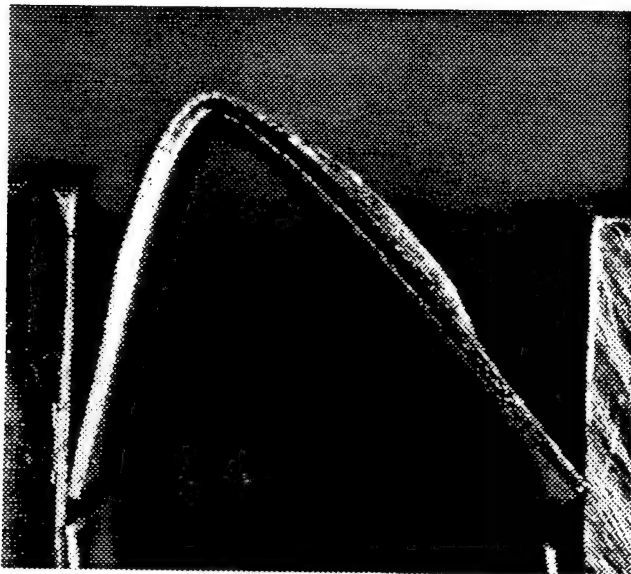
178-4 VER-2
122 Degrees, Coating Fracture
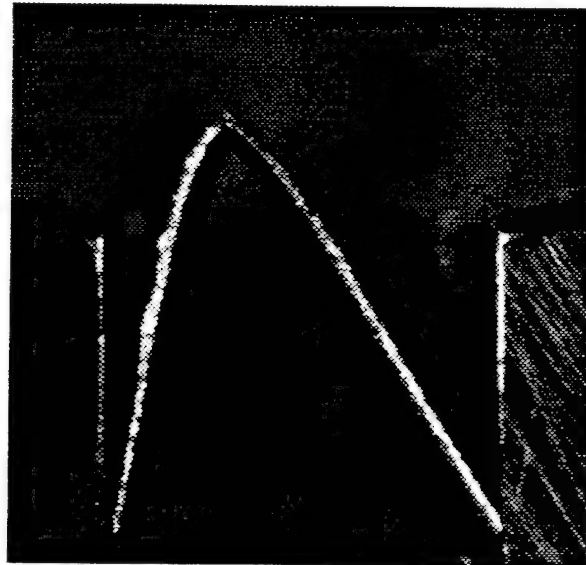
178-4 VER-3
137 Degrees, Coating Fracture

Figure 49.   Bend Test Specimens from the Last Tin-Coated Vertical Steel Strip.

D. ADHESION STRENGTH MEASUREMENTS

As earlier explained, bend-testing was primarily a relative indicator
of coating ductility, although a few samples with especially weak bonding
delaminated from the steel base metal before the coating could fracture.
Accordingly, adhesion strength had to be measured in a direct, absolute
manner in order to quantify this important aspect of coating quality.

Adhesion strength can be determined in two substantially different
ways--by pulling the bonds apart under gradually increasing tension and by
peeling a coating off at a constant load. Both approaches involve first
attaching gripping pieces to the coating and to the base metal, such that
controlled loads can be applied for inducing separation. The uniaxial
pull-test method was chosen because: (1) sample preparation is easier,
since pull grips are directly opposed, rather than offset for peel tests;
(2) sample geometry can be accurately controlled by trimming to the edges
of pulling grips, whereas peel tests require a constant cross-sectional
area at the separation front; and (3) bond strength is clearly defined in
a pull test by the tension at which delamination suddenly occurs, but peel
tests must measure the rate of separation at a constant load. This rate
may not be constant and an optimal load value is not obvious in advance.

Adhesion studies were conducted on an Instron Model 1128 load-test
machine, which is normally used on tensile specimens. It was equipped
with threaded fixtures for attaching samples to the crosshead drive, so
the easiest way to make pulling grips was to fabricate them from bolts.
After machining off two bolt heads and gluing one shank to the tin layer
and the other shank to the steel backing, the pulling grips could simply
be screwed into the Instron fixtures. Standard quarter-inch bolts were
selected, since several coatings were barely wider than this diameter.

Of course, the glue used to attach the pulling grips must be stronger
than the tin-steel bond. Numerous epoxy-based formulations are capable of
high bond strength, but relatively few of these epoxies are designed to
chemically react with metal surfaces. Consequently, a miniature project
had to be undertaken to evaluate commercially available adhesives for
purposes of satisfying Phase I adhesion measurement objectives.

81

Seven different epoxies were tested in this exercise. For each test, an uncoated strip of low carbon steel was cleaned and roughened by grit-blasting with Number 30 alundum. After epoxy was applied, each strip was sandwiched between the machined-off, grit-blasted surfaces on two bolt shanks. When the epoxy had cured, the steel strip was trimmed with Dremel Tool cuts down to the quarter-inch shank diameter, so the Instron tension loads would be distributed over exactly 0.049 square inch of bonded area.

Only one epoxy survived beyond a 58-pound load (1200 psi)--Scotch-Weld No. 2214 Nonmetallic Adhesive (3M Corp.). The sample epoxied with this formulation exceeded the 200-pound load cell capacity, and a later effort established a bond strength to grit-blasted steel of at least 11,000 psi. This value is five times the 2100-psi tensile strength of wrought tin, so this epoxy would certainly surpass tin-on-steel adhesion.

The Scotch-Weld epoxy had to be cured under compression for 1 hour at a temperature of 120°C. Ordinary C-clamps were used to hold the bolt shanks against steel surfaces while curing, as well as during later trimming. However, no means were devised to consistently tighten the clamps, and this caused considerable difficulty on actual coated samples. In practice, over-tightening would occasionally cause samples to buckle and delaminate while curing, such that bond separations occurred before load-testing. In one instance, most of the epoxy was squeezed out of the joint, resulting in a peel-type test with gradual failure at low tension. Corrective actions would have been implemented early on, but the exact source of the sample damage was not diagnosed until late in Phase I.

Ultimately, performance conclusions could only be based on two-thirds of the prepared adhesion samples. As discussed below, the premature failures were apparently concentrated among samples with relatively weak bonds, while surprisingly strong adhesion was definitely observed in many cases. Thus plenty of samples were correctly prepared and successfully tested for confirming the feasibility of spraying high-quality coatings. Although Phase I objectives were not compromised, this difficulty focused considerable attention on the practical aspects of performance testing. Appropriate activities will be devoted toward developing reproducible sample preparation techniques early in Phase II.

The load arms were not thoroughly tightened when each adhesion sample was screwed into the Instron attachments. That is, some slack always existed that had to be taken up by the crosshead drive before significant tension was applied to a sample. The crosshead drive was deliberately set at the slowest speed available--0.002 inch/minute--to prevent abruptly tearing a sample apart. At this speed, however, 10 minutes or more could elapse before a test would begin in earnest. In the figures that follow, this effect artificially displaced all of the load test plots in time. These arbitrary time lags could have been removed after the strip-chart recordings were digitized, but it conveniently separated the plots for overlay comparisons and thus aided in visualizing the data.

Load-test plots from the first specimen set (on radially grit-blasted steel sleeves) are presented in Figure 50. As mentioned in the bend test discussion, all of these samples were sheared, so sectioning damage may have been primarily responsible for pre-test failures on four of the nine samples extracted. In any case, the three 150 RDL samples exhibited very similar testing behavior, with sharp transitions upon load application and nearly identical slopes. No significant difference was found from base metal preparation, since Sample 1 was deposited on a region peened with glass beads, while Sample 5 straddled bands blasted with coarse alundum. Sample 4 failed at a lower load than Sample 5 (36 versus 61 pounds, 735 versus 1245 psi), although spraying conditions were quite similar.

The two 153 RDL samples tested straddled the bands peened with glass beads and blasted with fine silica grit. However, their behavior was markedly different from Sample 150 RDL-1. Not only did they fail at much lower loads, but the slope transitions upon load application were gradual. The cause of this anomalous performance is unclear for Sample 153 RDL-1, but the C-clamp on Sample 2 was definitely over-tightened, squeezing out most of the epoxy. What remained was attached to opposite corners, and the coated sample bent into an S-shape when pulled, later peeling from a grip shank at one end. The tin coating and base metal never delaminated.

Recall that the 153 RDL experiment yielded a much thicker deposit than 150 RDL, due to slower sleeve speed. Unfortunately, no valid conclusions can be drawn on relative adhesion merits, with such suspect 153 RDL data.

83
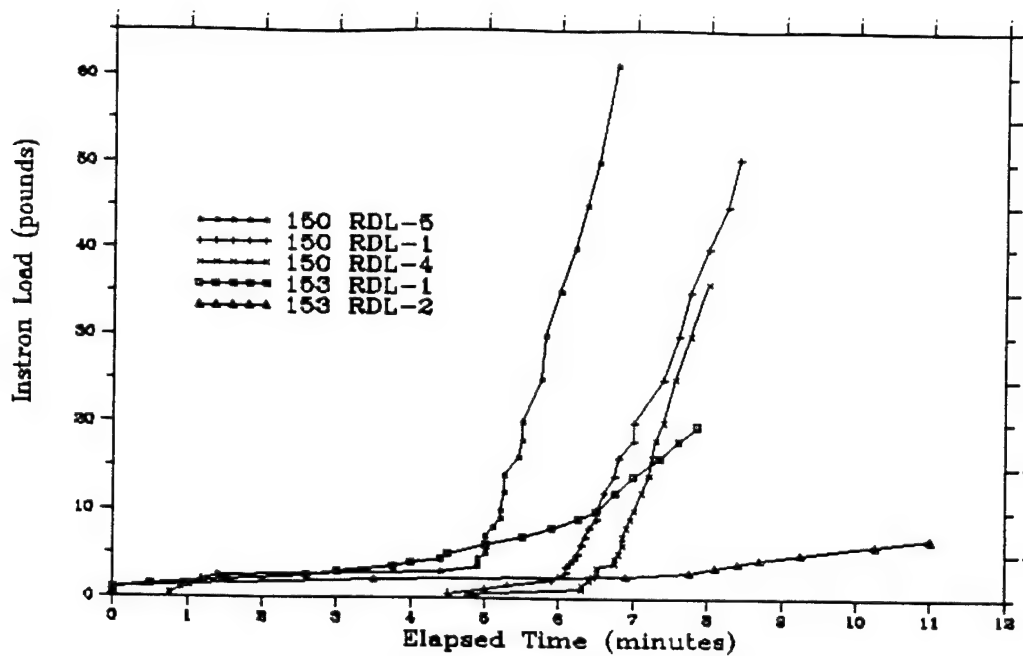
Figure 50.   Adhesion Tests on Radially Grit-Blasted
             Sleeve Specimens.
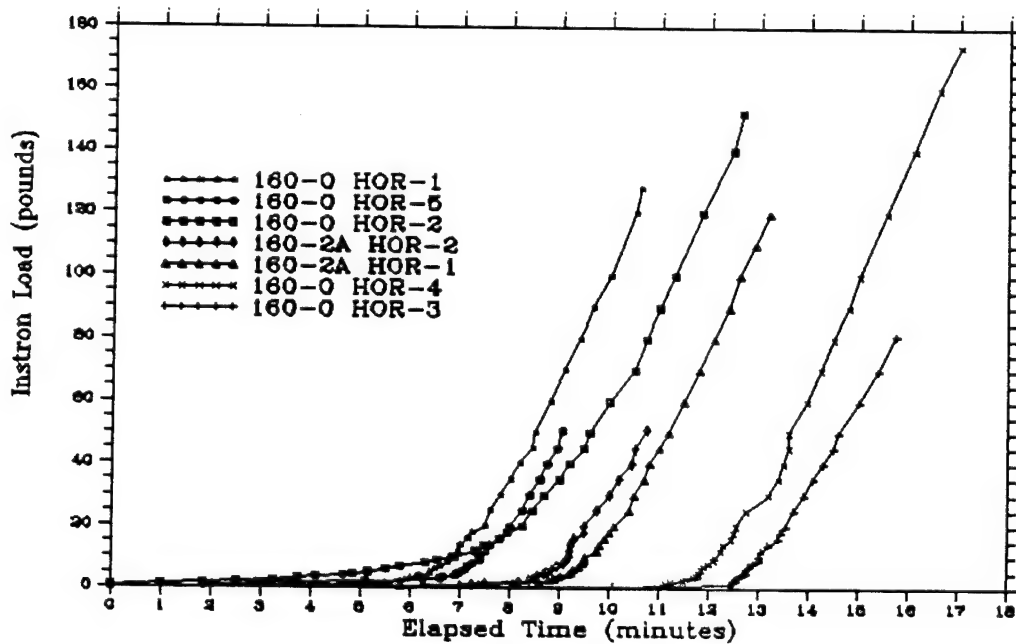
Figure 51.   Strong Adhesion Results from Wide Coatings
             Sprayed onto Steel Sleeve with Horizontal
             Grit-Blasting Pattern.

84

The best overall adhesion results are displayed in Figure 51. These samples were sectioned by Dremel Tool cuts, and all are from wide coatings deposited under cool conditions. All of the plots show sharp transitions in slope when slack was removed, as with the 150 RDL samples--although the maximum load values achieved here were much higher in all but two cases. Some preparation damage may have occurred, but the fact that none of this set failed prematurely is highly significant. That is, coatings with the largest adhesion strength seemed to be most resistant to C-clamp buckling.

After division by the trimmed 0.049 square-inch cross-sectional area, four of the samples in Figure 51 exceeded the 2100-psi tensile strength of wrought tin. One of these samples (160-0 HOR-1, 2600 psi) was extracted from the thin (0.001 inch) molten layer smeared by the preheater, which simulated a hot-dipped tin coating. Here the 500 psi of extra strength was caused by epoxy penetration of pinhole perforations in the tin layer, which were later found during a cursory metallographic inspection. The tin had been smeared over an area blasted with coarse grit--filling in the valleys on the steel sleeve surface but not covering the taller peaks--so epoxy bonded the grip shank directly to the base metal at these positions.

By contrast, the remaining three strong samples were normal sprayed coatings--much thicker, well consolidated, and absent of any perforations. Samples 160-2 HOR-2, 160-0 HOR-4, and 160-2A HOR-2 delaminated at 3100, 3545, and 2440 psi, respectively. In these three cases, the tin layers would probably have failed at lower loads without the benefits of rapid solidification (small grain size and no impurity segregation). Grit sizes had no influence on bond strength, since Sample 160-0 HOR-4 was roughened with fine silica, while coarse Number 46 alundum was used on the others.

The last three samples tested poorer. Bits of tin were found on the base metal on Sample 160-2A HOR-1 (1040 psi), so the coating partially ruptured instead of delaminating. Sample 160-0 HOR-3 (1650 psi) was over a region blasted with coarse Number 30 grit, and its strength should have been close to Sample 160-0 HOR-2; the likely cause was damage by excessive clamp compression. Sample 160-0 HOR-5 was from the same parent section as 160-0 HOR-4, cut later to confirm preparation damage. Deliberately over-tightenening the C-clamp dropped adhesion strength 70 percent to 1030 psi.

85

Results from the remaining three adhesion samples in the second set of coating specimens are presented in Figure 52. All three were sectioned from narrow coatings with partially or mostly molten surfaces from being deposited close to the nozzle exit with relatively high mass and thermal fluxes delivered to the base metal. All three failed at very low Instron loads, by comparison to samples in Figure 51. Of equal significance is the fact that three companion samples (including two from 160-3A HOR) fell apart when the C-clamps were removed. That is, this sample subset was susceptible to preparation damage at about the same frequency as the first specimen set from the 150- and 153-RDL experiments. Furthermore, these adhesion samples were extracted with relatively delicate Dremel Tool cuts, rather than by shearing as with the first set.

Of the three samples in Figure 52, SAmple 160-2B HOR-1 failed at the highest load value--10.8 pounds, or 220 psi. The coating here had a shiny, incipient melting appearance unlike the dimpled, faceted surface observed in 160-2A HOR and earlier experiments. Its companion sample, 160-2B HOR-2, failed at a low 3.8-pound load, evidently indicating significant preparation damage. The remaining sample from the 160-3B HOR experiment represented a molten tin layer, where the deep pool was pushed sideways by incident nozzle gas to form two parallel ridges. Intermittent transverse ridges also formed between major lateral ridges. This effect was less pronounced in the 160-3B HOR experiment than in 160-3A HOR, which may explain why one of the two samples escaped delamination during sample preparation, whereas neither sample from 160-3A HOR could be load-tested.

Grit size used during base metal preparation appears to have had some influence in the limited case of partially or mostly molten coatings. All three of the samples in Figure 52 represented coatings on surfaces blasted with coarse Number 30 and Number 46 grits. Meanwhile, all coating samples extracted from the fine Number 240-grit regions on all three experiments detached completely during the initial sectioning process. It thus seems that very rough surfaces are required to anchor molten coatings to even a tiny extent. This may mean that such layers warp from differential thermal stress while cooling, especially if the thickness is uneven from ridging. This hypothesis will be explored later in greater detail in connection with metallographic investigations.

86
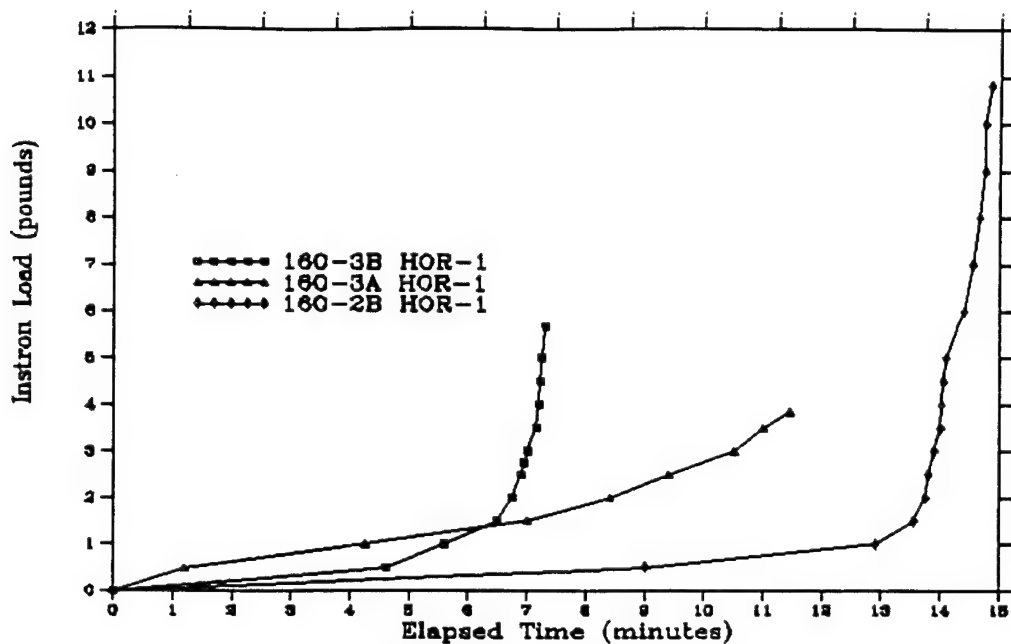
Figure 52.   Relatively Weak Adhesion from Narrow Coatings
Sprayed onto Horizontally Grit-Blasted Steel   .
Sleeve.
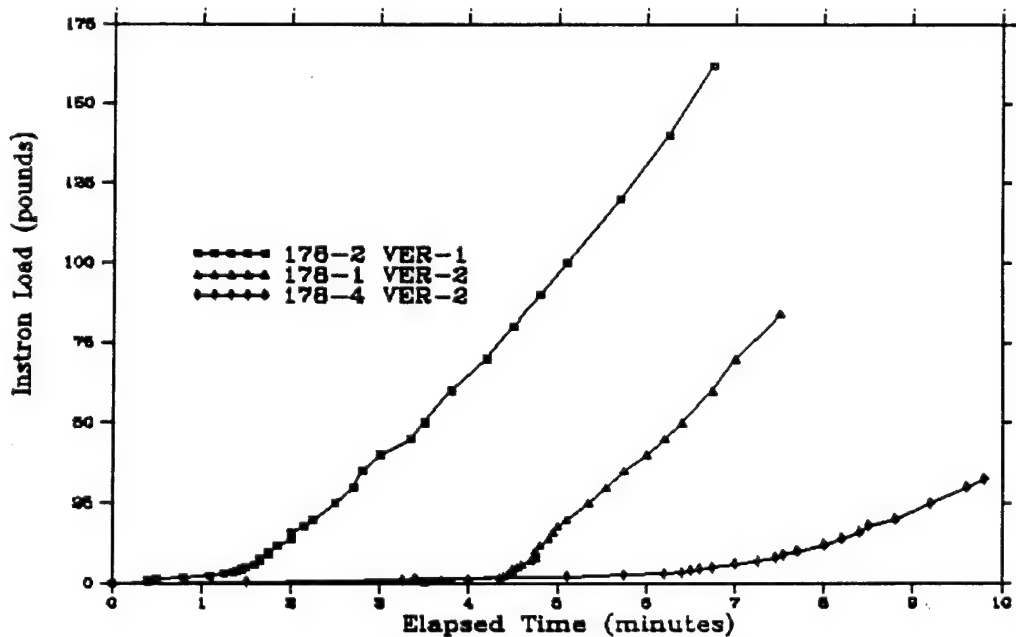
Figure 53.   Adhesion Test Data from Vertical Strip Specimens.

Adhesion test data from the flat steel strips coated in the 178 series of experiments are given in Figure 53. Only three plots are shown, since four of the seven samples failed prematurely from improper preparation. This unfortunately included the two samples representing thin molten coatings without ridges. However, the postulated damage mechanism of buckling under excessive clamp compression was more than conjecture for this third specimen set. In two cases, buckling was sufficiently severe to cause misalignments over 10 degrees between the opposing grip shanks. These observations forced the direct comparison between the two adjacent Samples 160-0 HOR-4 and 160-0 HOR-5 mentioned earlier, which finally confirmed C-clamp pressure at curing temperature as the source of damage.

Sample 178-2 VER-1 failed at a surprisingly high load of 162 pounds, which converts to 3300 psi. This result was not expected, because the sample was taken from the molten ridged region on this specimen and such areas produced very weak adhesion on 160-3A and 160-3B HOR samples. The anomaly was later explained during a cursory inspection of the companion metallographic sample, when numerous areas of bare steel (much bigger than pinholes) were seen between the ridges. Consequently, the high strength largely reflects epoxy bonds between the steel strip and steel grip shank.

Sample 178-1 VER-2 produced a respectable failure load of 84 pounds, or 1500 psi. This sample represents a 0.004-inch thick tin layer coated without preheating. As such, it is similar in origin to the 160-2A HOR samples, where Sample 1 failed at 1040 psi and Sample 2 delaminated at 2440 psi. Like Sample 160-2A HOR-1, this sample left small bits of tin attached to the steel base metal, so the tin layer evidently ruptured here, too. In this case, mid-layer porosity was discovered at an isolated location on the companion metallographic sample. (See Figure 65.)

Sample 178-4 VER-2 was from the 0.016-inch thick coating deposited at a slow speed over the unheated portion. It delaminated at a low strength value of 545 psi, as compared to samples with a similar coating thickness from the 150 RDL and 160-0 HOR experiments that were preheated. However, it was much weaker than unheated Sample 178-1 VER-2, as well, so sample preparation damage is most likely responsible. Metallography (Figure 65) shows no interfacial porosity from poor wetting of the cool steel surface.

88

E. METALLOGRAPHIC INVESTIGATIONS

Small sections were cut from all parent specimens for metallographic studies, and each one had a transverse orientation such that variations could be assessed across the width of a coating. This orientation was selected for determining any differences between the deposit center and edges in terms of porosity, interfacial matchup, surface roughness, and thickness uniformity.

Substantial coating porosity from incomplete consolidation of metal droplets would be detrimental to strength, hardness, wear resistance, and other mechanical properties. Any interconnected porosity would be particularly harmful wherever corrosion resistance was essential, since direct pathways to the base metal would be open to attack by aggressive chemical species. In addition, porosity collected along the coating/base metal interface would reduce mechanical bonding and weaken adhesion strength. That is, with rapidly solidified sprayed coatings, droplets at the leading plume portion must consolidate almost perfectly against a grit-blasted base metal surface, wetting this interface and interlinking with roughened features there, in order to adhere strongly without high-temperature metallurgical bonding.

Roughness on a coating exterior and coating thickness uniformity are both of interest from the standpoint of subsequent grinding or machining--either to achieve dimensional tolerances or to polish a coated surface for better reflectivity or for reduced friction and less wear. In many cases, a uniformly thick coating with minimal roughness would be preferred, since relatively little deposited metal would have to be removed. In certain applications, however, some residual roughness would be desired to enhance paintability or to anchor lubricating films.

It also should be recognized in advance that the circular geometry nozzle used in this feasibility study sprays deposits with thinly tapered edges, where the extent of crowning is governed by the nozzle exit cone, nozzle-to-base metal distance, etc. In actual practice, the large-scale, rectangular version of this nozzle design (slot-shaped throat and multiple liquid orifices) would likely be adopted for spraying broad flat coatings.

Preparation of metallographic samples proved to be more challenging than anticipated. As with the adhesion test samples, shearing of the early metallographic sections frequently caused them to separate along the edges prior to mounting. This damaged region was removed in some cases by grinding deep into the mount, but this problem was not resolved adequately until sectioning was performed with more delicate Dremel Tool cuts. Even then, widely separated once-bonded regions were occasionally found.

Even more difficulty was encountered in grinding and polishing the samples for simultaneous examinations of bulk porosity and interfacial matchup. Standard techniques for steel samples using disks impregnated with diamond and silicon carbide grit not only removed the softer tin layer preferentially, but prohibitive amounts of these grits smeared into the tin--appearing round and dark on photomicrographs, much like porosity. This soft coating-on-hard base metal situation forced a lengthy effort to develop a custom grinding and polishing procedure. Ultimately, acceptable results were produced with a wet slurries of alumina powder in steadily decreasing size ranges, although this process was very time-consuming.

Because of the above problems, not all of the metallographic samples sectioned could be examined in detail. In the following figures, samples from the first two specimen sets generally include those best suited for metallography--especially where both the steel-tin interface and the bulk tin coating were within the metallograph's limited depth-of-field. Those samples relatively free of sectioning damage were also given preference to study interfacial bonding. Similarly, anomalous areas such as the region smeared by heater contact and the "running globule" merely received brief visual inspections to explain adhesion behavior. Studies on vertical strip specimens were confined to those with successful adhesion tests.

This sample selection was sufficient to facilitate understanding the spray-coating process, although it did not constitute fully randomized coverage. Similar subjectivity was employed in detailed examinations of each individual metallographic mount. High-magnification photomicrographs on sample cross sections were typically taken to investigate distinctive features and to quantify porosity extremes, rather than to establish a statistically representative assessment of normal porosity distributions.

90

Figure 54 shows Sample 150 RDL-1, which was sectioned from the coating segment deposited on the outer sleeve band peened with glass beads. The composite photograph of the sample cross section reveals a thickness taper from approximately 0.010 inch over the upper portion to 0.003 inch near the bottom. where the constant 0.010-inch thickness of the steel base metal serves as a convenient reference. (The curved pieces at the bottom are from a spring clip, which holds the sample perpendicular to a mold base that contains the mounting epoxy during pouring and curing.) The coating thickness appears asymmetrical in this cross section because the droplet plume was not centered perfectly on the glass-beaded band and part of the plume width missed the sleel sleeve.

All photomicrographs were converted to digital records by optical scanning at a resolution of 200 pixels per inch. This process blurred contrast slightly on low-magnification images, because a pixel appears to be gray whenever it straddles a black-to-white boundary. This tended to exaggerate indentations along the exterior coating surface in the 23X composite. Nevertheless, the actual surface roughness was 0.004-inch deep in the worst locations, and it was independent of underlying thickness. So at least 0.004 inch of coating must be removed for a smooth surface.

In the low-magnification composite the tin coating appears to have separated completely from the steel base metal, but this is an illusion related to preferential grinding of the interface and creation of a shadow there, which was subsequently exaggerated by the digital scanning. This effect becomes insignificant at higher magnifications, and the two 268X micrographs reveal that most of the tin is immediately adjacent to steel. Minor interfacial separation is still evident in both images. However, this can be attributed primarily to shearing damage, because the tin contour matches that of the steel and the two sides of the interface must have been in close contact at the time of deposition. Yet, the contours do not match perfectly, so some porosity was trapped at the interface.

Very low porosity values are listed beneath the two 268X images, but open surface roughness and interfacial delaminations are not included. In each case the Bausch & Lomb Omnicon image analyzer was manually directed to sum dark areas within a rectangle covering solely the bulk tin layer.

Polishing Grit

A. Excellent Interfacial Matchup,
   0.10 Percent Porosity, 268X

B. Incomplete Consolidation,
   1.8 Percent Porosity, 268X

23X
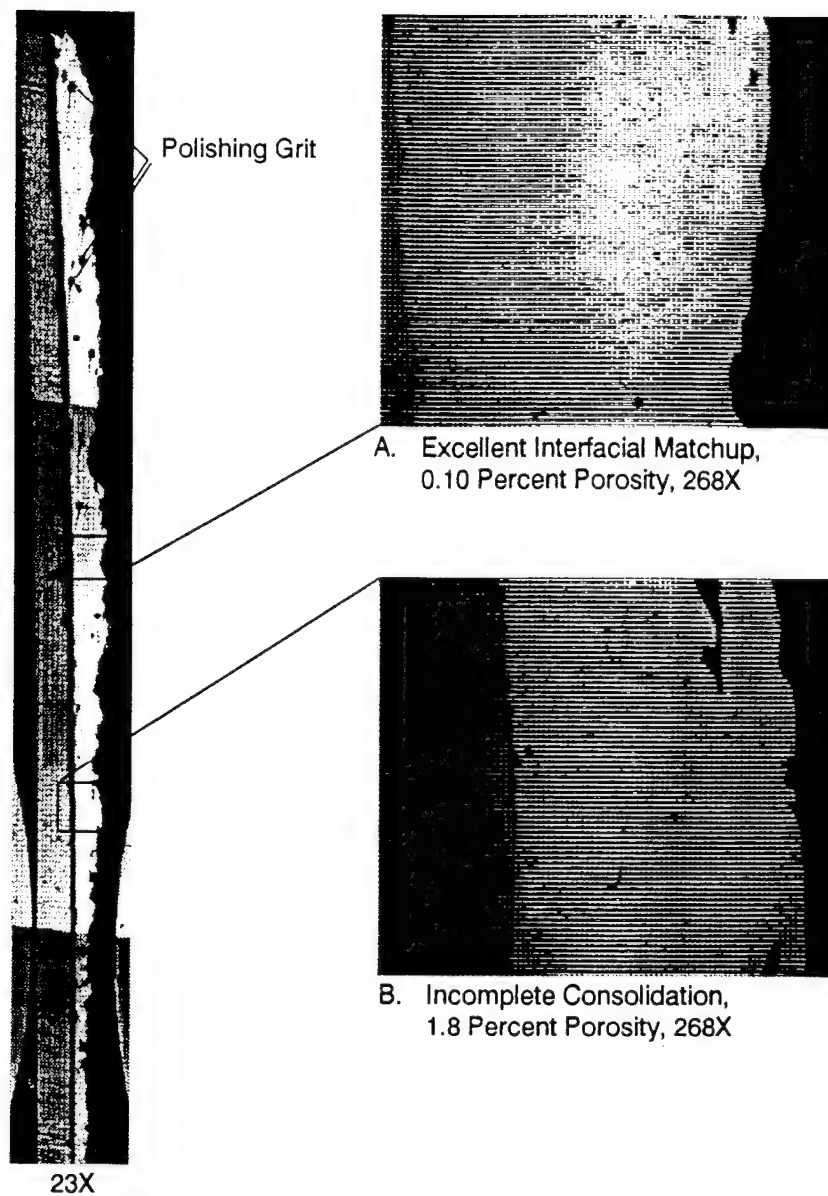
Figure 54. Sample 150 RDL-1 from Glass-Beaded Portion of First Tin-Coated Carbon Steel Sleeve with a Radial Grit-Blasting Pattern.

The full-thickness portion of Sample 150 RDL-4 is shown in Figure 55. This sample is from the third coating segment, which straddled the band boundary between coarse Number 46 and Number 30 grits. Here the average coating thickness was 0.012 inch due to briefly spraying at 23 psia, so more tin was aspirated than at the normal pressure of 24 psia for this experiment. Indentations on the outer coating surface are still up to 0.004 inch deep, and measurements of bulk tin porosity remain negligible.

The main difference from Figure 54 is that the tin layer clearly has been separated from the steel at most locations. Here grinding was not able to remove much of the shearing damage. Yet, inspection of the high-magnification micrographs demonstrates that the incident tin droplets did fill in nearly all of the rough steel surface from coarse grit-blasting, where crevices like that at the top of Image B were up to 0.001 inch deep.

A sample extracted nearby on the third coating segment is displayed in Figure 56. The coating thickness over the middle of the deposit width is back to 0.010 inch, as a consequence of returning to a 24-psia operating pressure on the spray nozzle. More significantly, grinding of this mount eliminated any distinctive shearing separations, so interfacial porosity could be studied accurately here. The tin-steel interlinkage is nearly perfect in Image A, although the tin next to the steel contained several microcracks--presumably caused by shearing. By contrast, mechanical bonding was noticeably poorer at the Image B position--the worst case of localized interfacial porosity observed on Sample 150 RDL-5. Instead of the porous area in the micrograph, the relevant quantity is the unbonded fraction of the interface--which can be estimated here at 36 percent. Local adhesion strength would be reduced by a corresponding amount.

Sample 153 RDL-1 was extracted from the second coated steel sleeve prepared with a radial grit-blasting pattern. This sample was taken from the outer circumferential pass, where the 1-inch wide coating straddled the bands peened with glass beads and blasted with a mixture of fine silica grits. After grinding and polishing, no shearing delamination was observed anywhere on this sample. Accordingly, bulk porosity extremes and interfacial matchup were explored in detail over both bands, and coverage of the central region of this sample requires more than a single figure.

A. Residual Bonding, 0.13 Percent Porosity, 200X

Polishing Grit

Pore

B. Residual Bonding, 0.02 Percent Porosity, 200X

Pore

23X
Polishing Grit

C. Interfacial Separation, 0.02 Percent Porosity, 200X
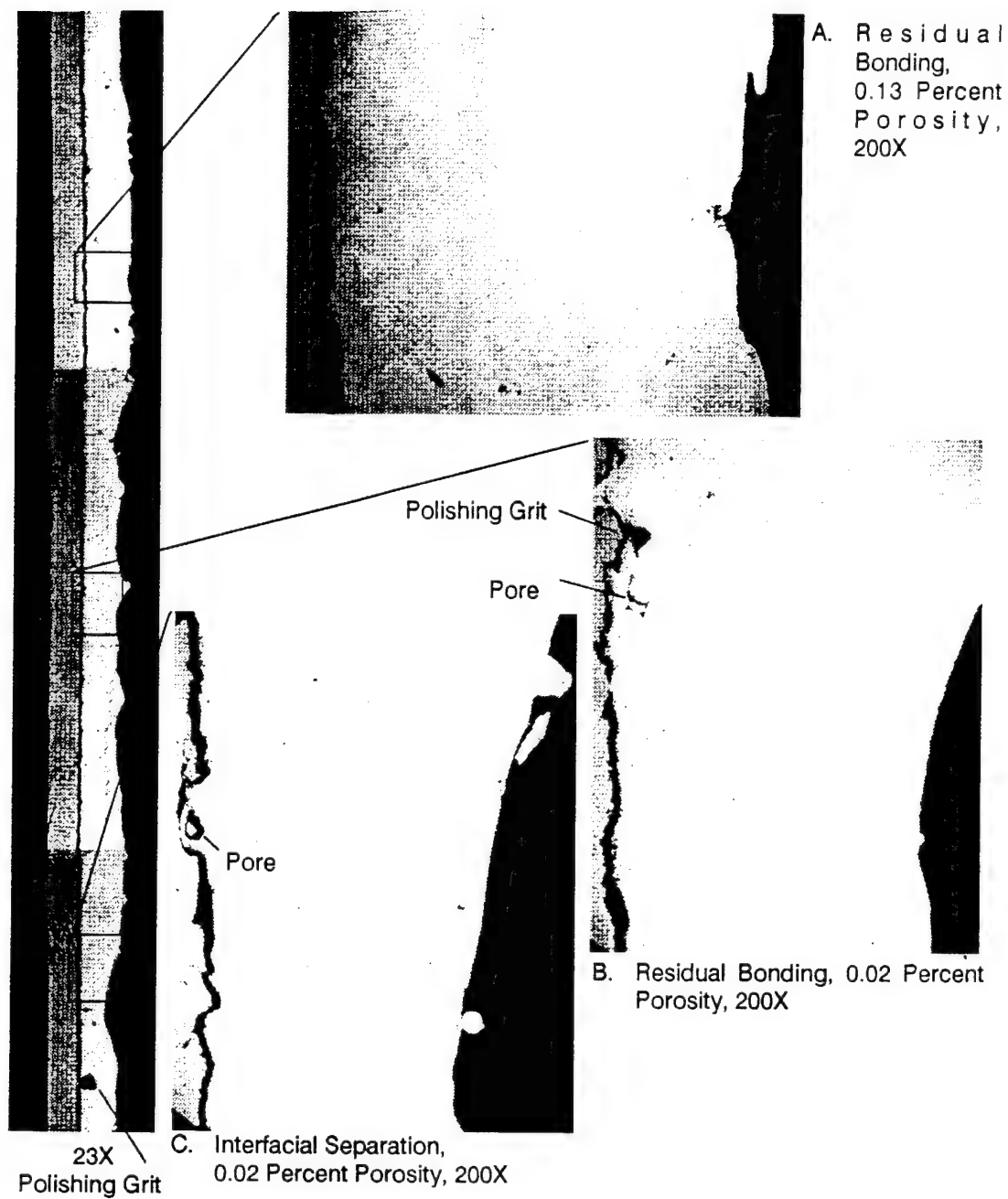
Figure 55.   Shearing Damage on Sample 150 RDL-4, from First Radially Grit-Blasted Steel Sleeve.

94

23X

A. Microcracks at Interface, 0.0 Percent Porosity, 168X

B. Interfacial Porosity, 0.0 Percent Bulk Porosity, 200X
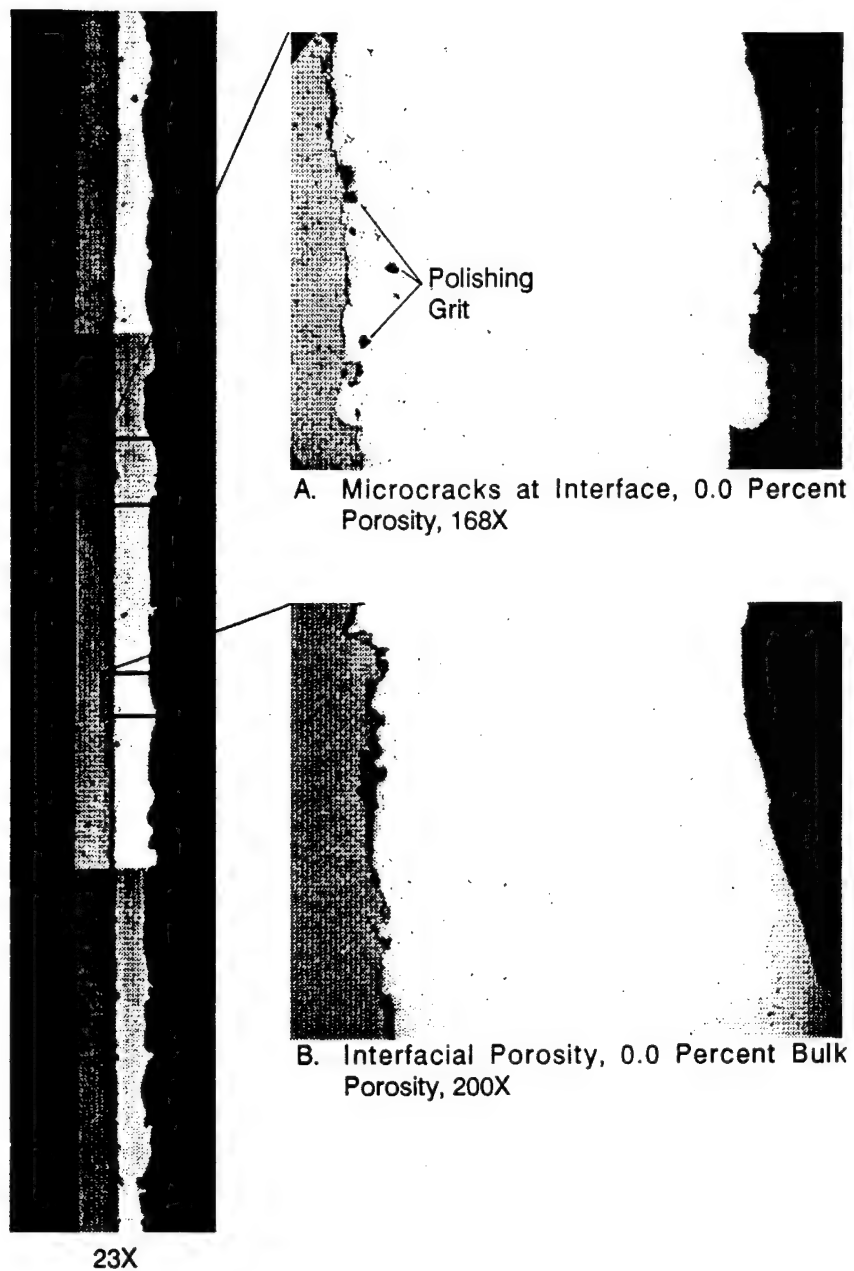
Figure 56.   Sample 150 RDL-5 from Number 30 Grit-Blasted Portion of First Tin-Coated Carbon Steel Sleeve.

Figure 57 shows the thicker portion of Sample 153 RDL-1 deposited on the finely grit-blasted band. (The thin tapered region was very similar to the 150 RDL samples.) Tin thickness in the composite photomicrograph increases from 0.015 to 0.025 inch, the goal for the slower base metal speed in the 153 RDL experiment. The smooth transition reflects the broad Gaussian mass distribution in the spray plume. The depressions in the outer tin surface are still in the 0.003- to 0.004-inch range, as with the 150 RDL coating. Since nebulizer operating parameters were similar in the two experiments, this finding again confirms that surface roughness is dominated by spraying conditions rather than coating thickness.

The two 168X images in Figure 57 reveal nearly perfect consolidation of incident tin droplets. Image A displays the worst case of porosity found on this portion of the sample, which is totally insignificant from the joint standpoints of mechanical properties and corrosion resistance. Mechanical bonding was also ideal everywhere along the interface.

The above results were essentially unchanged in Figure 58, where the excellent wetting and consolidation behavior were not compromised by using glass beads to clean and slightly roughen the steel surface. However, a few pores were discovered in the tin layer, and the isolated area shown in Image B contained several pores in close proximity. This unique porosity cluster includes one at the steel boundary. Nevertheless, this worst-case region would not impair corrosion resistance--much less other desired coating properties--because the porosity is far from being interconnected.

Figure 59 contains the examination results from Sample 153 RDL-4 from the second circumferential pass, where tin was coated over bands blasted with coarse alundum grits. The exerior tin surface is more irregular than on Sample 153 RDL-1, although the spraying conditions were identical over this experiment. However, this particular sample was sprayed around the 175-second mark, where Figure 34 shows a brief base metal temperature rise when the eccentric steel sleeve was closest to the preheater. Turbulence from the preheater plume may thus have been responsible. Shearing damage is evident in places, but the interfacial matchup was typically good, as in Image A. Image B is over the gap between grit-blasting bands, which explains the local interfacial separation but not the external porosity.

A. Incomplete Consolidation, 0.37 Percent
    Porosity, 168X

Polishing
Grit

B. Normal Density, 0.24 Percent Porosity, 168X

23X
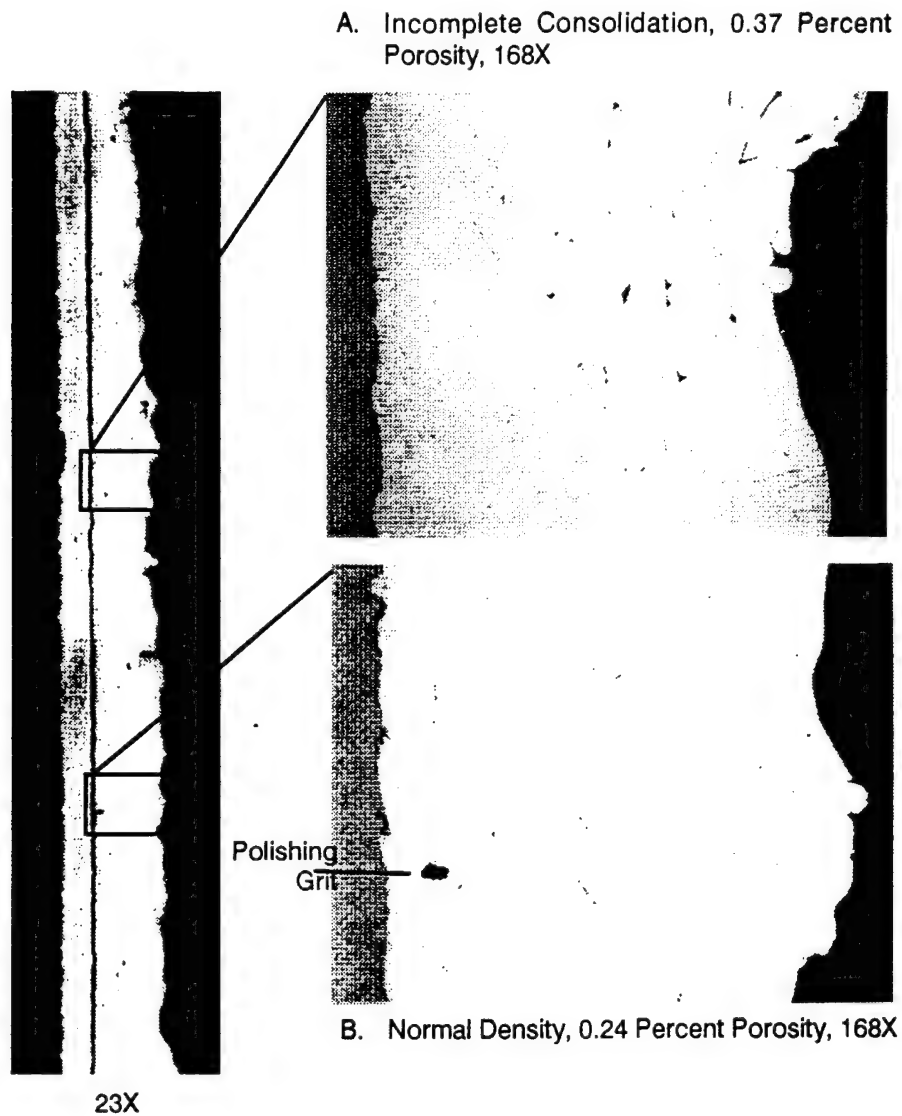
Figure 57. Representative Coating Structure from Left Side of Sample 153 RDL-1, where Steel Sleeve was
Blasted with a Number 60-120 Grit Mixture.

Polishing
Grit

Pore

Polishing
Grit

A. High-Density Region, 0.03 Percent Porosity,
    100X

B. Widely Distributed Pores, 1.38 Percent Bulk
    Porosity, 134X

23X
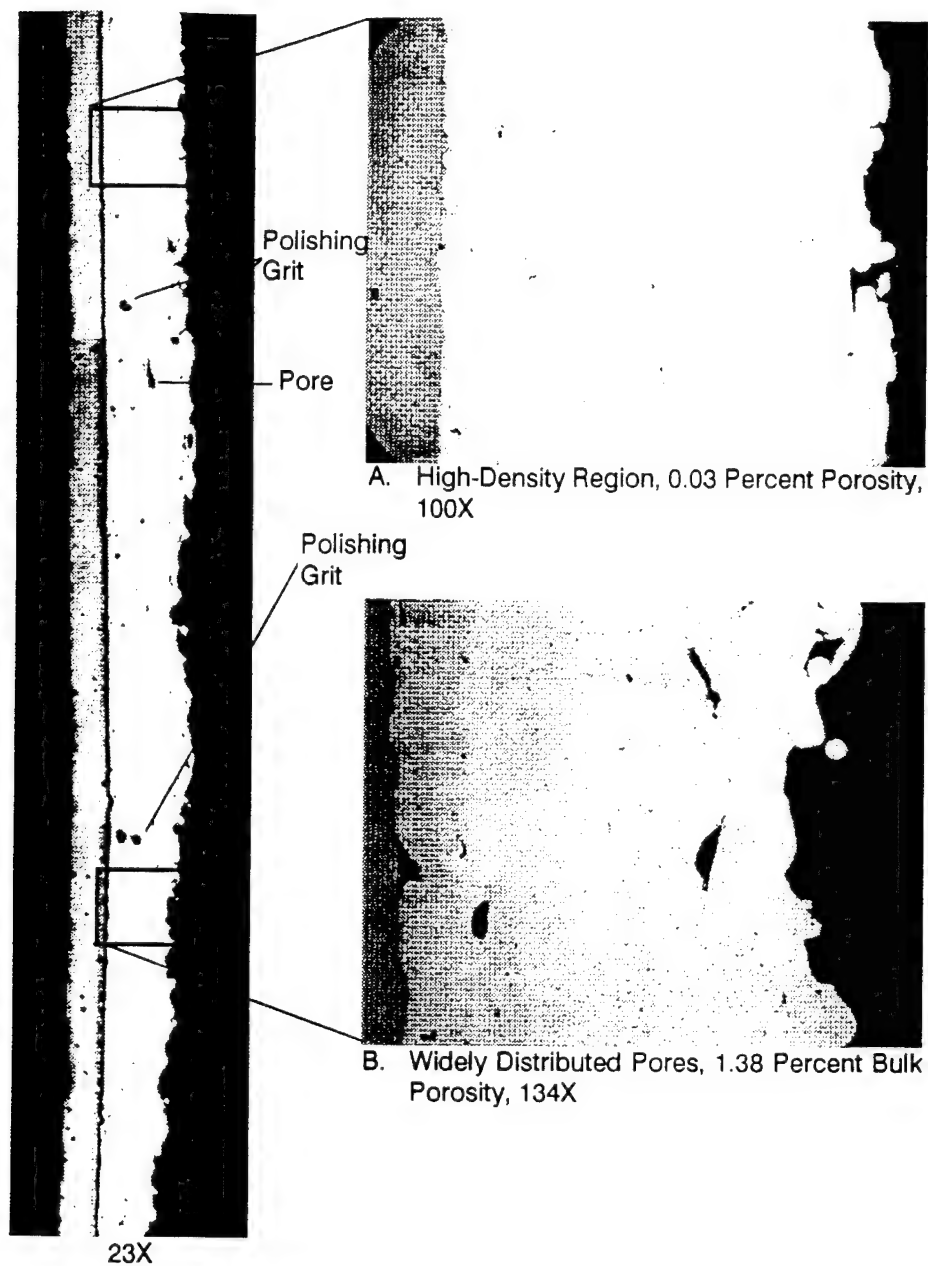
Figure 58. Porosity Variations on Right Side of Sample 153 RDL-1, where Carbon Steel Surface was
            Roughened by Glass Beads.

A. Normal Density, 0.14 Percent Porosity, 168X

Polishing Grit

B. Incomplete Outer Consolidation, 2.7 Percent Porosity, 168X

23X

23X

Separation from Sample Shearing
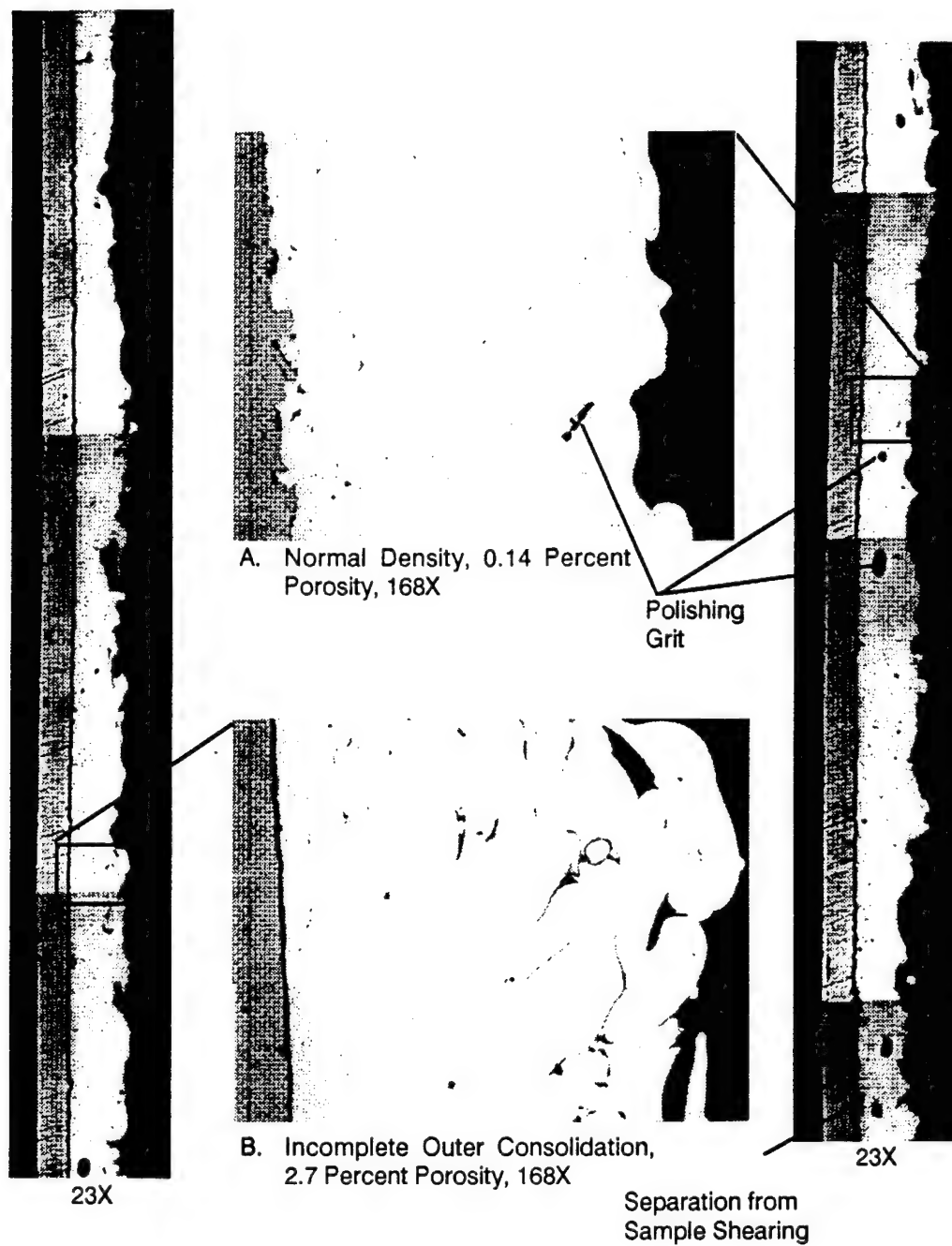
Figure 59.   Sample 153 RDL-4, where Left Half of Sleeve was Blasted with Number 46 Grit and Right Half was Blasted with Number 30 Grit.

The middle half-inch of Sample 160-0 HOR-2 is presented in Figure 60. Recall that this sample is from the first of five coatings sprayed around the circumference of a horizontally grit-blasted steel sleeve, and that this coating simulated 150 RDL conditions, including the base metal speed, nozzle-to-base metal distance, and nozzle operating pressure. This was also the only experiment in the 160 HOR series with base metal preheating. The coating thickness reaches 0.012 inch with identations up to 0.004-inch deep. The worst case of interfacial porosity is shown in Image A, but the tin-steel matchup was typically like the other two images--as required to account for the excellent 3100-psi adhesion strength on its companion. Bulk porosity in the tin layer was also very low, the only exception being the large outer pore in Image B, which was probably open to the surface.

Whereas the carbon steel in Sample 160-0 HOR-2 was blasted with coarse Number 46 alundum, metal underlying the coating in Sample 160-0 HOR-4 was blasted with Number 240 silica. Yet, Figure 61 reveals no outstanding differences in cross-sectional coating appearance. Image A contains a wide delaminated area, but the tin and steel contours match well, so the inference can be made that Dremel Tool cuts also caused occasional sample damage. Furthermore, the companion's adhesion test yielded the greatest strength (3545 psi), which indicates that interfacial porosity was rare.

For the 160-2A HOR experiment the sleeve was moved from 3 to 2 inches from the nozzle exit, reducing total coating width to 0.7 inch--much of which is displayed in Figures 62 and 63 (same transverse cross-sectional view of Sample 160-2A HOR-2). Increasing the rotational speed to 3 rpm decreased deposit thickness at mid-width to approximately 0.004 inch. Meanwhile, removing the preheater tube and the associated turbulence from spray plume interference reduced surface depression depths to 0.002 inch.

The changes in deposition conditions had no adverse effect on wetting of the grit-blasted steel surface by incident tin droplets. The highly magnified images in Figures 62 and 63 contain no interfacial porosity, which accounts for the impressive 2440-psi adhesion strength on Sample 160-2A HOR-2. These micrographs also show incomplete consolidation at the low 66°C sleeve temperature--especially in Figure 63A. This explains the early 120-degree fractures on 160-2A HOR samples during bend tests.

100

A. Interfacial Porosity, 0.27 Percent
   Bulk Porosity, 268X

Polishing
Grit

23X

B. Poorly Consolidated Exterior,
   10.0 Percent Porosity, 134X

23X

Polishing
Grit

C. No Detectable Porosity, 235X
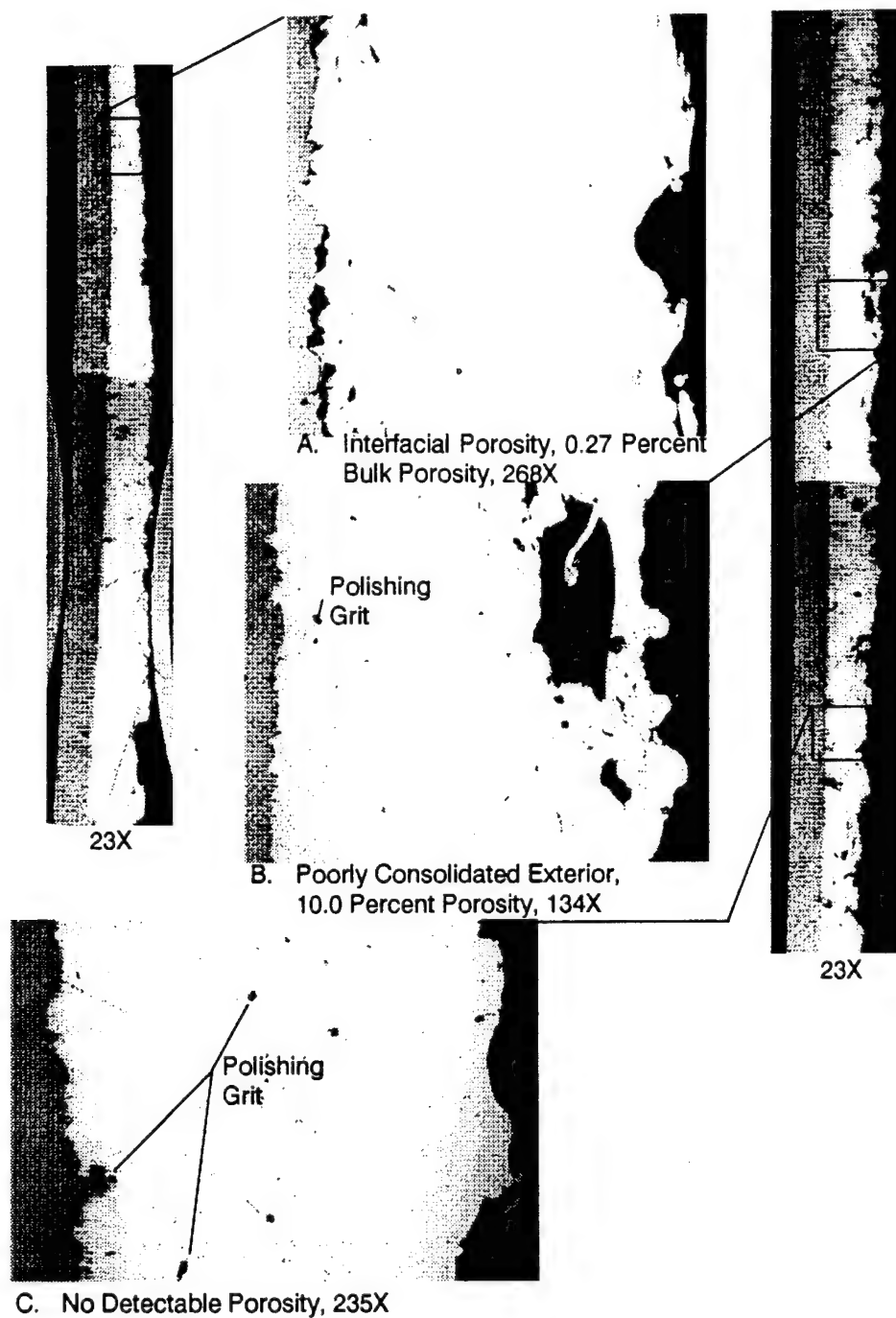
Figure 60. Porosity Variations from Edge through Middle of Sample 160-0 HOR-2, from Number 46 Grit-Blasted Portion of Horizontally Prepared Carbon Steel Sleeve.

A. Separation from Sample Extraction, 0.47 Percent Porosity, 200X

B. High-Density Region, 0.02 Percent Porosity, 200X

23X

23X
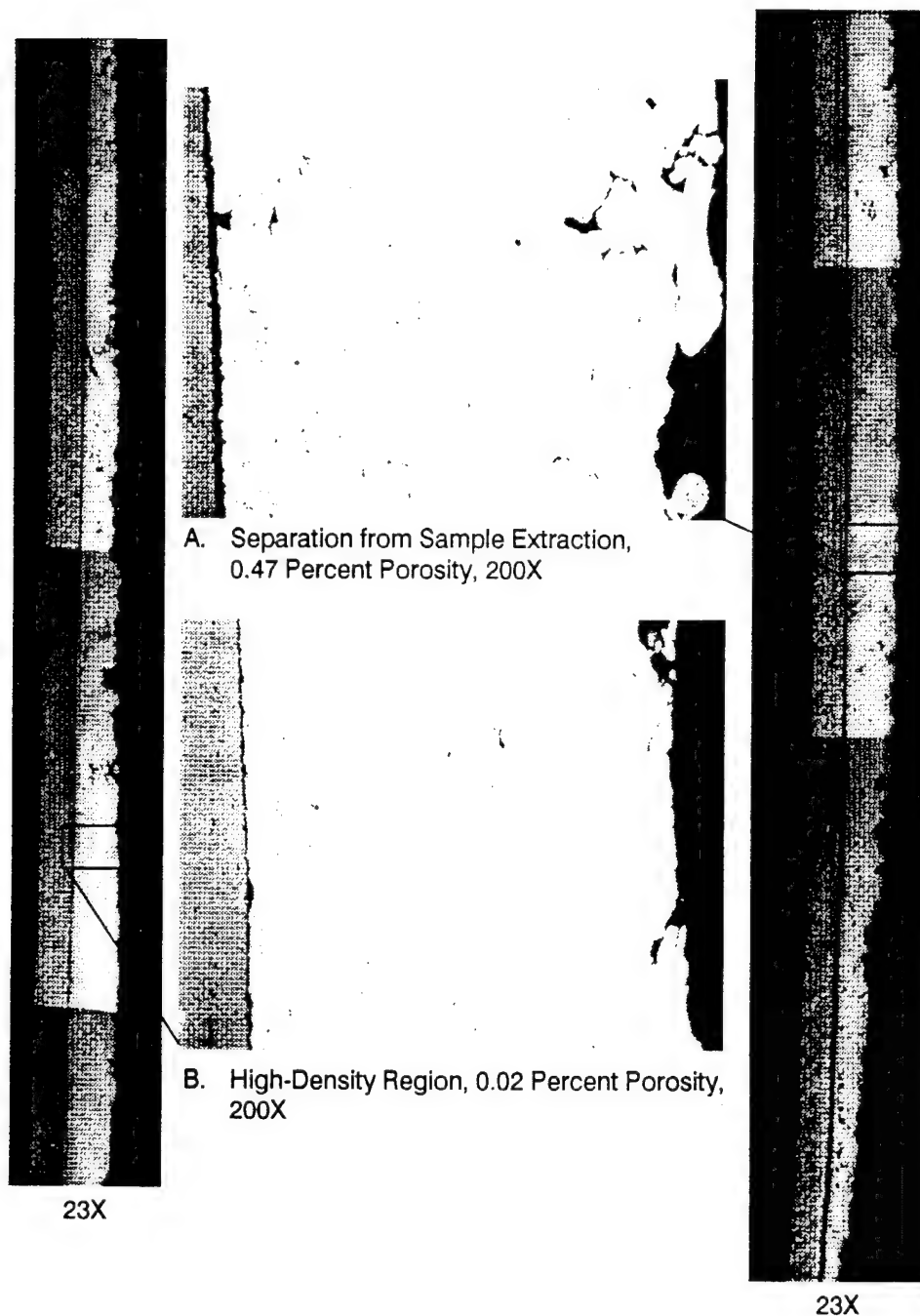
Figure 61. Characteristic Coating Structures from Full-Thickness Portion of Sample 160-0 HOR-4, Sprayed onto Number 240 Grit-Blasted Steel.

A. 0.004-Inch Thickness, 0.80 Percent Porosity, 268X

B. 0.002-Inch Thickness, 0.60 Percent Porosity, 536X

23X
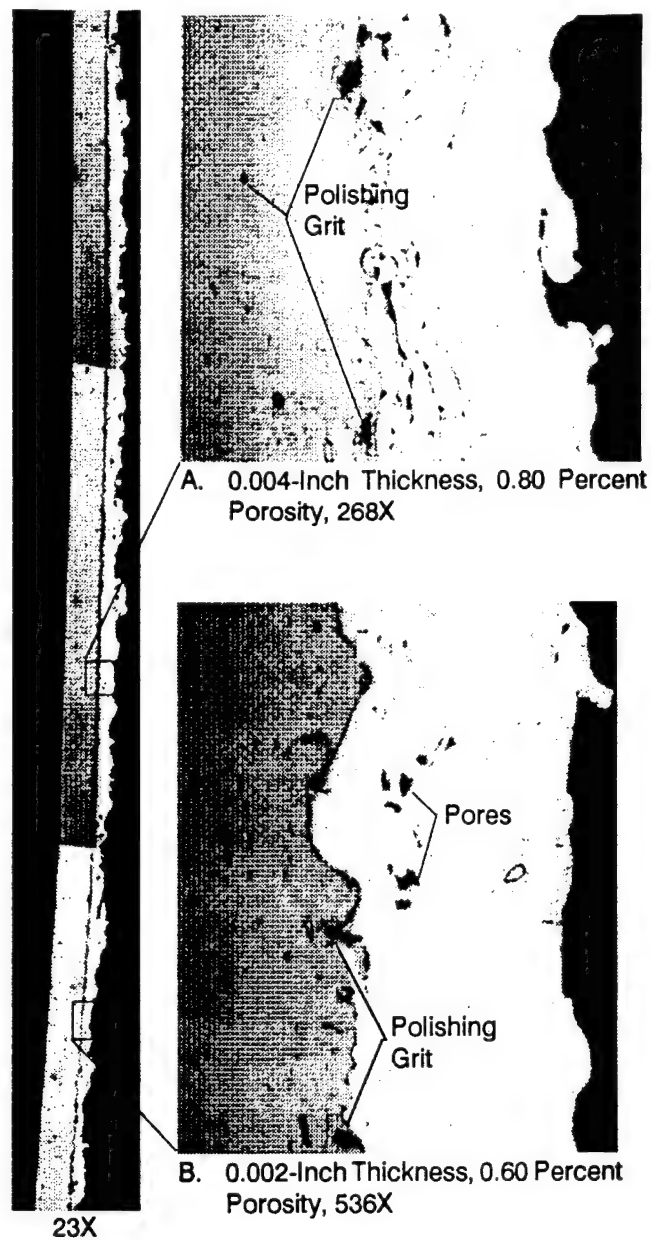
Figure 62. Average Porosity Regions on Sample 160-2A HOR-2, Illustrating Excellent Mating of Thin Sprayed Tin Layer to Number 46 Grit-Blasting Steel Surface.

A. 5.8 Percent Porosity, Including
    Unconsolidated Exterior, 268X

B. Nearly Complete Consolidation,
    0.25 Percent Porosity, 268X

23X
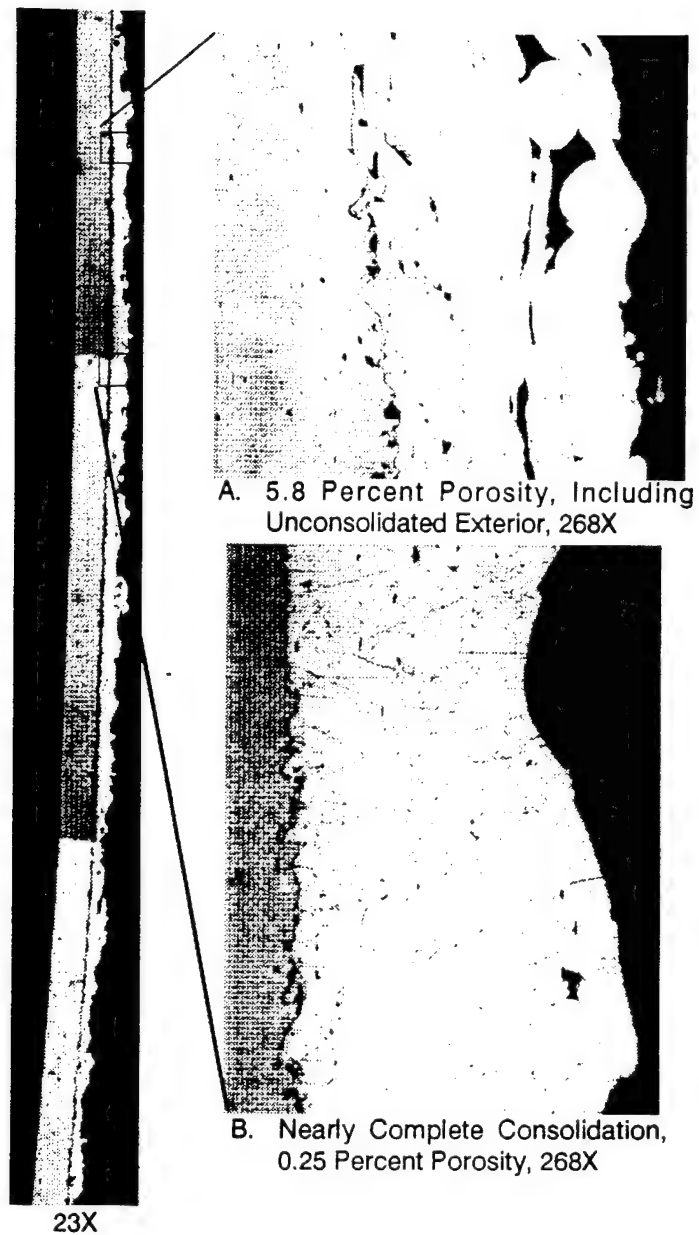
Figure 63. High- and Low-Porosity Regions on Sample 160-2A HOR-2, Showing Equivalent Mechanical
            Bonding.

The base metal was moved closer to the nozzle exit for the 160-2B HOR experiment, to a 1.2-inch separation that lowered the coating width to 0.45 inch. As indicated in Figure 64, the tightly concentrated plume increased the deposit thickness and also accentuated its Gaussian profile. In addition, the higher heat flux created a smoother, reflective coating surface here on Sample 160-2B HOR-1, which was referred to earlier as an "incipient melting" appearance. Surface roughness in the Figure 64 cross section is markedly reduced, with indentations only 0.001-inch deep.

Sample 160-2B HOR-1 exhibits a major interfacial separation along all of its length. The gap was more than wide enough for mounting epoxy to flow through it and later trap grinding and polishing grit. Although this sample yielded a weak 220-psi adhesion test, the separation very likely occurred during Dremel Tool cutting, since tin was found still bonded to steel at a few locations. Image A provides the best example of this, and it further reveals a local fracture parallel to the interface in the tin layer. Image B shows another case where a small piece of tin fractured free, but the nearby steel fragments were probably dislodged by grinding. Both images suggest that limited metallurgical bonding may have taken place here, despite the low 90°C base metal temperature recorded then.

Another interpretation of this fracturing behavior is more likely. Close inspection of Images A and C enables individual tin grains to be resolved, albeit barely after image digitization. Some porosity in all three images is from perceptible grain boundaries, especially in Image C. Grain sizes are in the 20- to 25-micrometer range in this sample, whereas the typically 10-micrometer grains in previous samples could only be discerned after chemical etching. (The etched microstructure photographed very poorly.) Therefore equiaxed grains grew here upon deposition due to the larger heat flux from the concentrated spray plume. Grains grow by movement of voids and dislocations, which also allows any impurities to segregate at tin grain boundaries, weakening intergranular coating bonds.

With this interpretation, the 160-2B HOR coating may have lost many benefits of rapid solidification. Wetting of the steel and bonding still occurred, so adhesion might otherwise have been good. But, attempting to induce metallurgical bonding in this way may have been counterproductive.

105

A. Tin Fracturing, 0.65 Percent Porosity, 268X

Steel
Fragments

Tin
Fragments

B. Interfacial Fracturing, 0.25 Percent Porosity, 200X

23X

C. Trapped Polishing Grit, 0.56 Percent Porosity, 268X
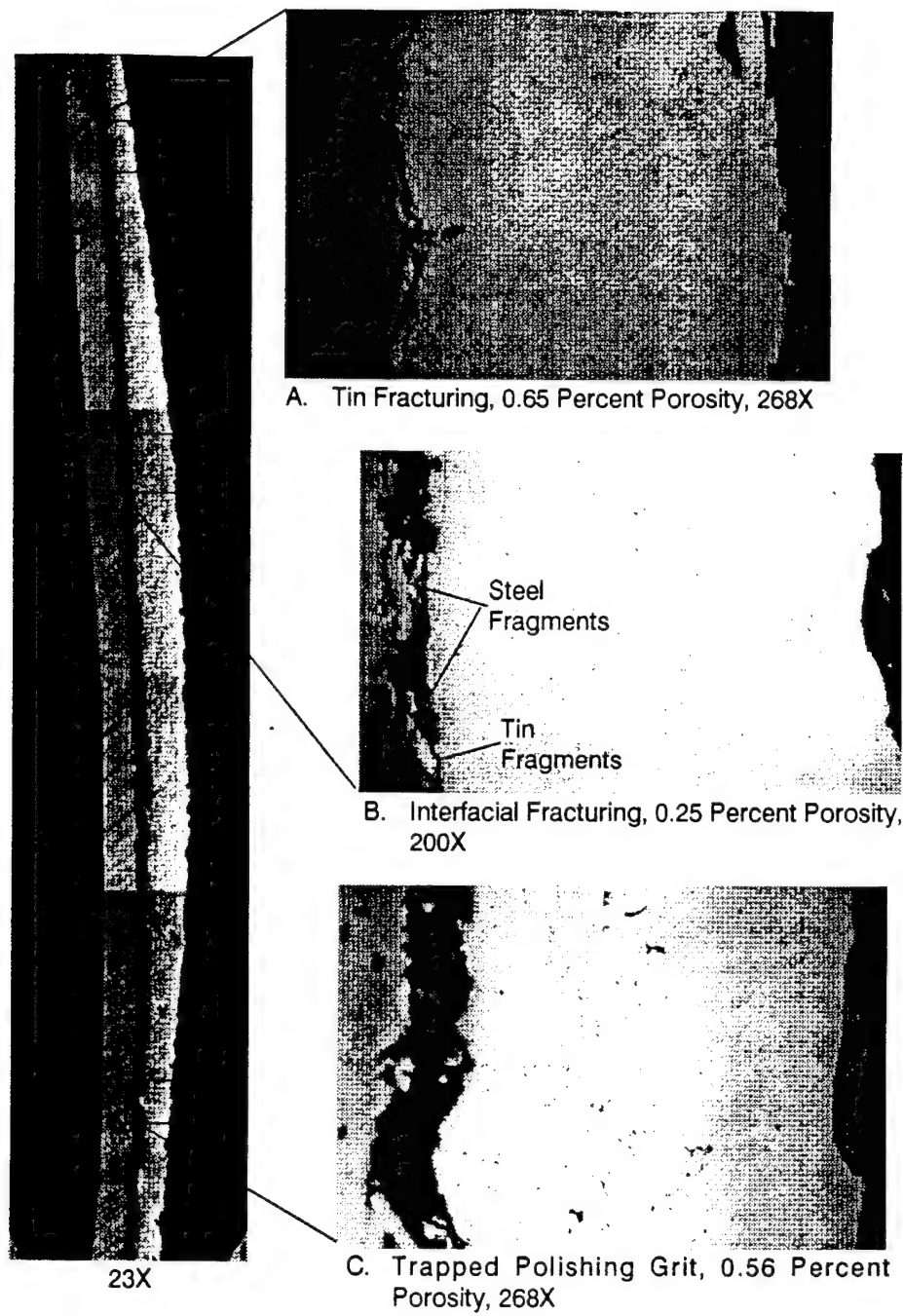
Figure 64.   Sectioning Damage and Polishing Grit Accumulation at Interface on Sample 160-2B HOR-1.

106

No examples of the fully molten, ridged coatings from the 160-3A HOR and 160-3B HOR experiments are presented here. Their highly nonuniform thicknesses included perforations in the tin layer all the way to steel base metal. Once-molten tin coatings were also very soft, and the problem with grinding grit smearing into the tin was never overcome on these samples. Consequently, the best views available were already shown in Figure 47 from the bend tests performed on their adjacent companions.

Nevertheless, visual examination of the metallographic samples did provide several important observations. Most significantly, the failure mode was very different from that seen in Figure 64. No tin remained attached to the steel and no intergranular fractures occurred. Instead, in all four cases the tin layer separated cleanly from the base metal, evidently during sectioning. In addition, the twin ridges pushed toward the sides by plume pressure were curved away from the base metal. This curvature may have happened during sectioning, but warping by differential cooling stress is more likely. That is, heat may have been conducted into the steel sleeve faster from the ridge edges than from the molten ridge interiors, whereupon thermal contraction could have pulled the ridge edges away from the steel, leaving relatively little tin in firm contact.

This differential thermal contraction possibility was noted already in connection with adhesion results, where only the ridged coatings over the coarsest steel surfaces were able to be load-tested after preparation of samples. Rougher surfaces either resisted warping-induced separations better or stuck better to the tin that stayed in contact. In either case, this effect could only be eliminated by depositing uniformly thin molten coatings. Such molten coatings would also have to be wide to counteract extra heat removal by base metal on both sides, unless the base metal was preheated to a temperature near the melting point of the coating material.

Uniformly thin molten coatings were produced during the 178-2 VER and 178-4 VER experiments. Furthermore, the steel strip temperatures exceeded 200°C, near the melting point of tin. Yet, unlike most cool coating samples, the two thin molten adhesion samples failed during preparation. So, whether or not such coatings could be made strong remains speculative. Rapid solidification benefits would surely not occur at such temperatures.

Sample 178-1 VER-2 is displayed in Figure 65. It was taken from the thinly coated portion of the first vertical steel strip. The rapid base metal speed reduced its maximum thickness to 0.004 inch, and the base metal was not preheated. These coating conditions were similar to those in the 160-2A HOR experiment, and Sample 178-1 VER-2 resembles micrographs from Sample 160-2A HOR-2 in Figures 62 and 63. The exterior tin surface is smooth, since the preheating gun gas flow (element off) was aimed at the back strip surface where it did not interfere with the spray plume. Only one 0.002-inch deep indentation is found in the cross-sectional composite over the full-thickness portion. Image B reveals that the other two apparent depressions are a grinding scratch and a water spot stain.

The tin-steel matchup shown in Figure 65 is uniformly tight with virtually no interfacial porosity. Thus it is to be expected that this sample's 1500-psi adhesion strength was very comparable to the two samples tested from the 160-2A HOR experiment (1040 and 2440 psi). A few small flakes of tin were found still attached to the steel base metal after adhesion testing, indicating local ruptures in the tin layer at isolated areas of high bulk porosity--such as that found at the Image A position.

Sample 178-4 VER-2 in Figure 66 was extracted from the 0.016-inch peak thickness part of the coating deposited before the preheater was engaged. Thus the main difference between this sample and Sample 178-1 VER-2 was a slower base metal speed, although 178-4 VER-2 was crowned and asymmetric. Mechanical bonding was comparably good between the two samples, so the lower adhesion strength here (545 psi) was likely due to preparation damage induced by excessive C-clamp compression during epoxy curing.

Other coatings deposited under cool conditions were like this sample in that any bulk porosity was generally found toward the outer surface. However, this tendency is especially exaggerated in Sample 178-4 VER-2, with no porosity whatsoever except near the peak of the crowned deposit. The external tin surface is very smooth, as well, outside this particular region. This unusual behavior may be related to the 500°C nozzle temperature selected for the 178-2 VER and 178-4 VER experiments. Further metallographic studies might have provided insights on nozzle temperature effects, but time and budgetary constraints prevented additional efforts.

108

A. 7.5 Percent Bulk Coating Porosity, 400X

B. Scratch and Stain Artifacts, 268X

C. Mechanical Bonding, 0.02 Percent Porosity, 400X

23X

D. Thin Coating Region, 0.35 Percent Porosity, 400X

Polishing Grit

Grit
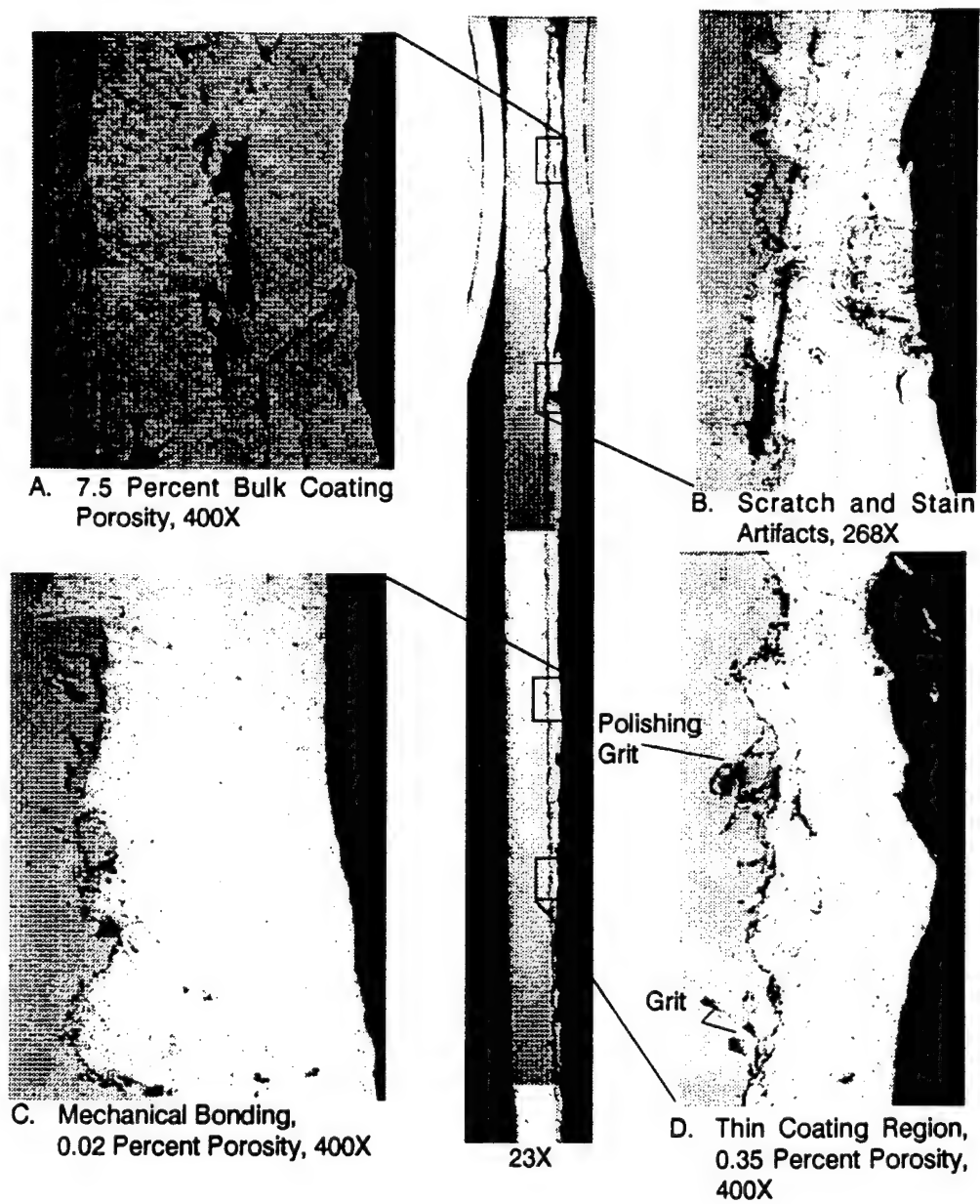
Figure 65. Sample 178-1 VER-2, from the First Tin-Coated Vertical Steel Strip.

109

A.   0.0 Percent Porosity, 268X

B.   External Voids, 5.1 Percent Porosity, 134X

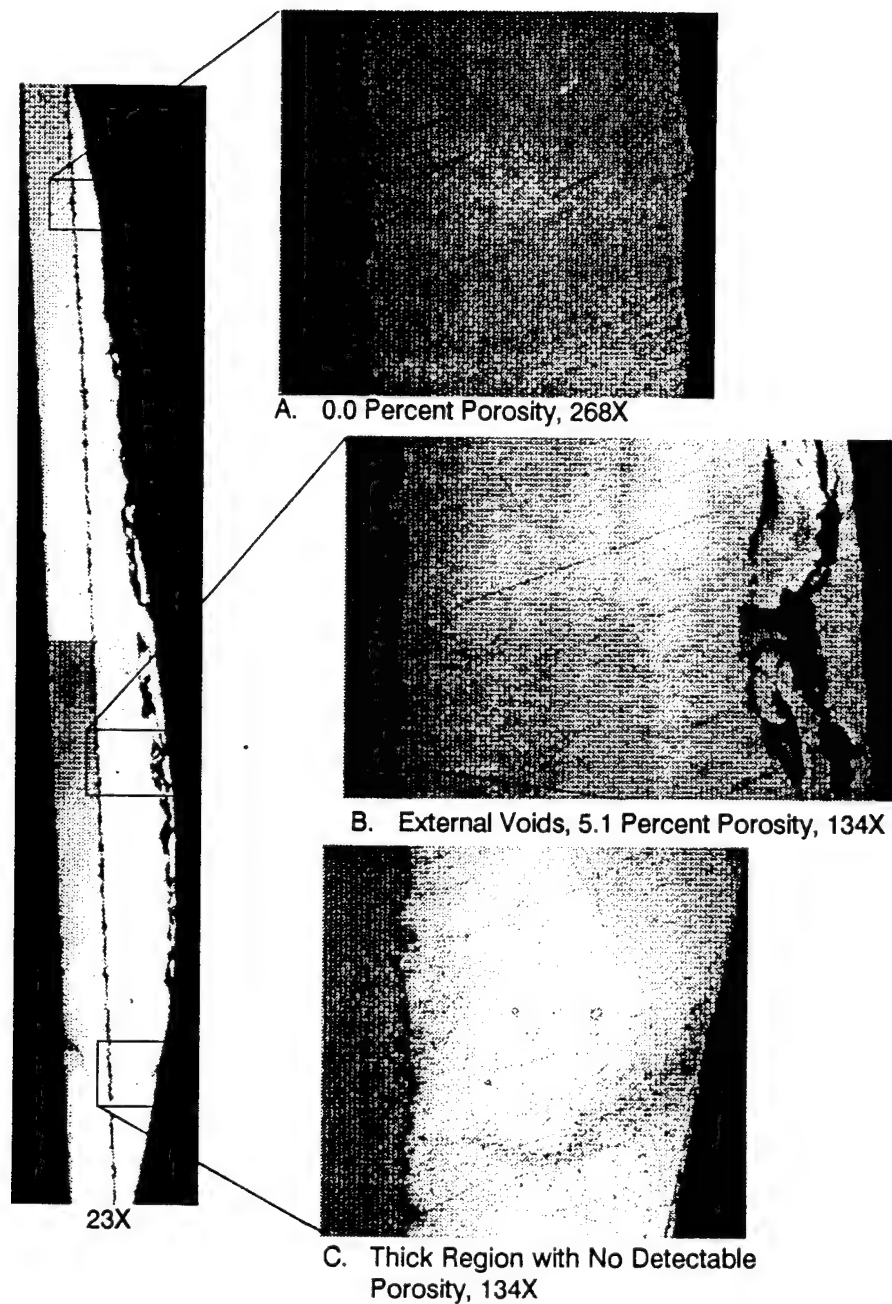C.   Thick Region with No Detectable
     Porosity, 134X

Figure 66.   Variations in Thickness and Outside Surface Porosity on Sample 178-4 VER-2, from the Last
             Tin-Coated Steel Strip.

SECTION V

OBSERVATIONS

Now that descriptions have been provided on spray-system components, the sequence of coating experiments, and testing of coated samples, several valid generalizations can be made. In reviewing and summarizing the previous information, three essential areas must be thoroughly considered in assessing the overall success of this Phase I feasibility study. These fundamental aspects are: (1) how well the new integrated spray-coating system performed, including the behavior of its individual components and subsystems; (2) what coating quality influences were found from different spraying conditions throughout the course of the Phase I experiments; and (3) what the Phase I results and the associated coating development methodology imply for subsequent efforts with high-melting-point materials and large-scale nebulizers.

A. PERFORMANCE OF SPRAY-COATING SYSTEM

As has been shown repeatedly, the data acquisition system was an indispensable part of the aggregate experimental apparatus. Besides displaying and recording essential information from each experiment, the data acquisition system was invaluable for characterizing performance of each component during assembly of the nebulizing system. In addition, the menu-driven screen approach selected for categorizing acquisition modes and standardizing recording formats proved most helpful during subsequent reduction and analysis of the numerous data sets.

The acquisition electronics functioned almost perfectly throughout Phase I, including the measurement transducers, signal conditioners, and computer programs. After installation of hardware and early debugging of software, the only changes made were to augment capabilities and enlarge versatility. The sole difficulty experienced with instrumentation was occasional handling damage to the custom-built thermocouples, which were particularly delicate for fast thermal response. No TC failures occurred during component characterizations and actual coating experiments.

111

The furnace/melt delivery system performed exactly as designed. The full 100-gram crucible charge was more than sufficient for all of the experiments conducted. This amount of tin could be melted and brought up to the desired 400°C temperature within a few minutes, while other spray system components were warming up, as governed by their temperature controllers. The furnace was well-insulated, such that heat losses in the absence of a cover could be tolerated easily. The tilting and pouring mechanism functioned smoothly and accurately, with no spillage around the tundish mouth. The mechanism's remote linkage occupied significant space and tended to restrict positioning of other components, however, so an electric tilt motor will be installed for Phase II.

The gas supply heater met its design requirements of raising inert gas temperature up to 600°C between inlet pressures of 12.4 and 50 psia over argon flow rates from 0 to 10 scfm. As discussed previously, the commercial gas heater had to be adapted with an exterior housing for chamber mounting and to protect personnel against burn injury when it was used for bench-testing. Furthermore, a portion of the inlet gas flow had to be diverted around the coil heaters for internal cooling in order to permit continuous heating operation. The modification successfully achieved maximum heating efficiency and the desired high temperatures at gas flows above 3 scfm, which was substantially more gas than would pass through the nozzle throat. However, this surplus of heated gas was routed through a tee past the nozzle and used to preheat the cylindrical steel sleeves in coating the 150 RDL, 153 RDL, and 160-0 HOR specimens.

Performance of the nozzle/tundish assembly was also nearly perfect, since it was able to spray high-quality coatings without modifications. This success verified the concept of aspirating molten metal into the throat of a converging/diverging gas nozzle, forming a directed spray of small, rapidly cooling droplets that consolidated against a base metal into a dense, adherent layer. Depositing good coatings with relative ease upon the first serious attempt demonstrated the process capabilities and inherent versatility that can be achieved with spray-forming technology. Moreover, these desirable features are fundamental characteristics of the INEL Controlled Aspiration Process, so its basic suitability for coating deposition was confirmed in a highly encouraging fashion, as well.

112

Yet, all nebulizers based upon a converging/diverging nozzle will not behave identically; seemingly subtle design aspects play important roles. Consequently, the success of this feasibility study required an advance development effort to optimize the exit cone geometry. Three exit cone angles were pressure-profiled, with multiple exit cone lengths tried in each case. Results from the miniature design investigation were carefully factored into the final configuration. It was thus no coincidence that the nebulizer displayed smooth, continuous plume properties whenever any transitions occurred in operating pressure. The fact that no individual droplets could be observed in the mist-like plume further meant that no vortices were forming along the exit cone walls, which had previously trapped tin droplets and caused them to agglomerate in earlier designs.

This does not imply that that a nozzle of circular cross section is ideal for large-scale coating applications. Such configurations tend to spray crowned deposits with tapered edges, as was repeatedly observed on Phase I metallographic samples. Also, the deposit width is primarily determined by the nozzle-to-base metal separation distance, for a specific plume expansion angle. This distance influences the heat flux delivered to the base metal, as well, so the width, thickness, and temperature of a coating are interdependent--which reduces process flexibility. These variables can be decoupled to a large extent with the rectangular version of this nebulizer design, which would spray broad, flat coatings with minimal edge tapering (Reference 1). Besides coating large areas at a uniform thickness, a rectangular nozzle can produce a plume area that does not expand rapidly with distance. Here the nozzle exit-to-base metal separation would still affect deposited heat flux by in-flight radiative cooling and entrainment of cool surrounding gas, rather than by expansion.

The first base metal fixture rotated cylindrical sleeves of low carbon steel in front of the spray plume. This approach was adequate for two of the three sets of coated specimens. Samples from these specimens included those with the highest adhesion strengths measured, plus superior flexural strengths and good metallographic appearances. Therefore, the rotating base metal fixture was able to aid in demonstrating the feasibility of spraying high-quality coatings at relatively low deposition temperatures. No modifications were required to accomplish critical Phase I objectives.

Nevertheless, as detailed previously, several problems of a nuisance nature were found when the rotating base metal fixture was actually used. The worst drawback involved preheating the steel sleeves with the surplus flow of heated gas that bypassed the nozzle/tundish assembly. The bypass tube was rigidly attached in front of the nebulizer, and it was inflexible in order to handle gas at temperatures of 500°C and above. Although base metal specimens could be raised to 150°C, the nozzle exit-to-base metal spacing essentially could not be changed without installing a new bypass tube. So, when experiments had to be performed to deposit coatings at higher thermal fluxes, the tube preheater was abandoned for the sake of expediency. The base metal fixture then had to be moved somewhat closer to the nozzle than otherwise desired to make up for the heat loss. This movement subjected fully molten coatings to spray plume turbulence that, in turn, caused poor-quality coatings from formation of pronounced ridges.

This combined positioning and preheating difficulty was eliminated by developing a radically different fixture for the third specimen set. The new fixture incorporated flat steel strips that were easier to prepare for coating. Furthermore, an integral gun-type preheater was attached to the fixture back, such that no interference occurred with the nozzle plume and such that coatings could be sprayed at any distance from the nozzle. In addition, the new design enabled base metal speed to be monitored directly on the computer screen, thereby permitting this variable to be changed in the course of a single experiment. The advanced features of the second fixture permitted spraying thin molten coatings without ridges--the sole type of coating that was not successfully attained with the first design.

The main intentions for the spray-system isolation chamber were to protect laboratory personnel from all potentially dangerous experimental situations, to limit gaseous reactions with molten metal droplets and hot components, and to filter out all metal particles before discharge to the environment. All of these goals were met with ample margin at a very economical cost by modifying a surplus glove box. The major elements of the spray system were operated remotely, eliminating possibilities for directly contacting molten tin, hot components, and exposed electrical leads. The sealed chamber prevented inhalation of metal particles and enabled purging of oxygen levels from 21 percent to less than 2 percent.

114

Chamber safety studies performed with laser aerosol spectrometers were both revealing and very encouraging. When spraying tin at high operating pressure--the worst-case condition--the highest chamber concentration of metal particles measured was 62 milligrams/cubic meter, whereas tin dust is considered moderately explosive at 100 to 500 grams/cubic meter. Thus personnel could not conceivably have faced an explosive hazard while spraying if the chamber had suddenly been flooded with air. A worst-case safety factor of at least 300 would exist even while spraying such highly explosive metals as aluminum and zirconium that become dangerous above concentrations between 20 and 50 grams/cubic meter.

Chamber concentration measurements were also compared to tin-spraying rates to estimate melt-to-deposit conversion efficiencies. Under normal low-pressure, high-aspiration conditions, 99.98 percent of the sprayed metal was consolidated into the deposit. With worst-case, high-pressure operation, the conversion efficiency was still a very high 99.82 percent.

Similar measurements on the filtered discharge stream found no clear indication that any tin passed through the high-volume ultrafine filter. Virtually all particles detected there were less than 1 micrometer in diameter, while tin particles sampled before the filter were in the 3- to 8-micrometer range. Nevertheless, the conservative assumption was made that all particles escaping the filter were tin, which yielded a small 6-microgram/cubic meter concentration leaving the laboratory stack for comparison to OSHA permissible exposure limits. Without taking credit for later dilution, this value is 333 times less than the OSHA PEL for tin dust, and similar margins would exist for other metals of interest. Thus spray coating must be regarded as an extremely clean and safe process from the joint standpoints of personnel exposure and atmospheric releases.

In summary, spray-system components generally performed better than expected, considering their number, complexity, and developmental nature. The entire spray-coating system functioned remarkably well in that dense, strong coatings were deposited directly from molten metal in the first attempt of its kind. Besides the versatility of spray-forming technology, this early success reflected the careful methodology employed, where valid coating parameter estimates came from comprehensive characterization data.

B. INFLUENCES OF SPRAYING CONDITIONS

The most straightforward fashion for evaluating process responses to different spraying parameters and base metal conditions is systematically reviewing coating quality data. Quantitative results include measurements of bend deflections, adhesion strengths, porous areas in tin layers, and roughness on external coating surfaces. Before beginning this assessment, however, it is worthwhile to recount the sequence of experiments.

o <u>150 RDL</u> Positioning the steel sleeve 3 inches from the nozzle produced a 1-inch wide deposit, while the 18.5-inch/minute base metal speed yielded a thickness of 0.010 inch. Nozzle operating pressure ranged between 23 and 24 psia. The coating was separated into three segments over four grit-blasted bands, and base metal temperature increased from 105 to 125°C as the preheater faced more of the sleeve. A "running globule" formed on one segment from excessive heat flux with too much aspiration at 23 psia.

o <u>153 RDL</u> The nozzle-to-sleeve separation was still 3 inches, but the speed was lowered to 7.3 inches/minute to increase coating thickness to 0.025 inch. Two circumferential passes comprised the coating--the first straddling bands roughened with glass beads and fine silica grit and the second over two bands blasted with coarse alundum. Nozzle pressure was held at 23.7 psia to prevent running globules, and the base metal temperature was steady at 130°C.

o <u>160-0 HOR</u> The preheater was still employed on the cylindrical sleeve with the horizontal pattern, where one 120-degree segment was blasted with fine Number 240 silica and the other two were blasted with coarse Number 46 and Number 30 alundum. The coating remained 1-inch wide, but the 15.7-inch/minute speed lowered the thickness to 0.012 inch. The temperature of the steel sleeve was a constant 125°C. The nozzle operating pressure was held at 23.9 psia. The overall intent was to reproduce the 150 RDL coating as a control experiment on the new base metal preparation pattern, but 50 degrees of coating was inadvertently remelted and smeared into a thin molten layer by contacting the preheater tube.

116

o   <u>160-2A HOR</u>   The preheater tube was removed so the sleeve could be
moved to 2 inches from the nozzle exit plane, which produced a
0.7-inch wide deposit. Speeding base metal up to 40 inches/minute
reduced the coating thickness to 0.004 inch. Operating pressure
was a constant 23.9 psia. Despite the more concentrated spray
plume, the absence of the preheater lowered the sleeve temperature
to 66°C. The outer surface was still dimpled and faceted.

o   <u>160-2B HOR</u>   The base metal was moved closer to the nozzle exit
plane to 1.2-inches, narrowing the deposit to 0.45 inch. The more
concentrated heat flux raised the sleeve to 90°C and coating
thickness to 0.009 inch. When the operating pressure was dropped
from 23.9 to 22.9 psia, the coating became shiny from incipient
melting induced by greater tin aspiration and higher heat flux.

o   <u>160-3A HOR</u>   The sleeve was moved closer in an attempt to foster
metallurgical bonding between the carbon steel and tin coating.
The 1.0-inch separation yielded a 0.41-inch width. The greater
spray concentration and lower 22.0-psia nozzle pressure produced a
molten pool that was pushed laterally by plume turbulence into two
primary parallel ridges 0.012-inch high. Temperature of the base
metal was not recorded, because the TC was no longer in contact.

o   <u>160-3B HOR</u>   The base metal was pulled back to 1.5 inches to reduce
molten ridge formation, widening the coating to 0.50 inch. Nozzle
pressure was lowered to 21.0 psia to ensure a predominantly molten
deposit. Molten ridges still formed under the incident plume, but
they were less pronounced, with maximum thicknesses of 0.010 inch.

o   <u>178-1 VER</u>   The vertical steel strip was blasted solely with coarse
Number 30 alundum grit, as with the two later 178 VER experiments.
The base metal was 1.5 inches from the nozzle exit for spraying a
0.50-inch wide coating, as in 160-3B HOR. The air gun heater was
not used, so a cool gas flow was directed against the back side of
the strip. This cooling and the higher 22.9-psia nozzle pressure
prevented deposit melting. Base metal speed was varied from 2.4
to 17.2 inches/minute, yielding 0.029- to 0.004-inch thicknesses.

117

o 178-2 VER Nozzle-to-base metal distance was still 1.5 inch, so
the coating width remained 0.50 inch. Operating pressure was also
held at 22.9 psia for consistency with 178-1 VER. To guarantee a
fully molten coating, the air gun heater was run at maximum power
and the nozzle temperature was raised from 400°C to 500°C.
A thin molten film was achieved once the base metal speed was
increased from 2.4 to 16.1 inches/minute to eliminate any ridging.
The thin (0.009-inch deep) layer formed between 200 and 225°C.

o 178-4 VER Base metal distance, coating width, nozzle temperature,
and operating pressure were as in 178-2 VER. The air gun heating
element was not engaged until half of the strip was coated to get
baseline data on effects of the 500°C nozzle without strip
preheating. Base metal speed was from 17.3 to 10.0 inches/minute
over the cool strip portion, producing a dimpled deposit from
0.010- to 0.016-inch thick. Ridging began when the preheater was
turned on. The ridges disappeared when the speed was increased
back to 17.3inches/minute, leaving a thin (0.009-inch) molten film
at base metal temperatures between 190 and 200°C.

Bend test results from all ten experiments are displayed in Figure 67,
excepting two samples with supiciously low deflections--as noted in the
caption. In this figure the 160 HOR values are separated to highlight any
flexural strength differences between cool dimpled coatings and the mostly
molten layers. On average, the best performance is found on samples from
the 153 RDL and 160-0 HOR experiments. As well as being deposited at 125
to 130°C onto preheated base metal, these coatings were relatively
wide from the 3-inch nozzle-to-sleeve separation. These conditions also
apply to the 150 RDL coatings, but they tended to fracture at somewhat
lower deflections for indefinite reasons--perhaps more shearing damage.

Thickness was not an important factor in coating ductility on the
superior samples, because 153 RDL deposits were typically 0.025-inch deep
and 160-0 HOR samples were 0.012 inch in thickness. The amount of surface
roughening during base metal preparation also had no obvious influence on
flexural strength; in both sets fine and coarse grit sizes yielded similar
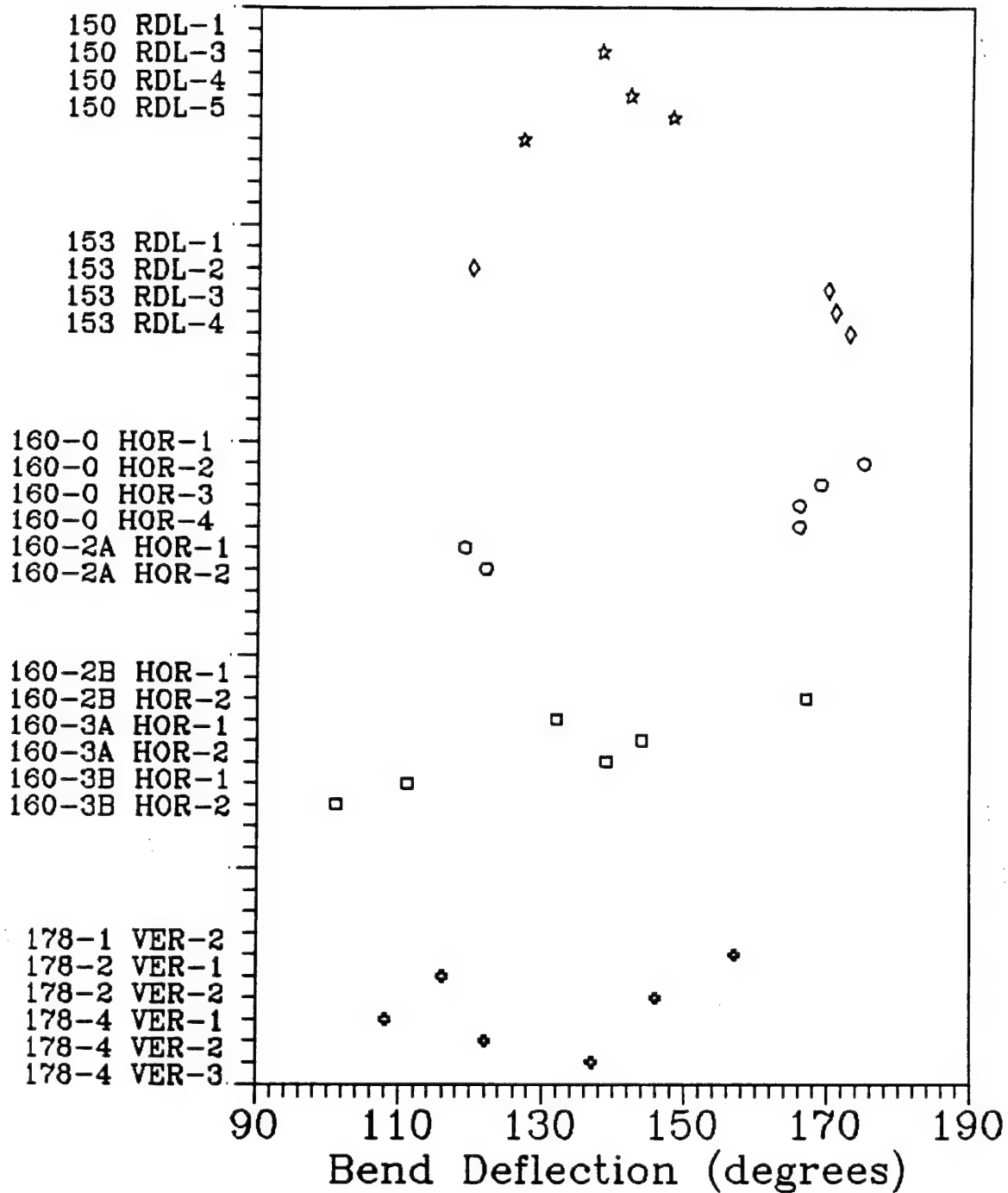results. This likely reflects comparably good consolidation and adhesion.

118

Figure 67. Histogram Summary of Bend Test Results, Excepting Anomalous Samples 150 RDL-2 (33 Degrees) and 178-1 VER-1 (15 Degrees).

119

The causes of poorer bend test performance on the remaining samples varied, as detailed in Section IV (C). Several specific observations are worth noting, however. The 160-2A HOR samples fractured at much lower deflections than the thicker preheated 160-0 HOR samples, but their early failures were evidently not related to the small 0.004-inch thickness and the low 66°C deposition temperature. Sample 178-1 VER-2 had the same thickness and an even lower base metal temperature (50°C), but its flexural strength approached the superior sample sets. Also, the mostly molten samples from the 160-2B HOR, 160-3A HOR, and 160-3B HOR experiments typically failed by delamination, rather than fracturing. Consequently, their results primarily reflect poor adhesion, instead of low ductility.

Adhesion results from the samples that were successfully load-tested are displayed in Figure 68. Approximately one-third of the samples taken delaminated before testing from a combination of sectioning damage and buckling from too much clamp compression, as described in Section IV (D). Furthermore, it is likely that many of the samples shown in Figure 68 were partially damaged from the same sample preparation sources. Nevertheless, certain generalizations can be made on overall adhesion behavior.

First, 10 of the 17 samples in Figure 68 yielded adhesion strengths that surpassed 1000 psi. This is a respectable threshold for many coating applications, especially when shear stresses are low. Samples 160-0 HOR-2 and 160-0 HOR-4 surpassed 3000 psi. These strengths are impressive at an early stage of development, already falling within the accepted range of commercial metal-metal bonds produced by plasma spraying (Reference 5), and no pickling or electrochemical cleaning steps were necessary. Note that plasma-sprayed metallic coatings often rely upon metallurgical bonds from the relatively high gas and deposition temperatures in that process.

The fact that three adhesion samples definitely exceeded the 2100-psi tensile strength of wrought tin is also significant. (Sample 160-0 HOR-1, from the preheater-smeared thin molten layer, was reinforced artificially by epoxy penetration at pinholes.) In these three cases the tin layers would themselves probably have failed earlier withhout the benefits of rapid solidification--smaller grains and negligible impurity segregation. Thus spray forming can yield better coatings, as well as strong bonds.
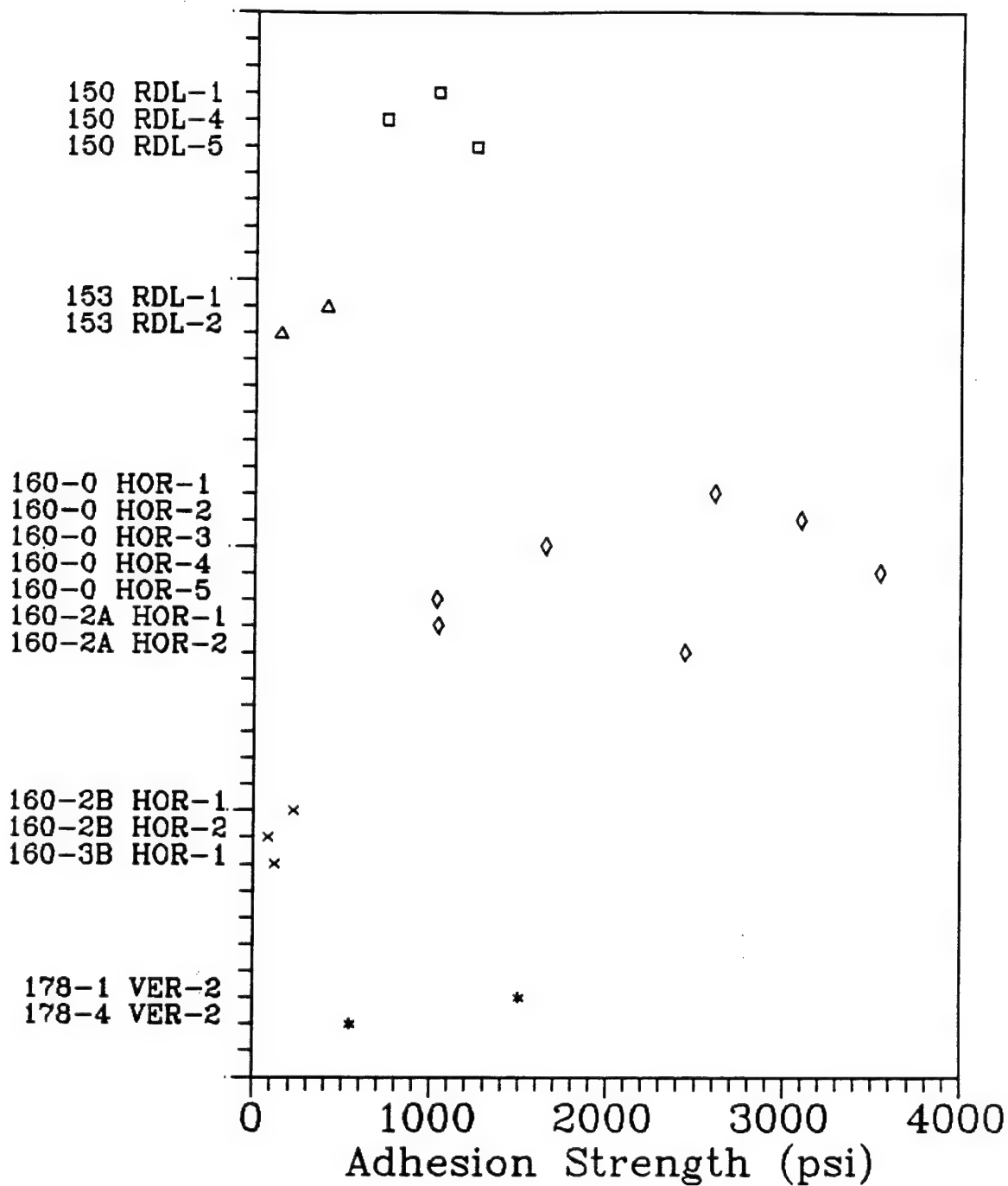
Figure 68. Histogram Compilation of Adhesion Strength
Measurements for All Pull-Tested Samples.

With the preparation damage problems, it was difficult to rigorously identify optimal conditions for spraying strongly adherent coatings. Nevertheless, the nonmolten coatings deposited at a large nozzle-to-base metal spacing in the 160-0 HOR and 160-2A HOR experiments produced by far the best adhesion strengths. Not only did they yield the largest strength values, but none of them failed during preparation--unlike all of the other sample sets. However, they were not totally immune to preparation damage, as positively confirmed by deliberately over-tightening the clamp on Sample 160-0 HOR-5, which was sectioned immediately adjacent to Sample 160-0 HOR-4 expressly for this purpose. Here the buckling definitely decreased adhesion strength by more than 70 percent. (Such difficulties with coating adhesion tests are not unusual, as discussed in Reference 6.)

The 160-0 HOR and 160-2A HOR coatings were typically wide and thin, and they were relatively cool (excepting remelted Sample 160-0 HOR-1). Yet, these conditions were not unique, occurring also in the 150 RDL and 153 RDL experiments. Metallography along the tin-steel interfaces on companion 160-0 HOR and 160-2A HOR samples showed near-perfect mechanical bonding, which is presumably critical for strong adhesion. (With such good interlinkage between metallic surfaces, electronic bonding may occur across the interface between atomic neighbors.) However, Figure 69 makes it clear that excellent interfacial matchups were formed in the thicker 153 RDL coatings, as well. Figures 54, 55, and 56 reveal that mechanical bonds were established at least occasionally on samples from the 150 RDL experiment, but shearing damage obscures the actual extent.

Preliminary tin-spraying efforts confirmed that some roughening of the base metal surface was required for substantial adhesion, as has been true for decades with conventional flame spraying (Reference 6). However, Figure 69 demonstrates that the grit size used to prepare a surface had little influence on mechanical bonding. In general, the incident tin droplets were able to wet even the roughest steel surfaces--filling in all depressions very well. This likely explains why grit size had no obvious effect on adhesion strengths among the 160-0 HOR samples. Similarly, it is doubtful that the radial grit-blasting pattern adversely impacted the 150 RDL and 153 RDL adhesion results. Consequently, shearing delamination was probably responsible for their low strengths, relative to 160-0 HOR.
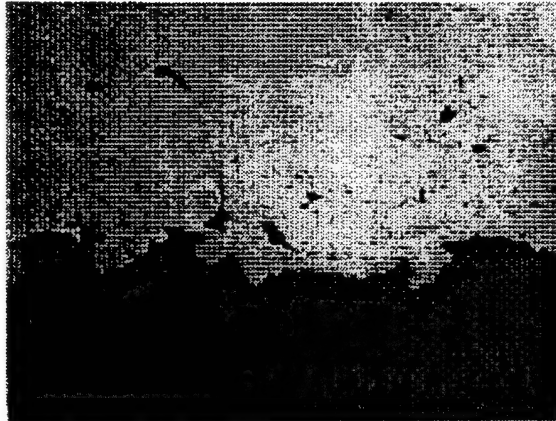
122
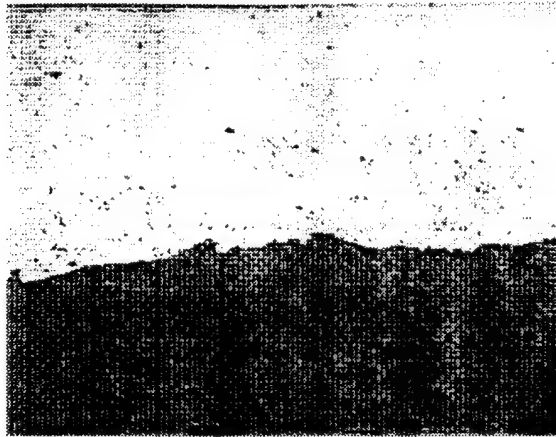
Sample 153 RDL-2, 536X

Mixture of Number 60 and Number 120 Grits.

Sample 160-0 HOR-2, 536X

Number 46 Grit.

Sample 153 RDL-4, 400X

Number 30 Grit, 0.50 Percent Porosity Measured Near Interface.

Figure 69. Good Interlinkage Between Tin Sprayed onto Grit-Blasted Carbon Steel, Independent of Grit Size Used.

Accounting for the poor adhesion behavior of the narrower, hotter coatings also involves some conjecture. Although shearing was no longer employed to extract samples, the high damage frequency of adhesion samples during the clamping and curing phase left a sparse data base. Moreover, metallography demonstrated that even the relatively delicate Dremel Tool sectioning could induce separation near the cuts. Consequently, better inferences can be made from metallography than directly from Figure 68.

Samples from the 160-2B HOR experiment, which displayed a reflective surface from incipient melting, apparently were weakened by grain gowth and impurity accumulation at grain boundaries. Figure 64 showed strong evidence of intergranular tin fracturing near the steel interface when Sample 160-2B HOR-1 was sectioned for metallography. Nevertheless, both adhesion samples from this experiment were able to be load-tested.

Three of the four adhesion samples from the 160-3A HOR and 160-3B HOR experiments failed during sample preparation. These mostly molten, badly ridged coatings incurred even higher temperatures and probably also were affected by grain growth. However, the cursory metallographic inspections of their companion samples showed no intergranular fracturing. Instead, the tin ridges had curled away from the base metal at their thin edges, leaving very little tin in firm contact with the base metal. Differential thermal contraction was apparently responsible for partial delamination immediately after these coatings were deposited.

Figure 53 presented a successful load test for Sample 178-2 VER-1, which also represented a molten, badly ridged coating. This sample produced a surprisingly high adhesion strength of 3300 psi. Nevertheless, later metallography on its companion sample revealed relatively large bare areas where the epoxy bonded the steel base metal directly to the steel grip shank, so the load test primarily reflected the tensile strength of the epoxy. Consequently, this sample was deleted from Figure 68.

The two samples in Figure 68 from 178 VER experiments were from cool, unheated strip areas. Sample 178-1 VER-2 was 0.004-inch thick and tested like 160-2A HOR samples. Sample 178-4 VER-2 was 0.016-inch thick and may have approached 160-0 HOR results, but for probable preparation damage.

124

As noted previously, thin molten layers without ridges were achieved in the 178-2 VER and 178-4 VER experiments. Unfortunately, both adhesion samples representing this type of coating delaminated from buckling during preparation, so potential adhesion strengths are unknown. Nevertheless, in both experiments, the base metal was preheated to 200°C or above-- near the 230°C melting point of tin. This should have reduced extra cooling along the coating sides and minimized any differential thermal contraction and the associated warping. In addition, these coatings were relatively narrow with high local heat flux to foster melting.

Consequently, considerable equiaxed grain growth can be assumed for the thin molten coatings, which would have eliminated any of the benefits of rapid solidification in the tin layers. The tensile strength of such tin coatings could not have surpassed 2100 psi, since the microstructure would be much like wrought tin. Thus the adhesion samples would not have equalled the performance of rapidly cooled samples from the 160-0 HOR experiment, no matter how good the bonding was along the steel interface.

All porosity values from digital image analysis of photomicrographs are presented in Figure 70. The area-averaged porosity concentrations are between 0 and 1 percent in the overwhelming majority of cases--independent of spray conditions, base metal preparation, deposition temperatures, etc. That is, excellent consolidation of the incident tin droplets typically was accomplished over the entire test matrix, and porosity was virtually never interconnected. Section IV (E) further confirmed that the isolated areas of relatively high porosity generally occurred near external coating surfaces--along with formation of surface roughness--where incomplete consolidation would be expected. In these worst-case positions, porosity was still very low near the steel interface, so corrosion resistance would not have been jeopardized. (See Figures 58, 59, 60, 63, 65, and 66.)

Valuable perspective on this Phase I achievement is supplied by Reference 5, wherein commercial plasma spraying is assigned an average porosity level of 5 percent for nonferrous metal coatings. Reference 7 states that plasma spraying can only achieve low porosity at near-vacuum conditions, due to gas entrapment at higher pressures. This is especially true for low interfacial porosity of the high quality shown in Figure 69.
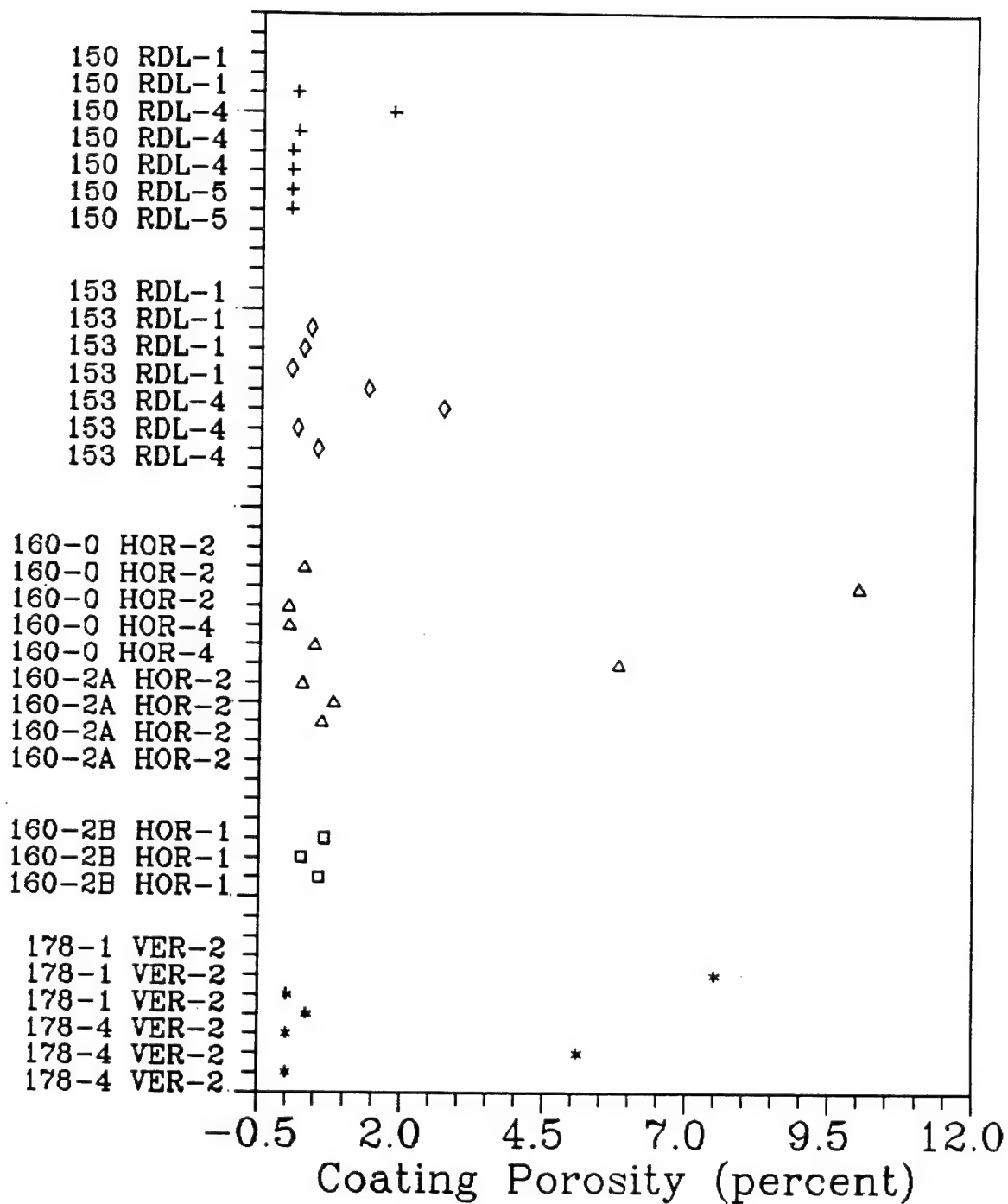
Figure 70.   Area-Averaged Coating Porosity Values Found by
             Digital Imaging of Photomicrographs from All
             Samples Examined.

126

The last aspect of coating quality to be quantified on Phase I samples was surface roughness. When coatings were deposited with a preheating flow directed against the front base metal surface, the indentations on the outer coating surface were 0.003 to 0.004 inch in depth. When the preheater was removed or directed against the opposite side of the base metal, the roughness decreased to approximately 0.002 inch. It thus appears that the front-directed preheater flow was interfering somewhat with the spray plume, inducing turbulence that caused slightly poorer consolidation of the last droplets to impact.

In both of the above situations, the roughness of the relatively cool coatings with dimpled surfaces was found to be independent of deposit thickness, base metal preparation, and other conditions. However, when the local heat flux was increased to form shiny "incipient melting" coatings or thin fully molten coatings, the roughness level was lowered even further to 0.001 inch--leaving very reflective surfaces. Of course, ridging of the thick molten layers increased surface roughness to an unacceptable degree, along with degrading most other important properties.

In summary, surface roughness can be controlled within reasonable limits according to heat deposition. For rapidly cooled coatings, at least 0.002 inch of material would have to be ground away to produce a smooth surface. Little or no grinding would be required for coatings deposited at higher temperatures. However, as noted earlier for certain applications, some roughness can be desirable--where lubricant retention or paint adherence are critical, for example. In such applications, the dimpled, faceted surfaces of the rapidly cooled coatings might be ideal.

C. VIABILITY OF SPRAY-COATING TECHNOLOGY

Projecting Phase I results toward accomplishments from Phase II and later efforts necessarily requires speculation. Yet, findings in certain categories can be extrapolated with considerable confidence. As might be expected, these presumptions apply more to fundamental features of the Controlled Aspiration Process and converging/diverging nebulizer designs than to high-melting-point coatings and large-scale applications.

127

Phase I clearly demonstrated that dense tin coatings can be deposited onto steel over a wide range of conditions. Furthermore, the typically excellent mechanical interlinkage achieved strong adherence between the coating and base metal without harsh cleaning steps and high-temperature metallurgical bonding. This experience can be applied directly to other metals with low melting points, such as lead, cadmium, zinc, and probably aluminum. Since sprayed droplets cool rapidly in flight, coatings can be placed onto heat-sensitive metals without fear of degradation, along with roughened plastics, cloth fibers, and even paper products.

Nebulizers based upon a converging/diverging nozzle should also work for spraying metals with much higher melting points. Higher temperatures will be essential for the nozzle body and the nebulizing gas to prevent metal freezing in the liquid orifices. However, converging/diverging gas nozzles have already been designed and tested for several high-temperature applications (rocket engines, etc.), so low pressures can definitely be created for aspiration into the throat region at certain upstream gas pressures. In addition, the aspirated metal streams will still be sheared by the perpendicular gas flows within the tightly confined interaction zone into a directed mist of droplets .

Although it is virtually certain that high-melting-point metals can be sprayed, the limitations of existing computer models preclude any advance judgments on important plume characteristics for coating deposition. The spray plume characteristics include droplet size distributions, gas/metal mass ratios, and in-flight droplet cooling rates. Therefore, indications on consolidation of hotter droplets into a dense deposit must be provided by experiment, along with whether or not the deposits will adhere strongly to a given base metal. In any case, the inherent parametric flexibility of the Controlled Aspiration Process offers an excellent likelihood that a suitable combination of spray-coating conditions can be developed.

The methodology employed during development is as critical as process versatility. Phase I performance relied heavily upon design expertise, thorough component characterizations, comprehensive control features, precise instrumentation, on-line computer readouts, and detailed recording of process variables. This fundamentally sound approach will continue.

To be economically attractive, spray-forming technology must be extended for covering large surface areas with uniformly thick coatings. Reference 1 has already established the ability of a rectangular INEL nozzle version for spraying broad, flat tin deposits 0.020- to 0.080-inch thick, where thickness uniformity was within 2 percent over much of the 4-inch width. However, this prototype nebulizer sprayed against a smooth metal substrate to produce free-standing deposits, so potential coating capabilities of the rectangular configuration of the converging/diverging design have not been completely confirmed, as yet.

Another important aspect of spray-coating economics is melt-to-coating conversion efficiency. Careful Phase I measurements verified efficiencies of 99.8 percent or better with tin coatings (neglecting any later grinding for smooth surface applications). Comparable conversions at larger scales and higher temperatures must be demonstrated experimentally, but initial results are definitely encouraging. Furthermore, any actual "overspray" could be collected within the sealed chamber and recycled. Similarly, the argon gas was found to be remarkably clean after filtration, so it could be conveniently recycled if argon were chosen as the nebulizing/purging gas. (Less costly nitrogen could be used for many types of coating.)

Personnel safety requirements and environmental emission limits are also concerns that cannot be avoided, especially since this project has the ultimate goal of eliminating hazardous wastes currently generated by electroplating of metal coatings. Phase I tin studies found minimum safety margins of approximately 300 to 1000 under the most conservative assumptions imaginable, both for particulate explosion hazards (chamber suddenly filled with air) and for discharge of the filtered exhaust stream out the laboratory stack (no dilution assumed).

Margins while spraying other metals must be confirmed in practice, but no grounds exist for suspecting different results. One strong reason to expect similar explosive hazard findings is that, once purged, the spray chamber is kept clean by the nebulizing gas, whose flow rate is nearly identical for a given mass of any sprayed metal. Thus the concentration of metal particles should be the same in any chamber. Meanwhile, the high-volume, ultrafine particle filter would function well for all metals.

129

As previously noted, adhesion of high-melting-point coatings requires experimental confirmation. The incident droplets must wet the base metal and consolidate within irregular surface features (from grit-blasting or a similar preparation technique) for sound mechanical bonding. The amount of interfacial porosity will likely be influenced by both the cleanliness of the base metal and any droplet-gas chemical reactions in flight, which would proceed at accelerated rates with higher droplet temperatures. Thus more attention will likely be required in order to achieve mechanical bond strengths of 3000 psi or higher, as accomplished during Phase I.

However, higher droplet temperatures would encourage metallurgical diffusion bonds along the base metal interface, which could increase adhesion strengths substantially. In principle, this could occur without the fully molten coatings attempted in Phase I and the associated problems of ridging and dripping globule formation. An alternative method for metallurgical bonding is annealing at moderate temperatures for extended periods--provided that the base metal would not degrade in the process.

Under suitable spray-coating conditions, high-melting-point deposits could still be rapidly solidified, as with the dimpled tin coatings that displayed greater tensile strength than their parent material. That is, relatively little grain growth and impurity segregation would occur in any rapidly solidified coating--by comparison to slowly cooled ingot stock--if sufficient cooling of droplets happened in flight and if the base metal preheating could be limited to moderate temperatures.

This could cause major improvements in certain coating properties, especially for certain alloys that are strengthened by finely distributed dispersiods or by metastable phase freezing. In theory, spray coating could deposit amorphous metallic layers of unequalled wear and corrosion resistance, due to the absence of grain boundaries (Reference 8). Here, however, service temperatures must be kept below 250 to 300°C, the typical transition temperature range for metallic glasses.

130

SECTION VI

CONCLUSIONS

1. The novel spray-coating system and its integral components functioned as designed, which reflected a comprehesive development methodology. The only significant modifications were to the base metal fixture and its preheater to finish the coating test matrix.

2. The molten metal nebulizer based upon a converging/diverging nozzle successfully sprayed fine tin droplets in a low velocity mist. By adjusting upstream gas pressure, the nebulizer could be turned on and off and the metal spraying rate could be throttled, in accordance with the Controlled Aspiration Process.

3. A tin particle concentration of 62 milligrams/cubic meter was measured while sampling the chamber atmosphere under worst-case (high-pressure) spraying conditions. No explosive danger would have existed upon an accidental air ingress, since tin dust becomes moderately explosive at 100 to 500 grams/cubic meter. Even highly explosive metal powders require concentrations from 20 to 50 grams/cubic meter.

4. Comparing tin particle concentrations in the chamber to metal-spraying rates showed melt-to-coating conversion efficiencies of99.98 percent under normal conditions and 99.82 percent in worst-case situations.

5. Sampling the filtered discharge stream found only submicron particles, indicating that no tin escaped the chamber. Conservatively assuming that all of this tiny particulate mass was tin yielded a discharge concentration of 6 micrograms/cubic meter, 333 times less than the Occupational Health and Safety Administration's tin dust limit for continuous breathing. No credit was taken for poststack dilution.

6. Tin coatings were successfully deposited onto low carbon steel with and without base metal preheating. Widths ranged from 0.4 to 1.1 inch and base metal temperatures were from 50 to 220°C. This spread in conditions showed the basic versatility of spray-coating technology.

131

7. Rapidly cooled coatings from large flight distances and more mixing with cool surrounding gas displayed a dimpled, faceted appearance from incomplete consolidation of the last droplets to impact. Thicknesses of such coatings ranged from 0.004 to 0.025 inch, depending on the plume expansion in flight and the base metal's speed of translation.

8. Thick molten layers from the high thermal flux of a concentrated spray plume caused dripping melt globules or formed high ridges under plume pressure, resulting in poor thickness uniformity and other properties. These effects were eliminated by increasing the base metal speed and the plume expansion while preheating the base metal back, creating thin molten coatings. This approach appears limited to molten layers no more than 0.010 inch in thickness.

9. The highest overall bend test deflections were obtained from wide coatings deposited by a cool spray plume, where the base metal was preheated to 125°C. Most samples failed by coating fracture above 160 degrees--where 180 degrees is the maximum possible deflection-- which shows good ductility in such rapidly solidified tin coatings. No significant influences were found from coating thickness and the grit size used to roughen the steel surface for mechanical bonding.

10. Relatively low bend test deflections near 120 degrees were measured on mostly molten coatings. These samples typically failed by separating, rather than fracturing, indicating poor adhesion--not low ductility.

11. Superior overall adhesion strengths were found on wide, cool coatings without high-temperature metallurgical bonding. Mechanical bonds on two of these samples exceeded 3000 psi, within the accepted range of metal layers coated by plasma spraying, a long-established commercial process with high temperatures that often induce metallurgical bonds. Spray coating can thus deposit strong coatings at low temperatures that will not compromise heat-sensitive base materials.

12. Adhesion results on three samples substantially exceeded the tensile strength of the wrought tin parent material, illustrating how rapid solidification benefits can improve properties in the coating layer.

13. The surprisingly strong adhesion values required prior roughening of the base metal surfaces, either by blasting with abrasive grits or by peening with glass beads. However, no harsh cleaning operations were found to be necessary. In particular, no pickling or electrochemical etching steps were employed.

14. Area-averaged porosity concentrations in tin layer micrographs were overwhelmingly between 0 and 1 percent, and the pores never provided an interconnected corrosion pathway to the base metal. This porosity level is superior to standard commercial plasma spraying and equal to plasma spraying conducted in a vacuum chamber. Spray-coated porosity is particularly low near the base metal interface, as compared to atmospheric-pressure plasma spraying where much gas is entrapped.

15. Tin coatings produced in Phase I had edges that tapered in thickness. The extent of the crowning was primarily determined by the flight distance and the associated amount of plume expansion. This thickness nonuniformity is a fundamental byproduct of the circular geometry nozzle design used for the small-scale Phase I feasibility study. The effect can be eliminated in future efforts by incorporating a nozzle of rectangular cross section, which contains a slot-shaped throat and multiple liquid orifices.

16. Surface roughness on rapidly cooled, dimpled coatings decreased from 0.004-inch deep indentations to 0.002 inch when the preheating flow was removed from the front base metal surface and later directed against the opposite side from the spray plume impact zone. On shiny coatings consisting of partially or fully molten layers, the complete droplet consolidation decreased the roughness level to 0.001 inch. Surface roughness can therefore be controlled according to the deposition conditions, which is advantageous because some roughness is desirable for certain coating applications.

SECTION VII

RECOMMENDATIONS

The level of success achieved during Phase I is remarkable, given that coatings were sprayed directly from the melt over a wide range of process conditions in the first attempt of its kind. Furthermore, many samples displayed good ductility, porosity, and surface roughness. In particular, low-temperature mechanical bonds proved capable of surprising adhesion strengths, offering a new option for coating heat-sensitive materials.

The Phase I feasibility study was confined to coating low carbon steel with tin at temperatures of 200°C or below. Meanwhile, the greatest immediate benefit of spray-coating technology to the U.S. Air Force would be to replace the current process of electroplating chromium and eliminate the associated generation of hazardous wastes. This requires experimental confirmation that high-melting-point metals can be sprayed to form dense adherent coatings. Accordingly, as detailed in Appendix B, the primary thrust of Phase II (as approved) will be to spray coatings of chromium or chromium alloys in a second bench-scale feasibility study. Increasingly sophisticated computer models will be developed to expedite this process.

Spray-coating technology will be of little practicle use unless it can be adopted on a much larger scale. Maximum benefit would be realized by spraying broad, flat coatings with good thickness uniformity in a single pass over large base metal areas. As previously described, a nebulizer of rectangular geometry has successfully sprayed tin in flat, 4-inch wide deposits, but coating capabilities were not verified on this prototype. In addition, high-melting-point metals have not been attempted yet with this design. However, preliminary evaluations will be conducted early in Phase II on small rectangular nebulizers aimed at uniformly thick coatings 1.0- to 1.5-inches wide with metal spraying rates of 3 to 4 grams/second-- approximately eight times the output of the Phase I nebulizer. If results are as expected, the rectangular nebulizer will be investigated (with no additional funding) both for coating deposition purposes and for spraying high-temperature metals. A successful Phase II outcome would thus satisfy most concerns over the viability of spray coating for actual applications.

134

Chromium electroplating normally requires very clean steel surfaces for good adhesion, and both pickling and cathodic etching are employed by ALCs. These cleaning steps not only generate hazardous wastes, but also cause hydrogen uptake, which must be removed after plating by a careful anneal. Sprayed coatings can adhere to grit-blasted or ball-peened surfaces, potentially eliminating electrochemical cleaning and annealing.

Although replacing chrome plating would be of greatest value, other hazardous "heavy" metals are also frequently coated by this method. Many have melting points close to tin--such as lead and cadmium-- where the Phase I experience would be directly applicable. However, these metals are often used for very thin layers on fasteners, bolts, etc., which have recessed surfaces. Spray coating is a line-of-sight technique requiring a 0.003-inch minimum thickness for full surface coverage. These fundamental limitations must be considered in any assessments of the spray-coating technique for remediating existing electroplating operations.

An inherent strength of spray-coating technology is the ability to deposit alloys of virtually any composition for specific purposes, but electroplating is normally restricted to pure elements. For example, the corrosion and galling resistance of specialty stainless steels can be superior to elemental chromium. Similarly, stellite-type alloys typically provide better hardness and wear resistance than "hard" chromium plates. Spray coating could thus increase the service lives of coated components, decreasing refurbishment frequencies and reducing ALC aircraft downtimes.

Further improvements in coating properties can probably be achieved by spraying state-of-the-art rapidly solidified alloys. Where superalloys are strengthened by dispersions, rapid solidification results in very small dispersoids with an especially homogeneous distribution in the metal matrix. The dispersions tend to block migration of dislocations, which is particularly effective for increasing service temperatures. Comparable benefits are created in other alloy systems by freezing metastable phases. Lastly, ceramic particulates can be mixed into the spray plume to deposit metal-matrix composites. Common choices of ceramic reinforcement in bulk composites are silicon carbide, alumina, and diamond, but such composites are just coming into reality in the coating realm (Reference 5).

135

SECTION VIII

REFERENCES

1. Watson, L.D. et al., "Nozzle-Aspirated Metal Forming," paper presented at the Metallurgical Society's <u>International Symposium on Casting of Near Net Shape Products</u>, Honolulu, 13-17 November, 1988.

2. Alvarez, J.L. and Watson, L.D., "Apparatus and Method for Spraying Liquid Materials," <u>U.S. Patent 4,919,853</u>, 24 April, 1990.

3. <u>The Metals Handbook</u>, 9th ed., Vol 7, Powder Metallurgy, American Society for Metals, 1984.

4. <u>The Metals Handbook</u>, 9th ed., Vol 5, Surface Cleaning, Finishing and Coating, American Society for Metals, 1984.

5. Dibble, M.A., "Coatings Cover New Ground," <u>Machine Design</u>, 22 June, 1989, pp. 40-48.

6. Kubel, E.J., "Thermal Spraying Technology: from Art to Science," <u>Advanced Materials and Processes</u>, December 1987, pp. 69-80.

7. Herman, H., "Plasma-sprayed Coatings," <u>Scientific American</u>, September 1988, pp. 112-117.

8. Kubel, E.J., "All Eyes on Metallic Glasses," <u>Metal Progress</u>, May 1986, pp. 61-70.

APPENDIX A

PRELIMINARY TESTING OF NOZZLE DESIGNS

APPENDIX A

PRELIMINARY TESTING OF NOZZLE DESIGNS

Behavior of a converging/diverging gas nozzle is influenced by many geometric features. For a nozzle with a circular cross section, these specific features are the diameters of the entrance tube and throat, the angle of the entrance cone, the lengths of the entrance tube and throat, and the length and angle of the exit cone. The exact dimensions become even more important when one wishes to aspirate molten metal into the throat and spray it into a particular type of deposit in a carefully controlled fashion.

Past spray-forming research at INEL has successfully narrowed the range of design options for nebulizing molten metals, especially tin at low to moderate gas temperatures. Empirical correlations have thus been established that specify several of the above dimensions for any choice of metal spraying rate, particularly in the nozzle entrance region. However, the geometry of the exit cone typically must be tailored for a given spray-forming application.

Simple converging/diverging nozzles had to be built and tested to provide input to the final Phase I nebulizer design, since development of predictive computer models will not begin until Phase II--as outlined in Appendix B. Three distinct nozzles were constructed with exit cone angles of 6, 10, and 18 degrees. The exit cones were 1.25-inch long on the 10- and 18-degree nozzles, while the 6-degree nozzle cone was only 1.0-inch long due to a machining tool limitation. Small holes were drilled at one-sixth inch increments along the exit wall of each nozzle, beginning at the end of the throat region (often the optimal liquid orifice location for spraying molten metal). Local wall pressures were measured at these hole positions with an array of transducers as the operating gas pressure was sequentially increased.

After data had been obtained for each nozzle at its original exit area-to-throat area ratio, this ratio was changed by successively trimming down each nozzle's exit cone in one-third inch lengths, whereupon a new wall pressure data set was recorded. Four ratios (ie. four exit cone lengths) were tried for the 10- and 18-degree nozzles. Three ratios were studied on the 6-degree nozzle, which began too short for a third trim. All measurements were performed at room temperature with argon gas.

These local wall pressure measurements are plotted as recorded in Figures A-1, A-2, A-5, A-6, A-9, and A-10. In Figure A-1a Areas 2 through 8 designate successively larger distances from the throat (Area 1) in one-sixth inch steps. Trimming down an exit cone length by one-third inch reduced by two the number of holes where pressure could be measured, so only six areas are shown in Figure A-1b, and so on for later figures.

Normalized versions of the same wall pressure data sets are presented in Figures A-3, A-4, A-7, A-8, A-11, and A-12. In these figures the local wall pressures P were divided by the nozzle operating pressures $P01$, while the local cross-sectional exit cone areas A were divided by the constant throat area At. These dimensionless plots can be compared to classical nozzle characteristics, as well as used to predict shock wave formation.

Close examination of Figures A-1 through A-12 reveals relatively little difference between the 10- and 18-degree nozzles in that both the as-recorded and normalized pressure profiles are consistently smooth along their exit cone walls. Furthermore, this transitional behavior was not influenced strongly by changing the cone lengths. This flexibility in cone length is a desirable property, because it allows considerable freedom in designing related dimensions on other components, such as the width of the tundish mouth. By contrast, plots from the 6-degree nozzle contain irregular pressure profiles, and trimming induced rather abrupt shifts near its exit plane. Both trends suggest that cone wall pressure instabilities might occur with small changes in operating pressure.

An equally important aspect of the 10- and 18-degree nozzles is that the throat wall pressure (Area 1) shows first a decrease below atmospheric pressure (suction) and later an increase above atmospheric pressure, as the operating pressure is increased. This parabolic suction feature is absolutely essential for conveniently starting and stopping the spraying of liquid metal, plus using aspiration to precisely control the feed rate of liquid into the throat when spraying. However, this type of inflection is found in Figures A-9 and A-10 outside the 6-degree nozzle throat, too-- along the exit cone wall. This erratic behavior indicates a potential for local pressure instabilities such as shock fronts and wall separations.

Besides providing valuable input to the Phase I nebulizer design, these pressure profiles will be compared to computer predictions from a one-dimensional nozzle dynamics code, when code development activities are begun early in Phase II. After the code is verified for room-temperature gas flows using these data sets, the code will gradually be augmented for higher gas temperatures, for heavy liquid droplet loading of the exit stream (two-phase flow), and for two-dimensional effects (e.g. pressure differences between an exit cone centerline and the walls).
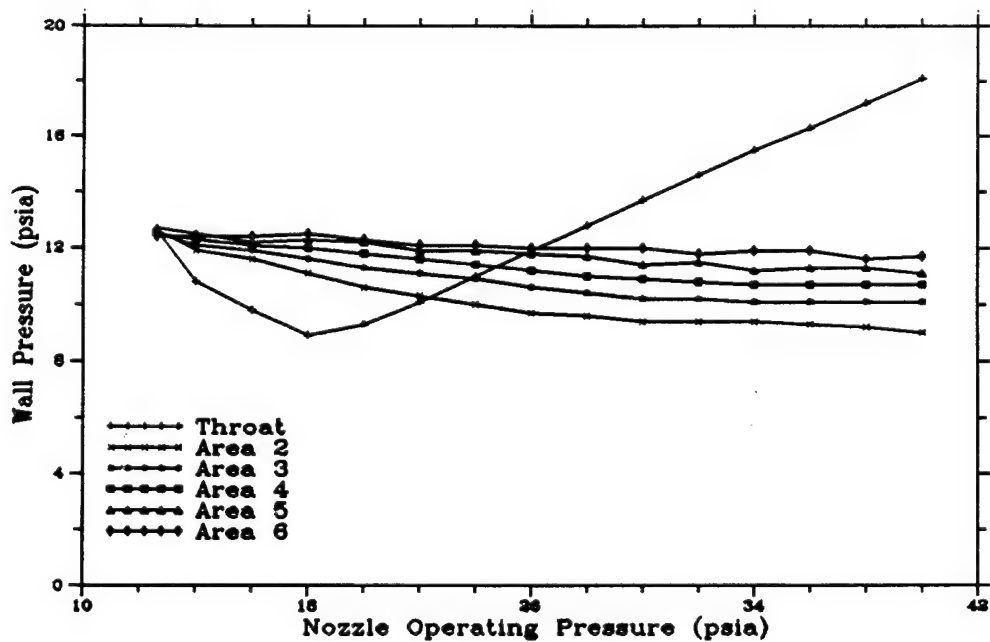
139
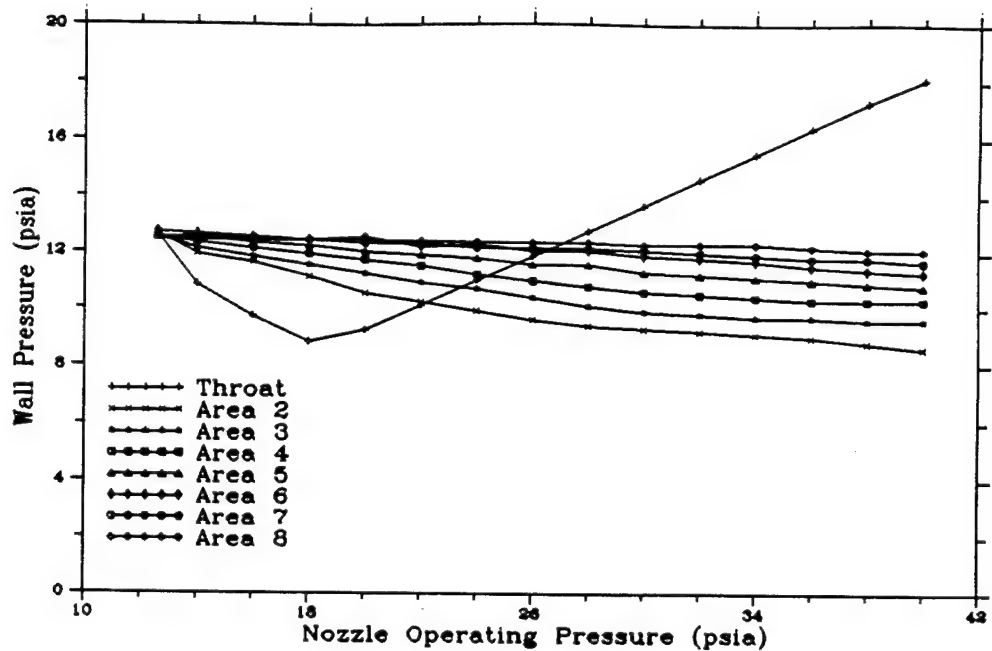
a) Exit to throat area ratio is 16
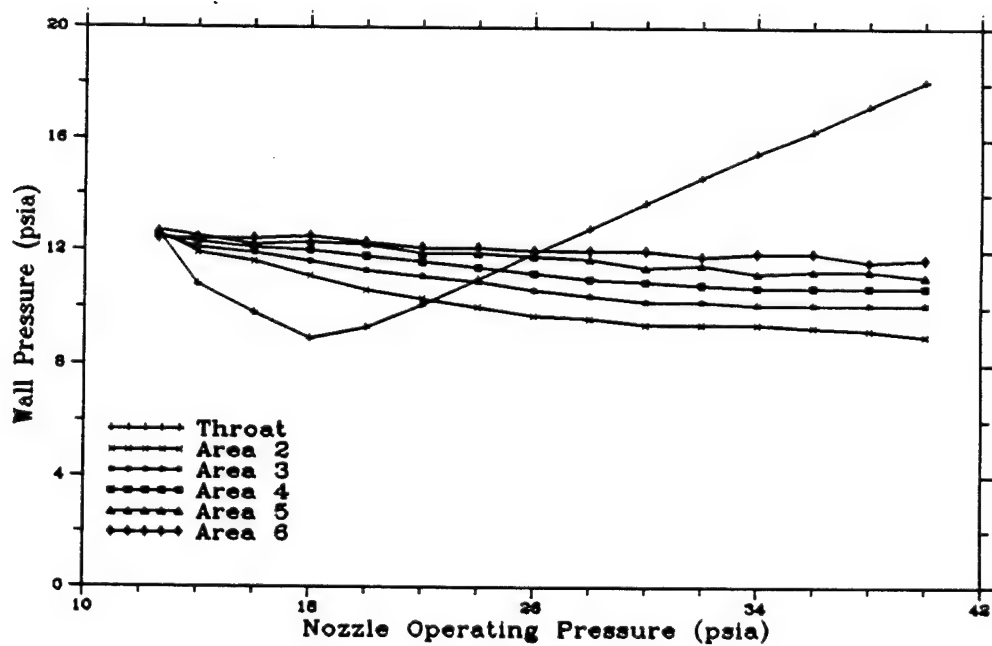
b) Exit to throat area ratio is 10

Figure A-1. Pressure Measurements along the Nozzle Exit Wall for an 18-Degree Nozzle with Exit Area-to-Throat Area Ratios of 16 and 10.
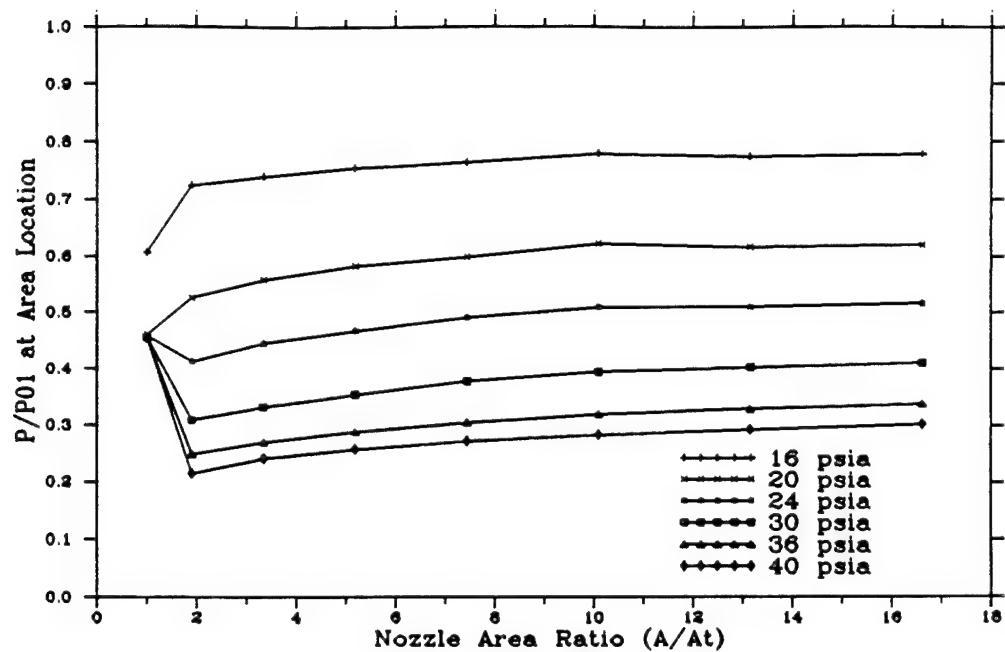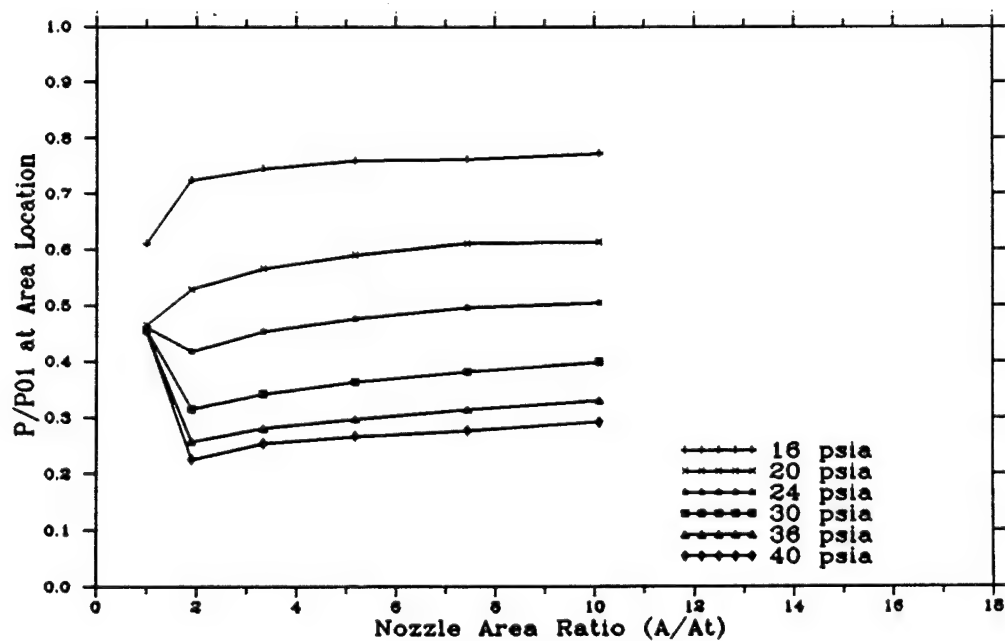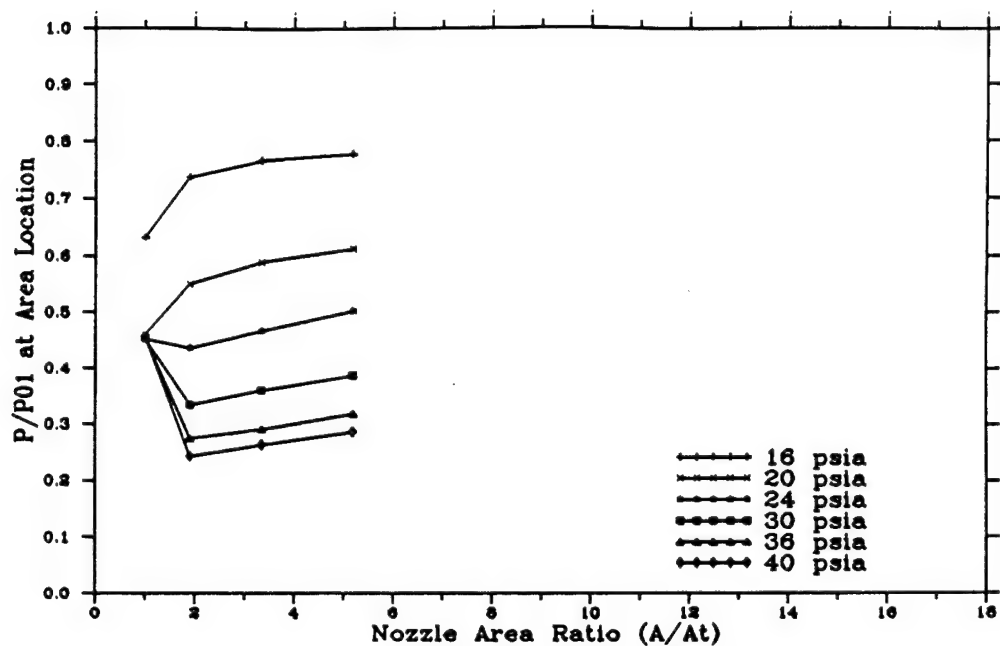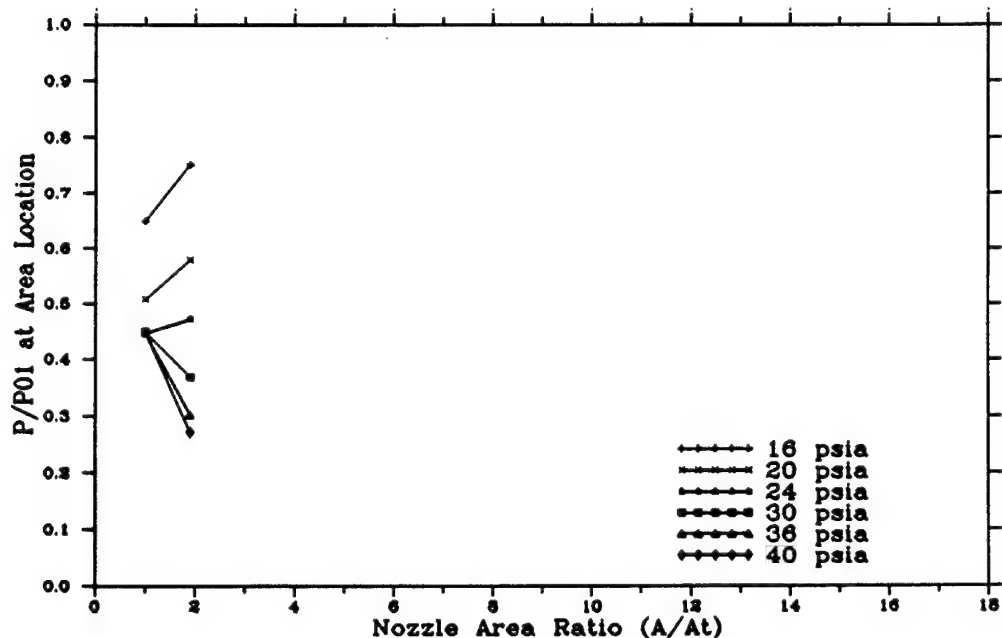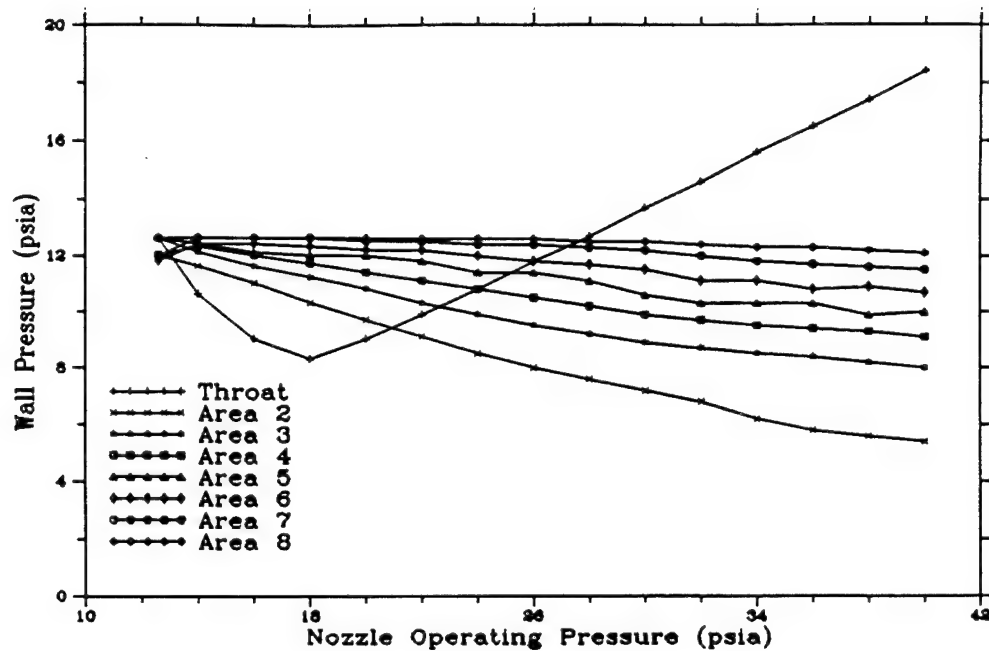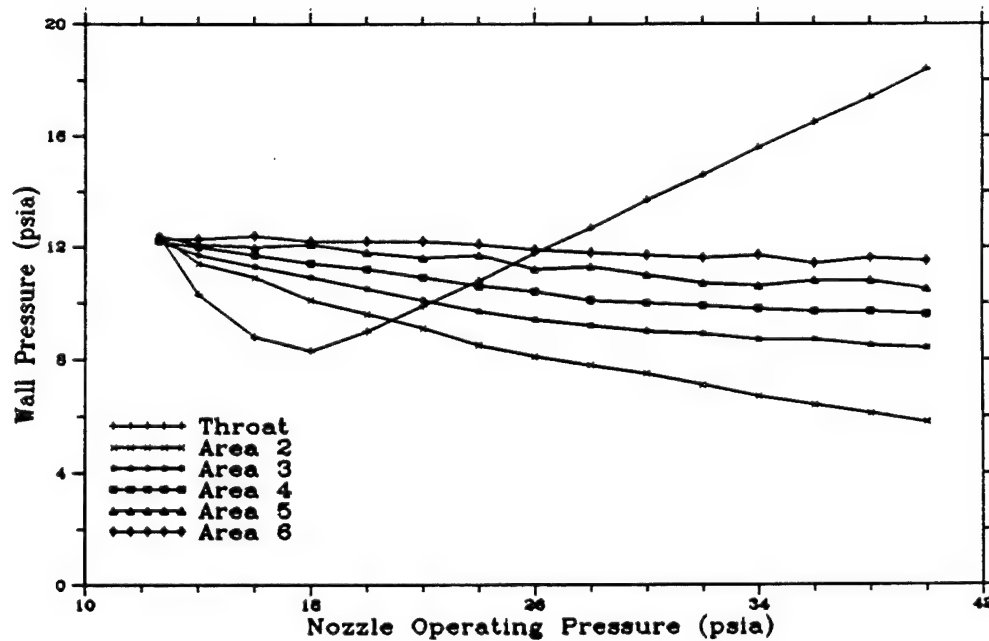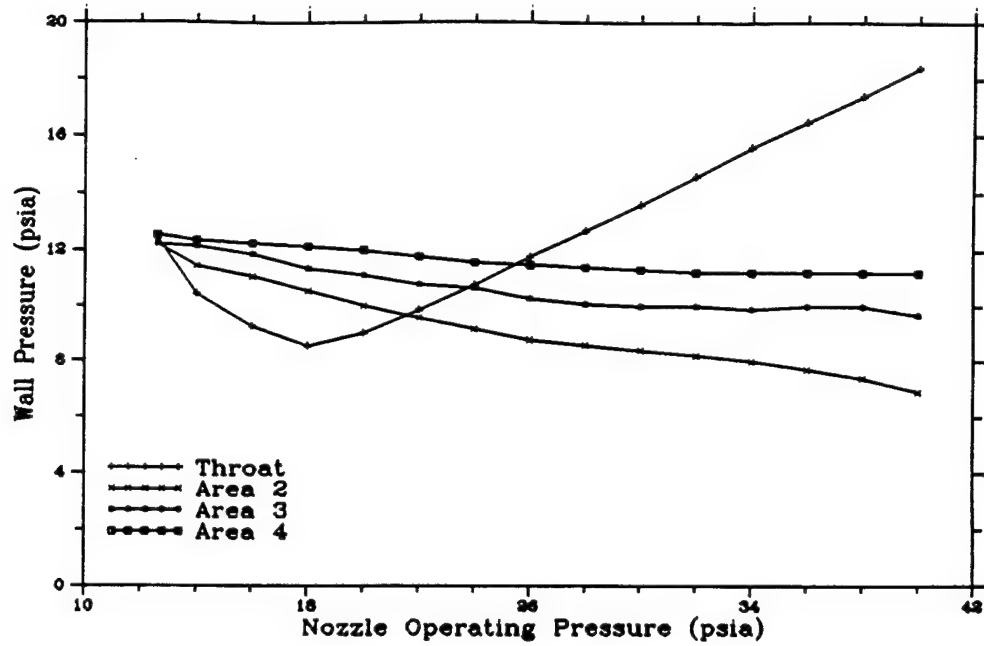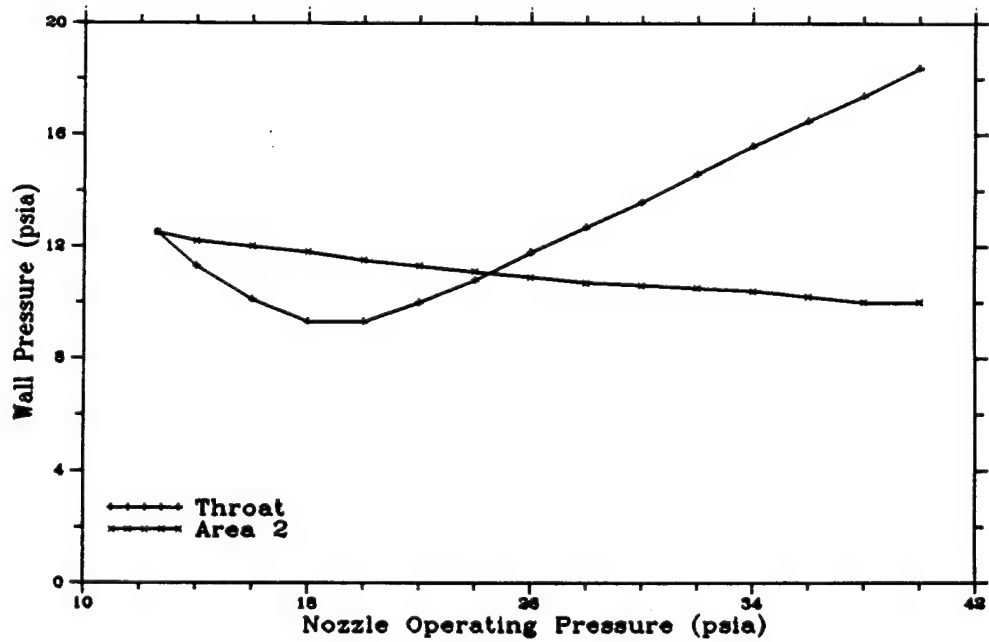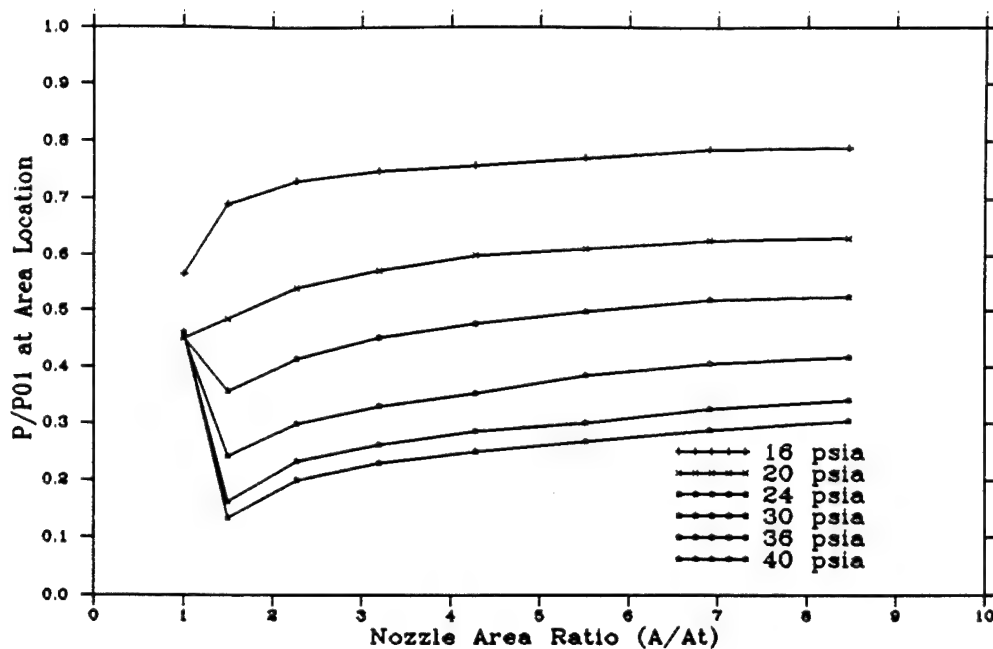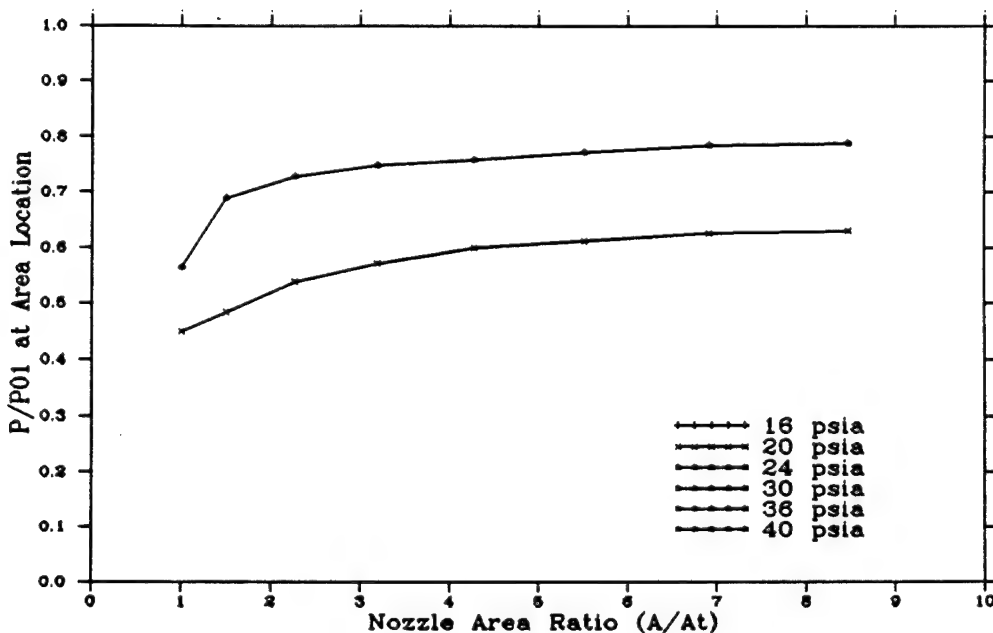
140
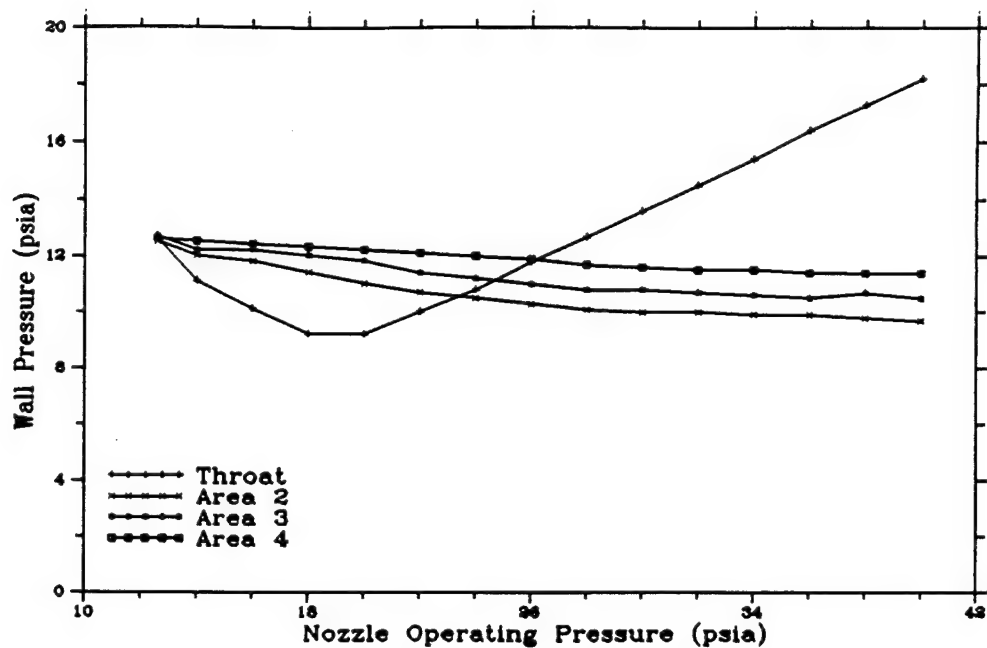
a) Exit to throat area ratio is 5

b) Exit to throat area ratio is 2

Figure A-2.   Pressure Measurements along the Nozzle Exit Wall for
an 18-Degree Nozzle with Exit Area-to-Throat Area
Ratios of 5 and 2.

141

a) Exit to throat area ratio is 16

b) Exit to throat area ratio is 10

Figure A-3. Normalized Pressure Ratios along the Nozzle Exit
Wall for an 18-Degree Nozzle with Exit
Area-to-Throat Area Ratios of 16 and 10.

142

a) Exit to throat area ratio is 5

b) Exit to throat area ratio is 2

Figure A-4. Normalized Pressure Ratios along the Nozzle Exit
Wall for an 18-Degree Nozzle with Exit
Area-to-Throat Area Ratios of 5 and 2.

143

a) Exit to throat area ratio is 8.5

b) Exit to throat area ratio is 5.5

Figure A-5.   Pressure Measurements along the Nozzle Exit Wall for
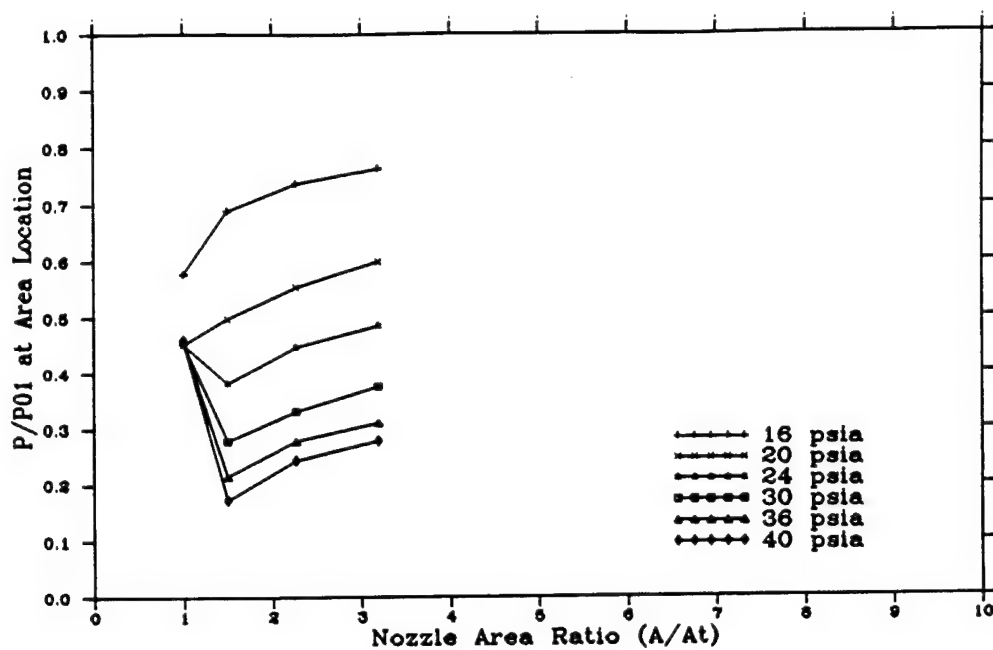a 10-Degree Nozzle with Exit Area-to-Throat Area
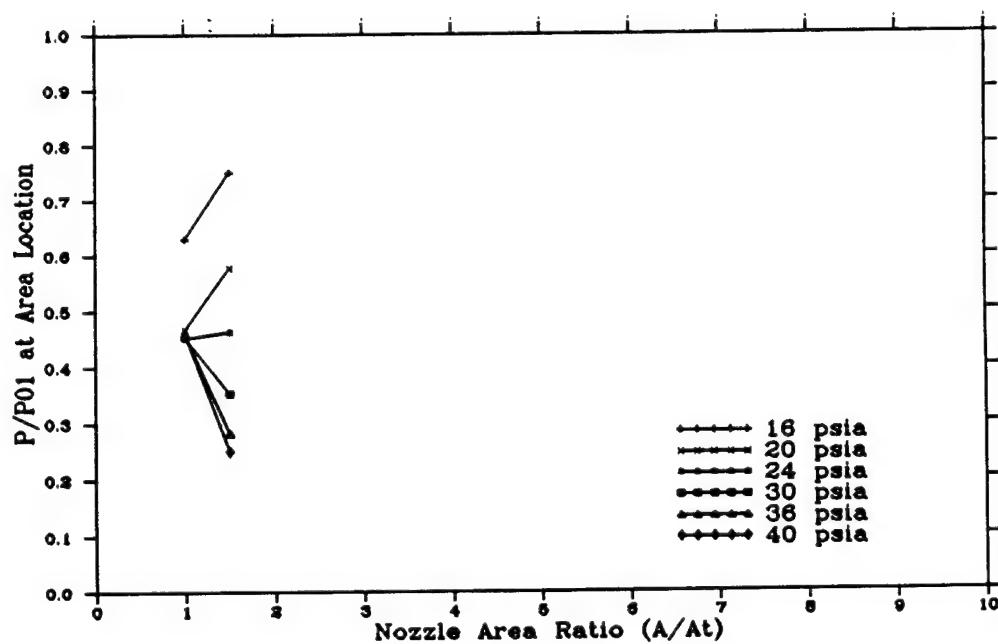Ratios of 8.5 and 5.5.

a) Exit to throat area ratio is 3.2

b) Exit to throat area ratio is 1.5

Figure A-6. Pressure Measurements along the Nozzle Exit Wall for
a 10-Degree Nozzle with Exit Area-to-Throat Area
Ratios of 3.2 and 1.5.

145

a)   Exit to throat area ratio is 8.5

b)   Exit to throat area ratio is 5.5

Figure A-7.   Normalized Pressure Ratios along the Nozzle Exit
             Wall for a 10-Degree Nozzle with Exit
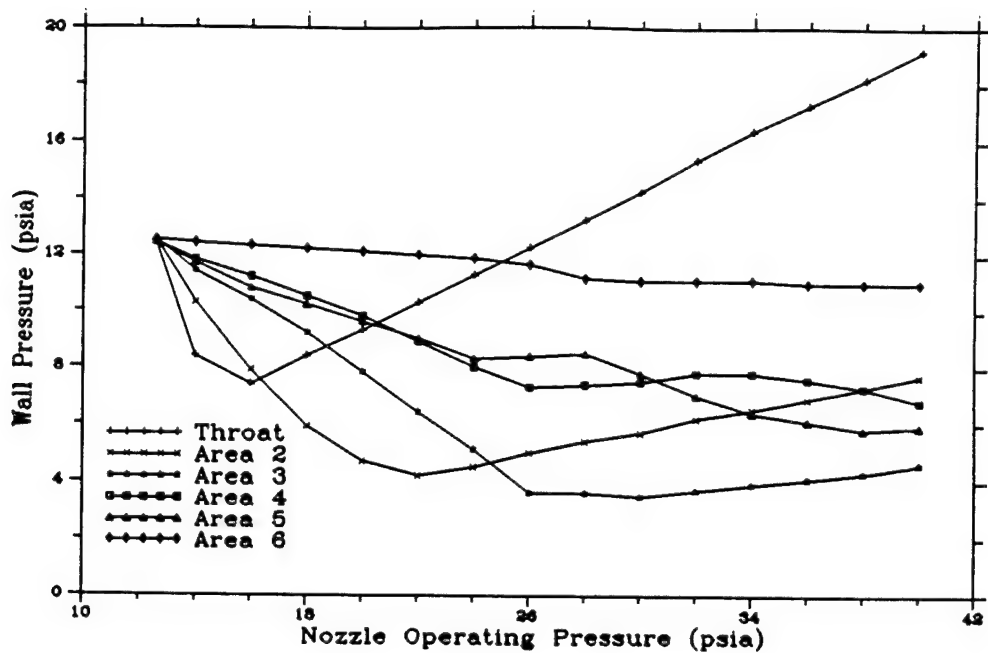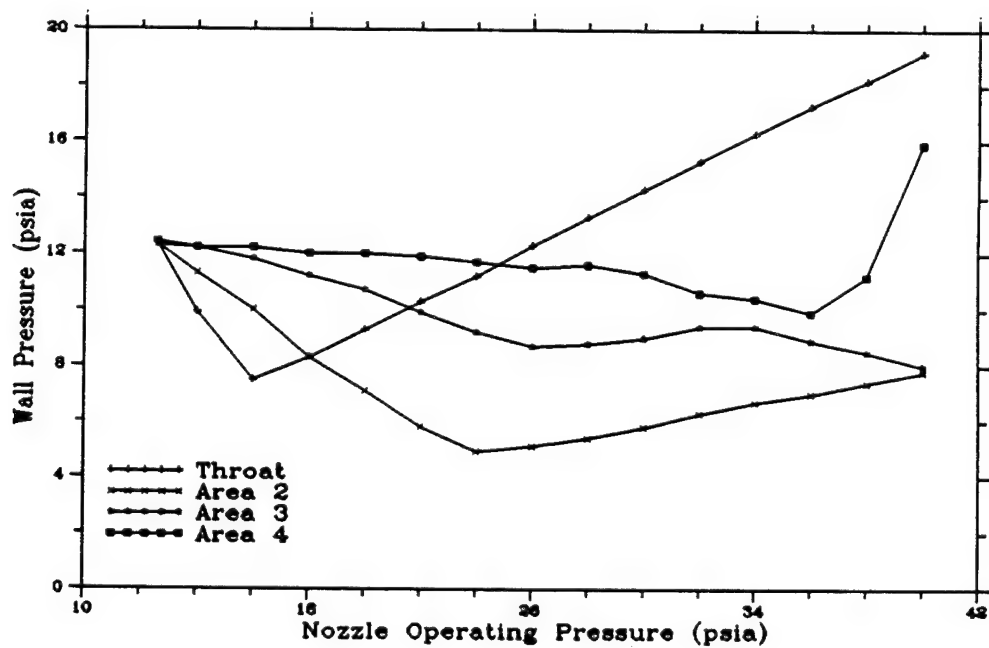   Area-to-Throat Area Ratios of 8.5 and 5.5.

146

a) Exit to throat area ratio is 3.2

b) Exit to throat area ratio is 1.5.

Figure A-8.   Normalized Pressure Ratios along the Nozzle Exit
Wall for a 10-Degree Nozzle with Exit
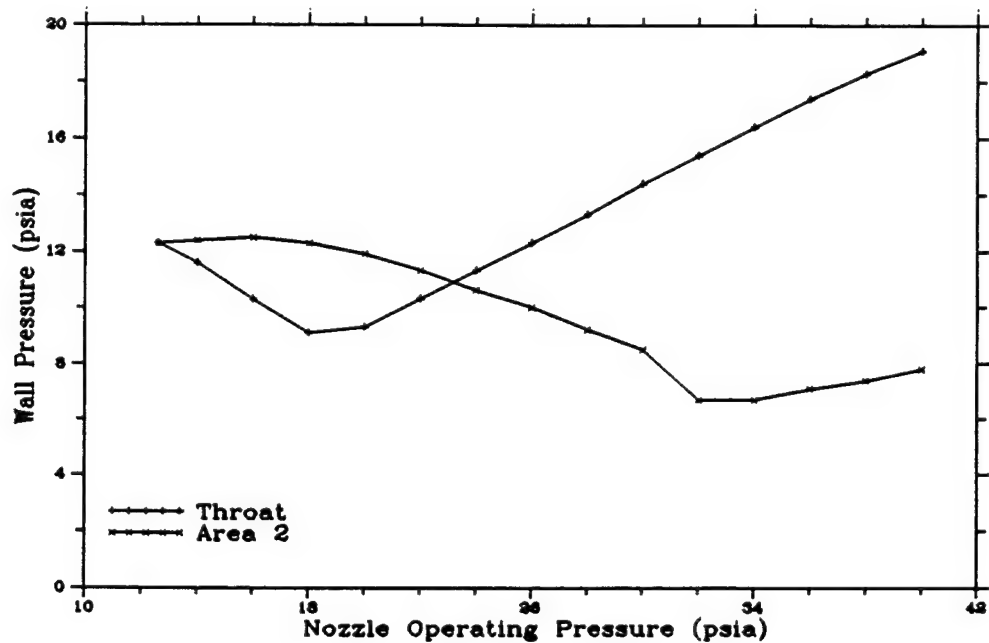Area-to-Throat Area Ratios of 3.2 and 1.5.
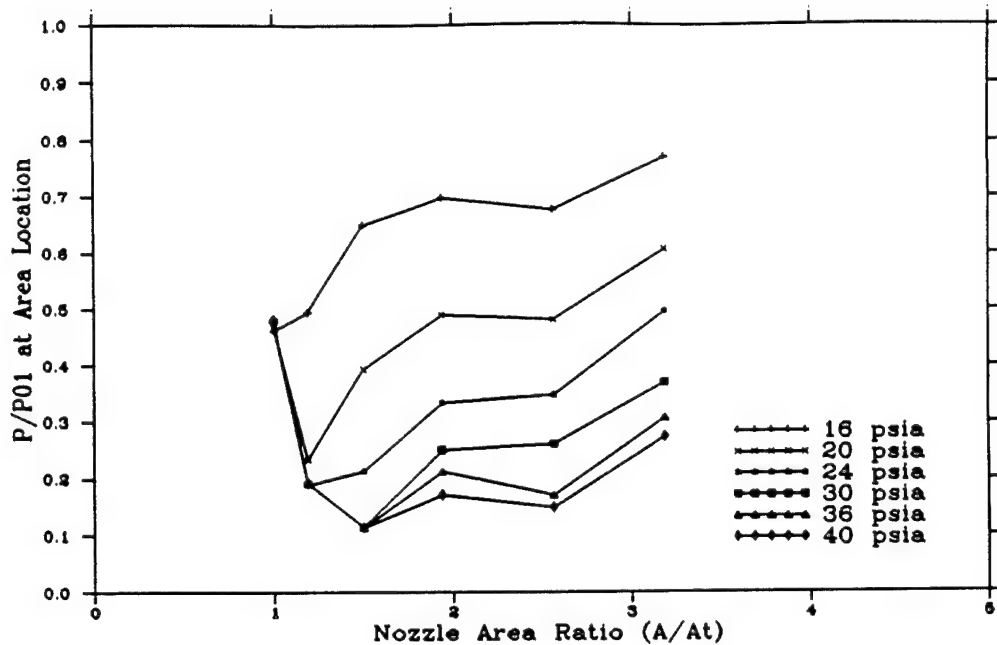
147

a) Exit to throat area ratio is 4

b) Exit to throat area ratio is 2.6

Figure A-9.   Pressure Measurements along the Nozzle Exit Wall for
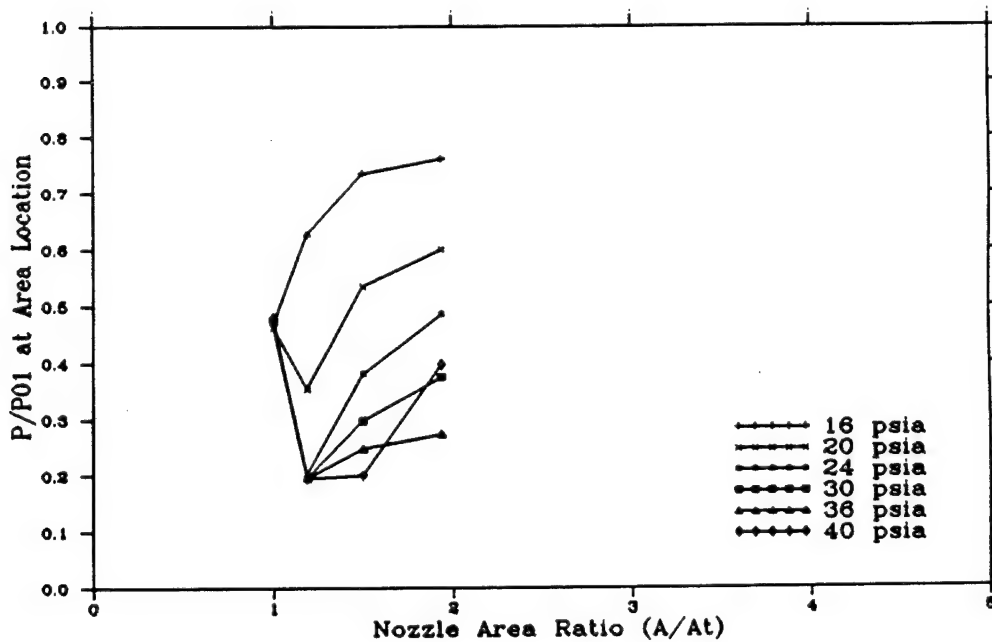a 6-Degree Nozzle with Exit Area-to-Throat Area
Ratios of 4 and 2.6.

148

a) Exit to throat area is 1.6

Figure A-10. Pressure Measurements along the Nozzle Exit Wall
for a 6-Degree Nozzle with Exit Area-to-Throat
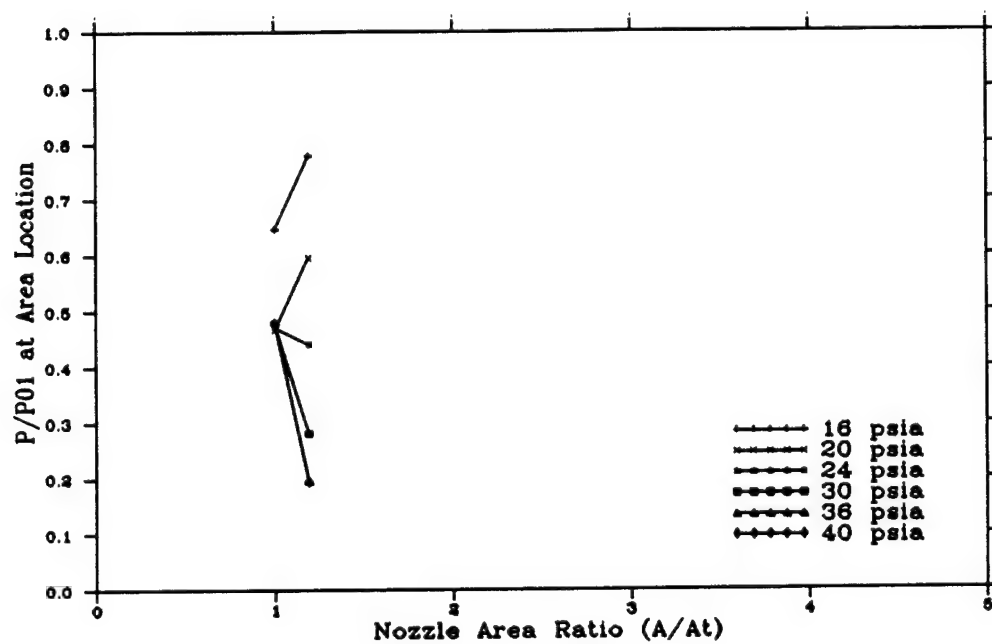Area Ratio of 1.6.

149

a) Exit to throat area ratio is 4

b) Exit to throat area ratio is 2.6

Figure A-11. Normalized Pressure Ratios along the Nozzle Exit
for a 6-Degree Nozzle with Exit Area-to-Throat
Area Ratios of 4 and 2.6.

150

a) Exit to throat area ratio is 1.6

Figure A-12. Normalized Pressure Ratios along the Nozzle Exit
for a 6-degree Nozzle with Exit Area-to-Throat
Area Ratio of 1.6.

APPENDIX B

PHASE II. SPRAY COATING OF METALS

APPROVED FISCAL YEAR 1990 WORK BREAKDOWN STRUCTURE

PHASE II. SPRAY COATING OF METALS

PROPOSED FISCAL YEAR 1990 WORK BREAKDOWN STRUCTURE

TASK 1: Upgrade System Components for High-Temperature Operation.

- o Modify chamber viewing ports to provide cooling. Install insulation at potential particle impact areas.

- o Install scrubbing system to minimize droplet oxidation.

- o Provide chamber safety features for overpressure and temperature transients.

- o Upgrade base metal fixturing for high-temperature deposits.

- o Upgrade furnace and tundish materials and capabilities for melting, pouring, and receiving high-temperature molten metals.

TASK 2: Initiate Modeling Efforts for Particle Consolidation.

- o Review Phase I particle consolidation results on base metal surfaces for input to modeling studies. Outline any supporting. experiments required.

- o Review existing models and evaluate their potential application for numerically simulating the droplet deposition process.

TASK 3: Develop High-Temperature Nebulizer Assembly.

- o Design, characterize, and test nozzles and nozzle/tundish assemblies for high-temperature operation.

TASK 4: Initiate Modeling Efforts for Nozzle Dynamics.

- o Initiate modeling efforts to numerically simulate two-phase nozzle dynamics, incorporating Phase I information on liquid breakup and plume geometry.

- o Incorporate Task 3 results on high-temperature gas characterization of nozzles and mass loading of gas stream. Special supporting experiments may be necessary.

TASK 5: Check Out High-Temperature Spray System.

- o Perform operational checks on diagnostic instrumentation, component parameter instrumentation, hardware-computer interfaces, software computer packages, and calibration modes of instrumentation.

TASK 6: Perform Initial Coating Trials.

o   Spray a coating of high-melting-point material (e.g. stainless steel) on a steel specimen.

o   Where necessary, revise spray-system features to obtain desired plume characteristics, to improve deposition behavior, or to stabilize nebulizer operation, using preliminary modeling results from Tasks 2 and 4.

o   Spray-coat specimens over a wide range of process variables to determine operating conditions likely to produce high-quality coatings.

TASK 7: Analyze Preliminary Specimens, Isolate Favorable Spray Conditions, and Design Experiment to Optimize Measured Coating Properties.

o   Visually evaluate all specimens coated during Task 6, selecting those worthy of detailed study. Subject this subset to bend tests, metallography, etc. to generate data on bonding, porosity, thickness uniformity, and surface finish.

o   Correlate results with spray conditions from Task 6. This will. identify governing variables and relatively narrow ranges over· which good coatings can be achieved.

o   Design an experiment to establish near-optimal spray parameters for producing desired coating properties.

TASK 8: Perform Designed Experiment to Optimize Individual Coating Properties.

o   Spray-coat specimens in accordance with variable setting combinations specified by the experimental design selected in Task 7. Trials will be performed in random order to minimize any time-dependent influences.

TASK 9: Evaluate Coated Specimens, Map Property Response Surfaces, and Design Experiment to Optimize Overall Coating Quality.

o   Evaluate all specimens from Task 8 in terms of bond strength, corrosion resistance, porosity content, and coating thickness and uniformity.

o   Correlate results with spray-system operating parameters to map coating process responses for each property measured, thereby identifying near-optimal conditions in each regard. Incorporate results into modeling effort of Tasks 2 and 4.

o   Select a second experimental design to map the process response surfaces at finer resolution. This would enable accurate determination of a total coating quality response surface.

TASK 10: Perform Designed Experiment to Optimize Total Coating Quality.

    o   Spray-coat specimens in accordance with variable setting combinations specified by the experimental design selected in Task 9. Trials will be performed in random order to minimize any time-dependent influences.

TASK 11: Analyze Final Specimens to Fully Optimize Coating Process.

    o   Evaluate all specimens from Task 10 for bond strength, corrosion resistance, porosity content, thickness uniformity, and surface finish.

    o   Correlate results with system operating conditions, which will produce a fully optimized coating process for high-temperature materials on a small scale.

    o   Incorporate results into modeling effort to project behavior and costs of spray-coating technique for a pilot-scale application.